ECSS-E-HB-10-12A
17 December 2010

EUROPEAN COOPERATION
ECSS
FOR SPACE STANDARDIZATION

Space engineering

Calculation of radiation and its effects and margin policy handbook

ECSS Secretariat
ESA-ESTEC
Requirements & Standards Division
Noordwijk, The Netherlands

Foreword

This Handbook is one document of the series of ECSS Documents intended to be used as supporting material for ECSS Standards in space projects and applications. ECSS is a cooperative effort of the European Space Agency, national space agencies and European industry associations for the purpose of developing and maintaining common standards.

This handbook has been prepared by the ECSS-E-HB-10-12 Working Group, reviewed by the ECSS Executive Secretariat and approved by the ECSS Technical Authority.

Disclaimer

Published by: ESA Requirements and Standards Division
ESTEC, P.O. Box 299,
2200 AG Noordwijk
The Netherlands

Change log

ECSS-E-HB-10-12A 17 December 2010	First issue

Table of contents

Figures

Tables

1
Scope

This handbook is a part of the System Engineering branch and covers the methods for the calculation of radiation received and its effects, and a policy for design margins. Both natural and man-made sources of radiation (*e.g.* radioisotope thermoelectric generators, or RTGs) are considered in the handbook.

This handbook can be applied to the evaluation of radiation effects on all space systems.

This handbook can be applied to all product types which exist or operate in space, as well as to crews of on manned space missions.

This handbook complements to ECSS-E-ST-10-12C “Methods for the calculation of radiation received and its effects and a policy for the design margin”.

2 Terms, definitions and abbreviated terms

2.1. Terms from other documents

For the purpose of this document, the terms and definitions from ECSS-S-ST-00-01 and ECSS-E-ST-10-12C apply.

2.2. Terms specific to the present handbook

None.

2.3. Abbreviated terms

The abbreviated specified in ECSS-E-ST-10-12C apply to this handbook.

3
Compendium of radiation effects

3.1. Purpose

This clause provides a brief summary of the various mechanisms for radiation damage and effects, and is summarised in the context in Table 1, which identifies important parameters to quantify effects, and gives units and examples. Table 2 can be used by the reader to cross-reference component/instrument technology to radiation effects discussed in detail elsewhere in this document.

Table 1: Summary of radiation effects parameters, units and examples.

Effect	Parameter	Typical units	Examples	Particles
Total ionising dose (TID)	Ionising dose in material	grays (material) (Gy(material)) or rad(material) 1 Gy = 100 rad	Threshold voltage shift and leakage currents in CMOS, linear bipolar (note dose-rate sensitivity)	Electrons, protons, bremsstrahlung
Displacement damage	Displacement damage equivalent dose (total non-ionising dose) Equivalent fluence of 10 MeV protons or 1 MeV electrons	MeV/g cm^{-2}	All photonics, e.g. CCD transfer efficiency, optocoupler transfer ratio Reduction in solar cell efficiency	Protons, electrons, neutrons, ions
Single event effects from direct ionisation	Events per unit fluence from linear energy transfer (LET) spectra & cross-section versus LET	cm^2 versus MeV·cm^2/mg	Memories, microprocessors. Soft errors, latch-up, burn-out, gate rupture, transients in op-amps, comparators.	Ions Z>1
Single event effects from nuclear reactions	Events per unit fluence from energy spectra & cross-section versus particle energy	cm^2 versus MeV	As above	Protons, neutrons, ions
Payload-specific radiation effects	Energy-loss spectra, charge-deposition spectra charging	counts s^{-1} MeV^{-1}	False count rates in detectors, false images in CCDs Gravity proof-masses	Protons, electrons, neutrons, ions, induced radioactivity (α, β±, γ)
Biological damage	Dose equivalent = Dose(tissue) x Quality Factor; equivalent dose = Dose(tissue) x radiation weighting factor; Effective dose	sieverts (Sv) or rems 1 Sv = 100 rem	DNA rupture, mutation, cell death	Ions, neutrons, protons, electrons, γ-rays, X-rays
Charging	Charge	coulombs (C)	Phantom commands from ESD	Electrons

Table 2: Summary of radiation effects and cross-references to other chapters (part 1 of 2)

Sub-system or component	Technology	Effect	ECSS-E-ST-10-12C Cross-reference	ECSS-E-HB-10-12A Cross-reference
Integrated circuits	Power MOS	TID SEGR SEB	Clause 7 Clause 9.4.1.6 Clause 9.4.1.6	Clause 6 Clause 8.6.2 Clause 8.6.3
	CMOS	TID SEE (generally)	Clause 7 Clause 9	Clause 6 Clause 8
	Bipolar	TNID SEU SET TID	Clause 8 Clauses 9.4.1.2, 9.4.1.3 Clause 9.4.1.7 Clause 7	Clause 7.4.2 Clause 8.7.1 Clause 8.7.5 Clause 6
	BiCMOS	TID TNID SEE (generally)	Clause 7 Clause 8 Clause 9	Clause 6 Clause 7.4.2 Clause 8
	SOI	TID SEE (generally exc. SEL)	Clause 7 Clause 9	Clause 6 Clause 8
Optoelectronics and sensors (1)	MEMS [a]	TID	Clause 7	Clause 6
	CCD	TNID TID Enhanced background (SEE)	Clause 8 Clause 7 Clauses 10.4.2, 10.4.3, 10.4.5	Clause 7.4.3 Clause 6 Clauses 9.2, 9.4
	CMOS APS	TNID TID SEE (generally) Enhanced background	Clause 8 Clause 7 Clause 9 Clauses 10.4.2, 10.4.3, 10.4.5	Clause 7.4.4 Clause 6 Clause 8 Clauses 9.2, 9.4,
	Photodiodes	TNID TID SET	Clause 8 Clause 7 Clause 9.4.1.7	Clause 7.4.5 Clause 6 Clause 8.7.5
	LEDs	TNID	Clause 8	Clause 7.4.7
	laser LEDs	TNID	Clause 8	Clause 7.4.6
	Opto-couplers	TNID SET	Clause 8 Clause 9.4.1.7	Clause 7.4.8 Clause 8.7.5
	γ-ray or X-ray scintillator	TNID (alkali halides) Enhanced background	Clause 8 Clauses 10.4.2, 10.4.3, 10.4.4	Clause 7.4.11 Clause 9.5
	γ-ray semiconductor	TNID Enhanced background	Clause 8 Clauses 10.4.2, 10.4.3, 10.4.4	Clause 7.4.10 Clause 9.5
	charge particle detectors	TNID (scintillator & semiconductor) Enhanced background TID (scintillator & semiconductors)	Clause 8 Clause 10.4.2, 10.4.3 Clause 7	Clause 9.5 Clause 9.3 Clause 6
	microchannel plates	Enhanced background	Clause 10.4.6	Clause 9.6
	photomultiplier tubes	Enhanced background	Clause 10.4.6	Clause 9.6

[a] MEMS refers to the effects on the microelectromechanical structure only. Any surrounding microelectronics are also subject to other radiation effects identified in “Integrated circuits” row

Table 2: Summary of radiation effects and cross-references to other chapters (part 2 of 2)

Sub-system or component	Technology	Effect	Main Section Cross-reference	ECSS-E-HB-10-12A Cross-reference
Optoelectronics and sensors (2)	Other imaging sensors (*e.g.* InSb, InGaAs, HgCdTe, GaAs and GaAlAs)	TNID Enhanced background	Clause 8 Clauses 10.4.2, 10.4.3	Clause 7 Clause 9.3
	gravity wave sensors	Enhanced background	Clause 10.4.7	Clause 9.7
Solar cells	cover glass & bonding materials	TID	Clause 7	Clause 6
	cell	TNID	Clause 8	Clause 7.4.9
Non-Optical materials	crystal oscillators	TID	Clause 7	Clause 6
	polymers	TID (radiolysis)	Clause 7	Clause 6
Optical materials	silica glasses	TID	Clause 7	Clause 6
	alkali halides	TID TNID	Clause 7 Clause 8	Clause 6 Clause 7.4.11
Radiobiological effects		Early effects	Clause 11	Clauses 10.3.3, 10.4.4
		Stochastic effects	Clause 11	Clauses 10.3.4, 10.4.4
		Deterministic late effects	Clause 11	Clauses 10.3.4, 10.4.4

3.2. Effects on electronic and electrical systems

3.2.1. Total ionising dose

Total ionising dose (TID) effects in semiconductor devices depend on the creation of electron-hole pairs within dielectric layers (oxides, nitrides, *etc.*) by the incident radiation and subsequent generation of:

- traps at or near the interface with the semiconductor;
- trapped charge in the dielectric.

This can produce a variety of device effects such as flatband and threshold voltage shifts, surface leakage currents, and noise [RDA.1].

TID effects in semiconductors are discussed further in Clause 7 of ECSS-E-ST-10-12C, and Clause 6 of the present handbook.

3.2.2. Displacement damage

Energetic particles such as neutrons, protons, electrons, α-particles and heavy ions can create damage in semiconductor materials by displacing atoms in the crystal lattice. Secondary electrons produced by high-energy photons also produce displacement effects. The result is that stable defect states are created within the bandgap that can give rise to a variety of effects depending on the temperature, carrier concentration and the location of the defect site [RDA.2]:

- Generation of electron-hole pairs (leading to thermal dark current in detectors).

- Recombination of electron-hole pairs (leading to reduction of minority carrier lifetime and effects in LEDs and laser diodes).
- Trapping of carriers, leading to loss in charge transfer efficiency in CCDs (minority carrier trapping) or carrier removal (majority carrier trapping).
- Compensation of donors or acceptors, also leading to carrier removal in some devices (for example the resistance in a lightly doped collector in a bipolar transistor can increase).
- Tunnelling of carriers (leading to increased current in reverse biased junctions – particularly for small bandgap materials and high electric fields).

Displacement damage effects in semiconductors is discussed further in Clause 8 of ECSS-E-ST-10-12C and Clause 7 of the present handbook.

3.2.3. Single event effects

Single event effects (SEEs) arise from the interaction of single particles (*e.g.* protons, neutrons or heavy ions) with the semiconductor causing either destructive (or potentially destructive) effects or transient effects.

- Destructive
  - Single event latch-up (SEL) in CMOS circuits – a potentially destructive triggering of a real or parasitic pnpn thyristor structure in the device;
  - Single event snapback (SESB) in NMOS devices, particularly in SOI devices – a destructive triggering of a lateral NPN transistor accompanied by regenerative feedback [RDA.3];
  - Single event gate rupture (SEGR) – Formation of a conducting path triggered by a single ionising particle in a high-field region of a gate oxide [RDA.4];
  - Single event dielectric rupture (SEDR) – destructive rupture of dielectric triggered by a single ionising particle in a high-field region of a dielectric *e.g.* in linear devices, FPGAs;
  - Single event burnout (SEB) in power transistors – a destructive triggering of a vertical n-channel transistor accompanied by regenerative feedback.
- Non-destructive
  - Single event upset (SEU) in memories and registers – *i.e.* bit-flips leading to change of stored information [RDA.5];
  - Multiple-cell upsets (MCU) in memories and registers (including single-word multiple-bit upsets (SMU)) – single particle impacts affecting several adjacent bits due to large particle ranges [RDA.6][RDA.7][RDA.8];
  - Several logically adjacent bits corrupted in a digital element that have been caused by direct ionisation from a single traversing particle or by recoiling nuclei from a nuclear interaction, *i.e.* multiple bit upsets within a single data word.
  - Single event functional interrupt (SEFI) in control circuitry, *e.g.* in processors, memories or ADCs – transient corruption of a control path [RDA.9];
  - Single event hard errors (SEHE) in SRAM and DRAM devices – where semi-permanent damage is sustained by the memory cell due to micro-dose effect from the ionising particle;
  - Single event transients (SET) in linear circuits – *i.e.* a current transient which can be interpreted as a false signal [RDA.10][RDA.11][RDA.12];

- Single event disturb (SED) in digital circuits – *i.e.* a signal transient that is propagated to cause an output error in combinatorial logic.

Further information on single event effects is presented in Clause 9 of ECSS-E-ST-10-12C and Clause 8 of the present handbook.

3.3. Effects on materials

Although TID effects are usually considered in the context of microelectronics or active sensors, exposure to ionising radiation at high doses can also degrade polymers (including those used in thermal blankets) and optical materials. In the case of the former, radiolytic reactions occur in which the bonds in the polymer chains are broken and formed with other reactive fragments. The result can be degradation of mechanical and dielectric properties, coloration, and production of gases that can contaminate and corrode nearby materials. Other optical materials such as silica glasses can also suffer coloration and therefore degradation of their optical properties, depending upon the purity of the material. These effects, together with TID effects in microelectronics, are discussed further in Clause 7 of ECSS-E-ST-10-12C and Clause 6 of the present handbook.

As with TID effects, displacement damage can also have deleterious effects on the properties of passive materials. Atomic displacements in optical materials based on alkali halides result in the production of colour centres (charge traps in the band-gap), and therefore darkening of the crystal. This is discussed further in Clause 8 of ECSS-E-ST-10-12C and Clause 7 of the present handbook.

3.4. Payload-specific radiation effects

Payloads can incorporate instruments which can suffer detrimental effects under irradiation, in the main resulting in enhanced background levels, *e.g.*:

- Direct ionisation from primary or prompt secondary particles (*e.g.* in CCDs);
- Added background noise in sensors due to the various mechanisms, *e.g.* random telegraph signals (RTS) discussed in Clause 8 of ECSS-E-ST-10-12C and Clause 7 of the present handbook;
- Gamma-ray detectors are sensitive to radioactive decays even outside regimes of intense particle radiation [RDA.13][RDA.14];
- It is known that high temperature superconductors, proposed for gravity-wave missions, can suffer a reduction in critical temperature under irradiation [RDA.15]. Intense radiation regimes can lead to macroscopic temperature changes in cryogenically cooled materials [RDA.16].

The use of high-mass spacecraft and detector systems necessitates the accurate computation of secondary radiation and its spectrum to the point of energy/charge deposition within the detector bandwidth.

Radiation background effects are discussed further in Clause 10 of ECSS-E-ST-10-12C and Clause 9 of the present handbook.

3.5. Biological effects

Ionisation produces free hydroxyl radicals which compromise one or more of the functions of the cell, this cellular damage becoming apparent after several cycles, or even resulting in immediate cell death. The effects of this can be deterioration of tissue or organ function, presenting within a matter of minutes to 30-60 days after exposure

(early radiobiological effects). Stochastic radiobiological effects can occur over the duration of the life of the individual exposed and appears in the form of neoplastic diseases (tumours). These are very probably the results of DNA damage to, and subsequent mutation of, a single cell. In addition to long-term stochastic effects, deterministic late effects are possible, such as the development of eye cataracts, which definitely occur beyond a threshold dose. Individual relativistic high-Z particles can also produce light flashes in the retina. These effects are discussed further in Clause 11 of ECSS-E-ST-10-12C and Clause 10 of the present handbook.

3.6. Spacecraft charging

Spacecraft charging can arise from energetic plasmas (10s of keV), leading to surface charging, or from energetic electrons (MeV), which can penetrate the spacecraft skin and collect in insulators leading to deep dielectric charging. The subsequent discharges can couple into spacecraft systems leading to anomalies and damage. Spacecraft charging is not discussed further in this document, but the reader is referred to a separate ECSS standard (ECSS-E-ST-20-06) for detailed information [RDA.17][RDA.18][RDA.19].

3.7. References

[RDA.1] P V Dressendorfer, “Basic mechanisms for the New Millennium,” IEEE Nuclear and Space Radiation Effects Conference, Short Course, Session III, 1998.

[RDA.2] P W Marshall and C J Marshall, “Proton effects and test issues for satellite designers,” IEEE Nuclear and Space Radiation Effects Conference, Short Course, Norfolk, VA, 1999.

[RDA.3] P E Dodd, M R Shaneyfelt, D S Walsh, J R Schwank, G L Hash, R A Loemker, B L Draper, P S Winokur, “Single-event upset and snapback in silicon-on-insulator devices and integrated circuits,” *IEEE Trans Nucl Sci*, **47**, No 6, pp2165-2174, December 2000.

[RDA.4] G K Lum, H O'Donnell and N Boruta, “The impact of single event gate rupture in linear devices,” *IEEE Trans Nucl Sci*, **47**, pp2373-2379, 2000.

[RDA.5] A H Johnston, “Radiation effects in advanced microelectronics technologies,” *IEEE Trans Nucl Sci*, **45**, pp1339-1353, 1998.

[RDA.6] G M Swift and S M Guertin, “In-flight observations of multiple-bit upset in DRAMs,” *IEEE Trans Nucl Sci*, **47**, pp2386-2391, 2000.

[RDA.7] A Makihara, H Shindou, N Nemeto, S Kuboyama, S Matsuda, T Oshima, T Hirao, H Itoh, S Buchner and A B Campbell, “Analysis of single-ion multiple-bit upset in high density DRAMs,” *IEEE Trans Nucl Sci*, **47**, pp2400-2404, 2000.

[RDA.8] C S Dyer, C Comber, P R Truscott, C Sanderson, C Underwood, M Oldfield, A Campbell, S Buchner, T Meehan, “Microdosimetry code simulation of charge-deposition spectra, single-event upsets and multiple-bit upsets,” *IEEE Trans Nucl Sci*, **46**, No 6, pp1486-1493, December 1999.

[RDA.9] S Bee, G R Hopkinson, R Harboe-Sørensen, L Adams and A Smith, “Heavy-ion study of single event effects in 12- and 16-Bit ADCs,” Workshop Record 1998 IEEE Radiation Effects Data Workshop, pp 58-67, 1998.

[RDA.10] A H Johnston, G M Swift, T Miyahira, S Guertin and L D Edmonds, "Single-event upset effects in optocouplers," *IEEE Trans Nucl Sci*, **45**, pp2867-2875, 1997.

[RDA.11] R Koga, S H Penzin, K B Crawford, W R Crain, S C Moss, S D Pinkerton, S D LaLumondiere and M C Maher, "Single event upset (SEU) sensitivity dependence of linear integrated circuits (Ics) on bias conditions," *IEEE Trans Nucl Sci*, **44**, pp2325-2332, 1997.

[RDA.12] R Harboe-Sorenson, F X Guerre, H Constans, J van Dooren, G Berger, W Hajdas, "Single Event Transient characterisation of analog IC's for ESA's satellites," Proceedings of RADECS99 Conference, IEEE 998471, pp 573-581, 1999.

[RDA.13] C S Dyer, J I Trombka, S M Seltzer and L G Evans, "Calculation of radioactivity induced in gamma-ray spectrometers during spaceflight," *Nucl Instrum Meth*, **173**, pp 585-601, 1980.

[RDA.14] C S Dyer, P R Truscott, H E Evans, N D A Hammond, C Comber, and S J R Battersby, "Calculations and observations of induced radioactivity in spaceborne materials," Proceedings of the 2nd European Conference on Radiation and its Effects on Components and Systems (RADECS) 1993, St Malo, France, IEEE Conference Proceedings 93TH0616-3, pp 77-83, 1993.

[RDA.15] G P Summers, D B Chrisey, W G Maisch, G H Stauss, E A Burke, M Nasatasi, J R Tesmer, "Electron and proton radiation effects on high temperature superconductor $YBa_2Cu_3O_{7-8}$," *IEEE Trans Nucl Sci*, **36**, pp1840, 1989.

[RDA.16] A L Vampola, R D Jiminez, J E Cox, "Heat loads due to the space particle environment," *J Spacecraft and Rockets*, **26**, pp474-476, 1989.

[RDA.17] Carolyn K Purvis, Henry B Garrett, A C Whittlesey and N John Stevens, "Design guidelines for assessing and controlling spacecraft charging effects," NASA Technical Paper 2361, 1984.

[RDA.18] "Avoiding problems caused by on-orbit internal charging effects," NASA-HDBK-4002.

[RDA.19] ECSS-E-ST-20-06 "Space engineering – Spacecraft charging".

4 Margin

4.1. Introduction

4.1.1. Application of margins

The application of a margin is ultimately a project management decision, but is based on consideration of a number of uncertainties in the radiation hardness analysis of a particular device or product.

Several issues contribute to the margin, and projects often adopt a “lumped” approach to margins in the domain by assuming that a single margin covers all the issues.

Applying a margin can result in problems for spacecraft development, including:

- The present component class can be unsuitable, and this can imply the use of a different one.
- COTS components can become unusable.
- The present shielding can be insufficient, and this can impliy the use of additional shielding.
- Alternative, it can imply the use of lower performance components.
- Conformity to the requirements cannot be ensured without additional and costly testing.

There is often pressure to reduce the margin. However, a margin should not be reduced without a risk analysis. Situations can result in which a mission becomes unfeasible with application of “standard” margins.

It is also important to consider the following issues:

- Criticality

  A target (component, experiment, astronaut) can be critical to mission success in which case it is important that the margin guarantees a high probability of survival, functioning, or both. Less critical functions (experiment mass storage, for example) can be affected in such a way as to represent a “nuisance”, and so a less stringent margin can be employed.

- Immunity

  If a target can be shown to be immune to radiation to a degree where the most conservative simplified assessment of the effects parameter(s) is considerably below the expected problem threshold, assuming worst-case margins, little further analysis is warranted.

This clause discusses the contributions to the margin and identifies ways in which the risk associated with the margins can be assessed. The domain is the subject of on-going research and understanding is limited in many areas. Therefore the advice provided is less solid than desired. Where possible normative requirements are indicated in Clause 5 of ECSS-E-ST-10-12C and expanded upon in this clause.

The contributors to the margin are:

- environmental uncertainty (models or other data);
- uncertainty in predicting effects parameters (shielding uncertainty, uncertainty in parameter prediction *e.g.* dose, SEU rate, *etc.*);
- testing: testing is complex and subject to both systematic and statistical uncertainties;
- procurement processes;
- project management decisions.

Each of these is treated below. They are also addressed in the individual clauses.

4.2. Environment uncertainty

ECSS-E-ST-10-04 space environment standard [RDB.1] is the formal location for information on the uncertainties and margins associated with the environment of a space system and related models and data. The standard models contained therein are based on satellite data. It is typically said that the models are accurate to "within a factor 2" as a consequence of uncertainties in these measurements due to:

- instrument calibration and characterisation difficulties;
- extrapolation and interpolation procedures employed in constructing models;
- representativity of the periods measured.

There is strong evidence that the AE-8 models for the electron radiation belts are compatible with the worst case, at least for the long-term average geostationary environment. In addition, geostationary environments are often specified for a "worst longitude" since there is arguably a dependence on longitude and in AE-8 this is a factor of two. The AE-8 models for the electron belts are only intended as long-term averages and the environment over short periods, months or various phases of the solar cycle can be considerably milder or more severe than the average model value. Evaluation of transient effects relates to extremes of the environment rather than the long-term averages represented by the models.

Radiation effects due to solar protons can be due to accumulated exposure or to transient effects. Certainly for the former and often with the latter, the environment is specified through use of statistical models. It is important to appreciate that when such models are employed *a margin is implicitly included*. Nevertheless, the same potential problems with instrumentation apply to solar particle measurements so a design margin can be appropriate. For example, for solar proton induced solar array degradation or total dose, the JPL-91 model can be employed [RDB.2], with a "90 % confidence level". It is often not appreciated that the environment specified is not a prediction but is rather a risk-level, or budget. A project can relax the specified confidence level, take a greater risk and "achieve" a lower dose.

A similar situation can arise with other environmental aspects when applying "worst case" methodologies – for example with the worst-case fluxes expected in the (dynamic) electron radiation belt.

Accuracy of environmental estimates are provided in the ECSS-E-ST-10-04 space environment standard [RDB.1].

4.3. Effects parameters' uncertainty

4.3.1. Overview

The process of deriving the radiation effects parameter (e.g. absorbed dose, SEE rate, dose equivalent, and background rates) are often complex and often the subject of simplification. In addition, calculation of shielding and interactions with materials around or within the target can be uncertain. As a result some margin are assumed and used for such calculations.

4.3.2. Shielding

For engineering purposes, three, progressively more detailed, levels of radiation shielding assessment are possible:

- Basic use of the "dose-depth" curve

  A mission environment specification usually specifies the dose (ionising, non-ionising), or particle fluence as a function of shield thickness (usually assumed to be aluminium). The minimum shielding between the target and space can be established by examining the actual configuration of the system under analysis The "dose-depth" curve, usually representing a spherical model of the shielding, indicates the dose through this minimum, and a worst-case dose can be estimated assuming all directions experience such minimum levels. Further, if other directions are particularly heavily shielded, they can be attributed a lower dose (according to the dose-depth curve) and the fraction of the total solid angle subtended used to weight the contribution (see ECSS-E-ST-10-12C Clause 6.2.2.2).

- Sectoring

  "Sectoring" (see ECSS-E-ST-10-12C Clause 6.2.3) is a method of estimating the effect of shielding surrounding a point of interest taking account of the complexity of the geometry. It samples all directions from the point and finds the total shielding in each direction. Each shielding value in the distribution corresponds to a dose in a "dose-depth curve" (see ECSS-E-ST-10-12C Clause 6.2.3). As a result, the total dose is found through integration of all contributions (weighted by the solid angle represented by the individual values). It is only an approximation in that the dose-depth curve is derived assuming the shielding is spherical (or sometimes planar). In reality, as radiation propagates through the spacecraft structure, it is scattered in direction and generates secondary radiation. Sectoring generally converts all materials to an equivalent amount of aluminium, thereby ignoring the differences in shielding, scattering and secondary production of materials. Slowing down behaviour also has a statistical scatter. Furthermore the environment is generally assumed isotropic. This is a reasonable assumption in most cases but can be incorrect in some circumstances.

  The error inherent in sectoring calculations depends on the environment, since electrons scatter more than protons and also generate significant bremsstrahlung – which also scatters. So in electron-dominated environments such as GEO and MEO, or close to Jupiter, it is important to consider the error.

- Monte-Carlo & finite difference models

  The full tracking of particles of representative type and energy through a 3-D model of the geometry, with correct attribution of material type, gives the best estimated (see ECSS-E-ST-10-12C Clause 6.2.4).

4.3.3. Ionising dose calculation

Ionising dose is calculated according to the methods defined in ECSS-E-ST-10-12C Clause 7, and Clause 6 of the present handbook. The dose is an integral of the product of the differential fluence of particles and the ionisation energy loss:

$$\int f(E) \cdot \left(\frac{dE}{dx} \right)_i \cdot dE \qquad \textbf{(1)}$$

The main uncertainties relate to the use of the appropriate energy loss for the correct material. Uncertainties are usually quite minor.

For thick materials, the dose deposition profile is important to consider, rather than the surface dose.

Some shielding calculations tend to generate TID predictions directly by computing local energy deposit through ionisation, whilst others convert estimates of particle fluence through a material into ionising dose (see Clause 4.5.1 of ECSS-E-ST-10-12C and Clause 6.4 of the present handbook). For the former, RDM factors associated with the TID can be assumed to be taken into consideration in the shielding calculation, whilst for the latter, the additional uncertainty associated with the conversion is very small compared to those incurred in from the fidelity of the shielding calculation and can in any case be neglected.

4.3.4. Non-ionising dose (NIEL, displacement damage)

By analogy with ionising dose, this is an integral involving the non-ionising energy-loss and so includes elastic and inelastic scattering from atoms. The main uncertainty is the non-ionising energy-loss function in a given material. This is often best derived from testing of individual materials or devices.

Solar cell assessment methods have been based in the past on a “damage-equivalence” methodology where extensive testing of cell types was used to derive the behaviour in space. With more complex cell types this approach is not suitable, and a more general approach, utilising direct calculation of the non-ionising dose in the cell materials, and an assessment of cell structure, is used.

4.3.5. Single event effects

Calculation of single event effects (see ECSS-E-ST-10-12C Clause 10 and in Clause 8 of the present handbook) often assumes that all the sensitive parts of “bits” on a chip are well approximated by identical rectangular parallelepipeds. This considerably simplifies the prediction of single event upset rates since a component can be characterised by a single “path-length distribution”. Modern electronics have many different logical elements on the chip and these are often not parallelepipeds. Memories often include control logic that can be susceptible to upsets, “locking” the component, or to latch-up. Consequently many of the assumptions made in the traditional prediction break down. Furthermore, many of the assumptions made in interpreting accelerator test data also break down. Tilting a component with respect to the accelerator ion beam is a common way of trying to mimic ions that produce greater ionisation, but this is only true for flat two-dimensional structures.

The single event transient (SET), which is an upset in analogue electronics – is also a complex problem to deal with. Generally the seriousness of the SET depends on where in the linear circuit the ion strikes, on the settings of the circuit, on the filtering of the signal and on the way in which the signal is used. So evaluation is very application-specific.

4.3.6. Effects on sensors

Radiation background in detectors is a related phenomenon, but is often much more complex to analyse because the specific sensitivity of a payload system depends on its application, what background event rates can be coped with, and whether there are specific energy (or energy-deposit) thresholds in play. Analysis depends increasingly on application of Monte-Carlo simulation to treat the passage of the radiation through the spacecraft and detector and of the interaction with detector elements.

4.4. Testing-related uncertainties

4.4.1. Overview

Testing has clear uncertainties related to systematic and random errors. The source of radiation, preparation of the device or sample, and means of measuring the effects all play a role.

The good calibration of radiation sources, as well as the availability of both the calibration data and estimates of systematic and statistical uncertainties, are fundamental issues. Equally important is a good understanding of the characteristics of the source.

Statistical analysis of results is important and if a limited sample size or number of single event effects observed in a test (or both) is not properly and rigorously accounted for, a good estimation of the measurement error cannot be establish.

It is important that the outcome of testing includes a quantitative error estimate, which can be used to demonstrate that the part or product satisfied the requirements that include a specified margin.

4.4.2. Beam characteristics

For particle beam sources, it is important to know:

- energy;
- energy spread;
- flux;
- beam size and uniformity;
- composition.

Beams used for total ionising dose, total non-ionising dose and SEU simulation can pass through “degraders” to reduce the energy and as a consequence what began as a well-defined mono-energetic beam can become broad in energy. Such energy spreading is taken into account in interpretation because effects can be energy dependent.

4.4.3. Radioactive sources

For radioactive sources, such as ^{60}Co, commonly used for total dose testing, the emission is normally characterised by a total ionising dose measurement. Account should be taken of the dose variation with location with respect to the source. Sources can emit a spectrum of (mainly) photons and electrons and it is important to take this into account.

^{252}Cf used for single event effects screening is a special case. In addition to its main emission (96.9 %) of alpha particles, it emits neutrons (2.3×10^9 neutron/s/mg) and a range of ions that have rather low energy. The source is usually used in a rough vacuum

to ensure sufficient particle range. Nevertheless, the penetration capabilities of the ions are poor.

4.4.4. Packaging

The effect that electronic component packaging has in modifying the source environment should be appreciated. Preparation of the sample can include removal of the lid of electronic components, *etc.* The purpose of this is often to ensure that particle from a source of low energy can reach the sensitive zones of a device. But such preparation can be difficult and residual layers can still obstruct the sensitive device regions under test.

4.4.5. Penetration

In electronic components, apart from problems of packaging in degrading low-energy sources, low-energy ions can slow significantly in the device and as a result their LETs, NIELs or dose profiles are not those of ideal un-slowed primaries.

For materials and solar cells, it is important to consider also the penetration behaviour. The profile of deposited dose (ionising or non-ionising) depends on the energy distribution and particle type of the radiation. While the "surface dose" can correspond to the in-orbit dose, if the spectrum of energies or particle types is very different, the resulting dose profile in the material can be very different from that in space. For example in optical materials, the resulting distribution of colour centres can be unrepresentative.

4.4.6. Representativeness

Space radiation is usually characterised by high energy and (relatively) low flux. Ground tests attempt to simulate this in a cost-affective and time-compressed manner. As a result, energies and particles are used which often do not correspond to space conditions. As mentioned in 4.4.5, particle penetration sometimes is not as desired and in addition, other properties of particle propagation and damage can come into play. Direct ionisation single event effects are assumed to be characterised by particle LET, independent of particle species and energy. However, there is evidence that different ion species possessing the same LET can give rise to different effects because of the details of the ionisation track structure. Tilting devices to change the "apparent LET" can cause range effects to come into play, invalidating the "non-slowing" assumption.

Dose rates in testing are generally different from in space and it is known that some devices respond differently to low and high dose rates.

While SEU testing devices with protons, a significant dose can be imparted to the device, degrading its behaviour and modifying its response. In order to achieve a statistically meaningful number of single event errors, this degradation can be difficult to avoid.

4.5. Procurement processes and device reproducibility

The device being flown should be as identical as possible to the one(s) tested. However, this is becoming more difficult to achieve as device manufacturing is a worldwide process, part codes do not guarantee the same manufacturing batch, and physical examination of devices is becoming very difficult.

4.6. Project management decisions

The ultimate authority to decide margins and margin policy is the project manager. In such decision making, it is important to clearly understand an analysis of the risks to the project as a result of changing the margins. Such decision-making cannot be supported if the analysis of the criticality and mission impact of a device or product, and of the uncertainties related to environment, and testing, are not available.

4.7. Relationship with derating

Derating is the "process of designing a product such that its components operate at a significantly reduced level of stress to increase reliability." Reference ECSS-Q-ST-30-11 [RDB.3]) discusses in detail the derating methods for a wide range of components.

If it can be demonstrated that de-rating improves the ability of the component to withstand radiation effects, it can usefully be employed. Nevertheless, it does not affect the margin to be used – it rather allows a component to comply with the specification, including the margin.

System de-rating can also be useful. For example, in the presence of single event transients (SET, see Clause 9.4.1.7 of ECSS-E-ST-10-12C, and Clause 8.7.5 of the present handbook), filtering and slowing the response of the circuit or system to analogue signals can protect the system against invalid responses to erroneous analogue signals induced by SET.

4.8. Typical design margins

A minimum RDM for long-duration operational geostationary missions where there is a lot of experience, and the environment is predicted on the basis of AE-8, is typically 1.2. However, certain assumptions are made on shielding and parts conservatism and this margin is established on a case-by-case basis.

For other missions the RDM can vary between 1.2 and 2 depending on mission reliability requirements.

Short duration missions or applications subject to episodic increases (*e.g.* SMART-1) should generally consider the risk of encountering a period of enhanced radiation (*e.g.* recurrent electron radiation belt enhancements due to coronal hole co-rotating region triggered storms).

4.9. References

[RDB.1] ECSS-E-ST-10-04 "Space engineering – Space environment"

[RDB.2] J Feynman, G Spitale, J Wang and S Gabriel, "Interplanetary proton fluence model: JPL 1991," *J Geophys Res*, **98(A8)**, pp13281-13294, 1993.

[RDB.3] ECSS-Q-30-11 "Space product assurance – Derating EEE components"

5 Radiation shielding

5.1. Introduction

In this clause we outline the interaction processes of particles found in the space environment, and trends in the importance of these processes as a function particle energy and target material. Key terms used, such as particle range and stopping power, are defined, shielding calculation approaches are described together with typical models used for these applications, and the standard techniques for mitigating radiation effects by radiation shielding are identified.

5.2. Radiation transport processes

5.2.1. Overview

There are many texts describing the transport of energetic particles through materials and it is not the intention of this clause to repeat this work. Instead this clause intends to highlight the main interaction mechanisms of electrons, protons, heavy ions, and electromagnetic radiation.

5.2.2. Electrons

Electrons interact with material mainly at the atomic level, producing excitation and ionisation, losing energy and being scattered in the process. Such scattering can lead to highly convoluted electron paths in the material. Electron acceleration in the strong electric field of the atomic nucleus results in the generation of energetic photons known as 'bremsstrahlung' (braking radiation). For electrons in the energy range less than 5 MeV (typical of the Earth's radiation belts) almost all energy loss during passage through a material is by bremsstrahlung and by interaction methods resulting in atomic excitation and ionisation of the material, *i.e.* the creation of electron-hole pairs with no momentum transfer to the atom.

The rate of loss of energy with distance traversed is known as the stopping power of the material. The amount of data available on stopping power for various materials at different incident particle energies is considerable. The range of an electron of a given energy is clearly an important parameter to understand in calculating the dose received by a component. Figure 1 and Figure 2 show the *continuous slowing down approximation* (CSDA) range and stopping powers for electrons in hydrogen, beryllium, aluminium, lead, water and polyethene[1] (these and similar data for other materials are

[1] Also known as polyethylene or polythene.

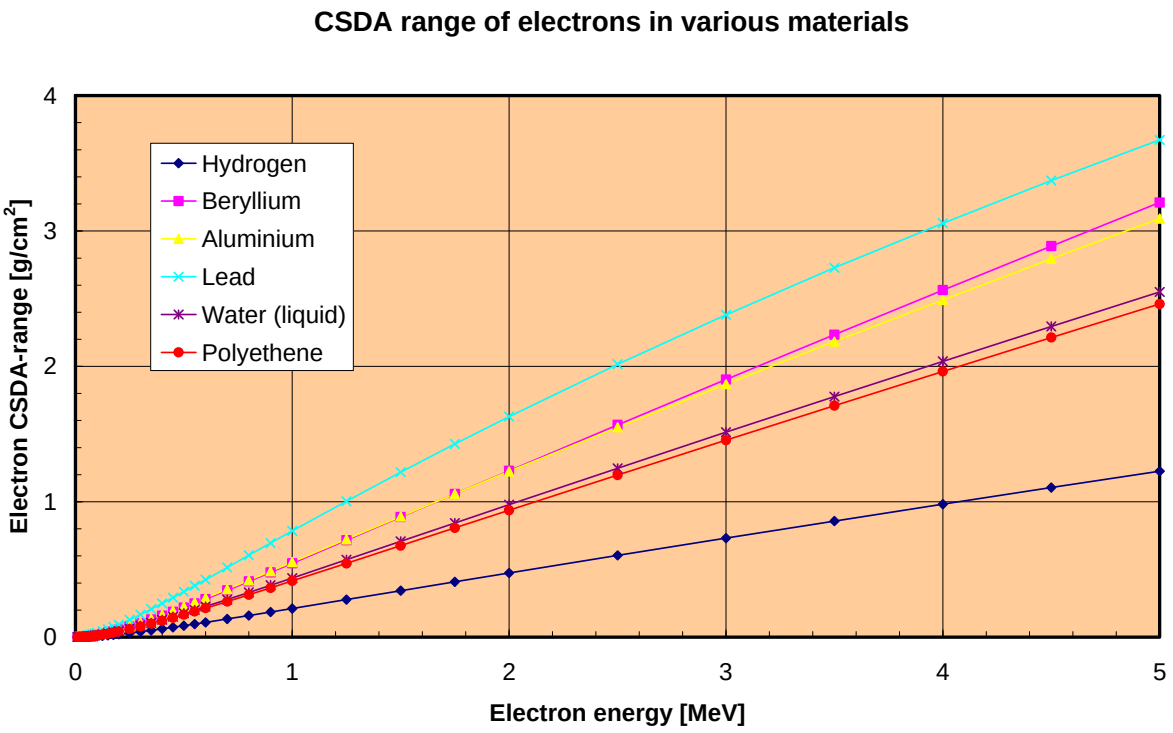

NOTE: CSDA refers to the average integral pathlength of the electrons in the material rather than penetration.

Figure 1: CSDA range of electrons in example low- and high-Z materials as a function of electron energy

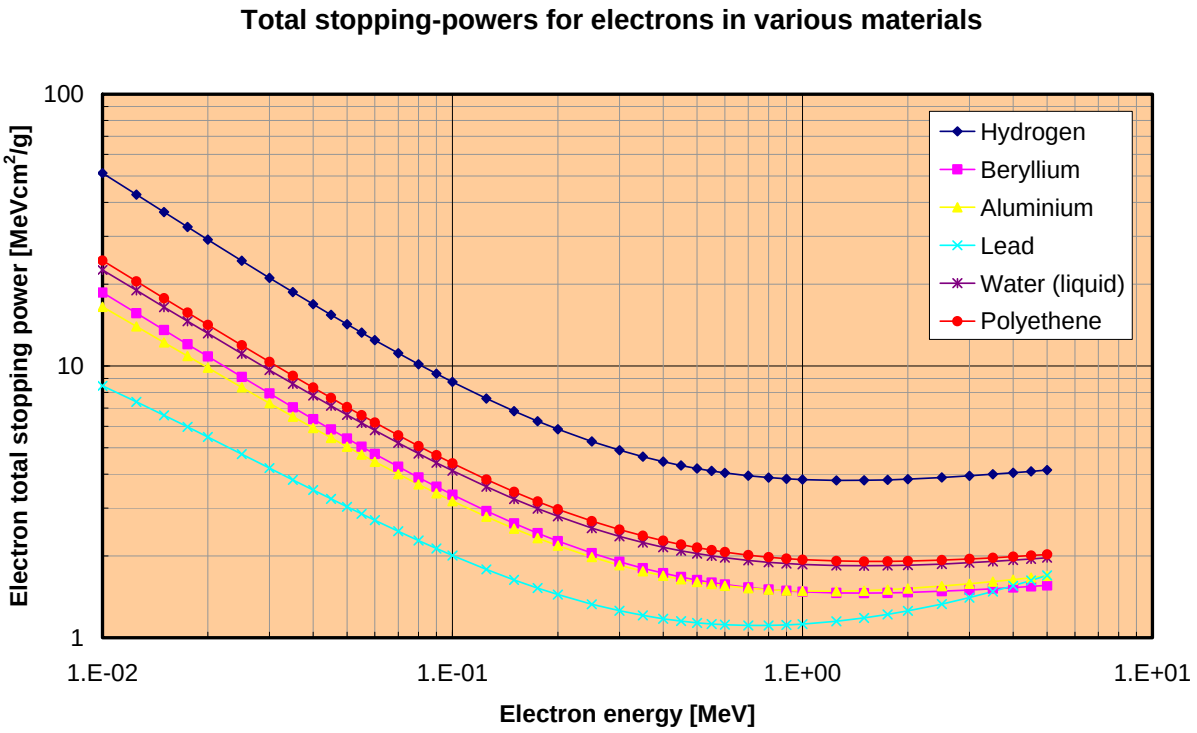

Figure 2: Total stopping powers for electrons in example low- and high-Z materials

available from the US National Institute of Standards and technology website [RDC.1]). The CSDA range corresponds to the integral pathlength travelled by electrons assuming no stochastic variations between different electrons of the same energy (see Clause 5.2.3). As already mentioned, electrons can suffer considerable multiple scattering, therefore, the *depth of penetration* is for most cases shorter than the CSDA range (depending upon the electron energy and material).

Typically for electrons in the space environment, the Z/A factor in the Bethe formula for the collision stopping power dominates [RDC.2]. Therefore, since there are fewer target electrons per unit mass in high-Z materials, the electron range (in units of g/cm^2) is greater in high-Z materials, such as lead, than in lower-Z materials, such as aluminium and silicon. This is illustrated in Figure 1. However for dose behind a shield, the increased scattering in high-Z materials reduces the dose more for thin high-Z shields than for thin low-Z shields. For thicker shields the bremsstrahlung becomes important, and low-Z shielding is more efficient than high-Z. An optimum shield employs a low-Z layer followed by a high-Z layer (discussed further in Clause 5.4). Such graded shields against electrons can give weight or dose advantages of as much as a factor of ten, depending upon the electron spectrum, and the degree of the dose attenuation to be achieved. It cannot be optimized without a careful application of radiation transport simulation codes.

5.2.3. Protons and other heavy particles

Inelastic collision with atomic electrons is the main mechanism of energy dissipation for protons and heavy ions in matter. Being heavier particles, these are not subject to the range of scattering experienced by electrons and their paths through materials are thus easier to compute. However, care should still be taken in interpreting published range data for protons and heavier ions, since particle range can be defined in several ways:

- ***CSDA range*** assumes no stochastic variations in the interactions for different protons of the same initial energy, and no angular deflections of the particles. In reality, the probabilistic nature of the interaction process gives rise to straggling, in which some protons have slightly longer pathlengths whilst others have shorter pathlengths. This is depicted in Figure 3, which shows the variation in intensity of a mono-energetic proton source as it passes through material. The *mean range* R_m is to a good approximation equal to the CSDA range and represents the integral pathlength after which the intensity is reduced by a factor of two, *i.e.* it is not the range at which all particles are stopped.
- ***Extrapolated range*** (R_e in Figure 3) attempts to compensate for range straggling, and is determined by extrapolating the line of maximum gradient in the intensity curve (Figure 3) until it reaches zero intensity.
- ***Projected range*** is the *average depth of penetration* of a particle measured along the initial direction of the particle. This value takes into consideration the deflection of the protons/ions due to multiple scattering.

The projected range (for low-energy protons/ions) or the extrapolated range (for higher energy protons/ions) are more appropriate quantities for assessing radiation-shielding effects.

Figure 4 and Figure 5 show the projected ranges and stopping powers for protons as a function of energy in hydrogen, beryllium, aluminium, lead, water and polythene. Due to the smaller scattering of heavy particles, the Z/A term in the Bethe-Bloch equation always means that low-Z materials provide more mass-efficient shields, as indicated in Figure 4.

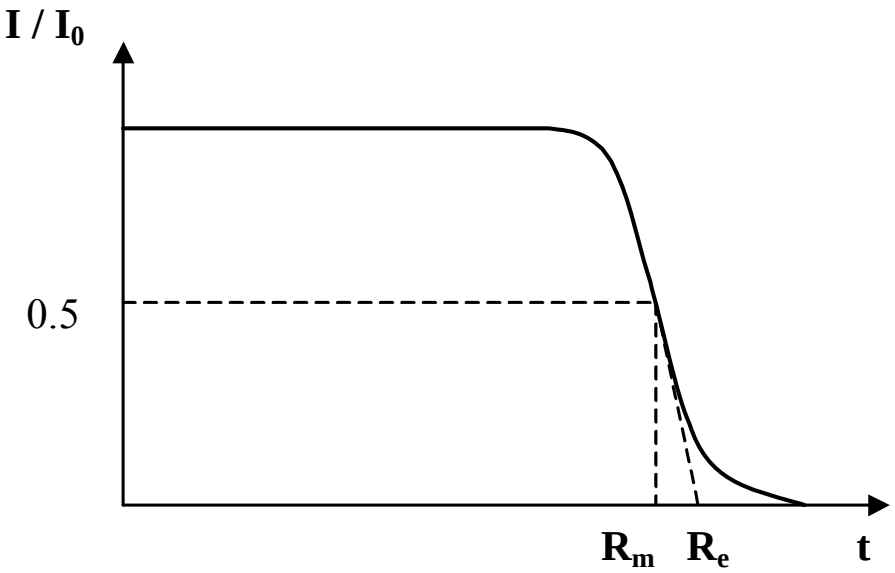

NOTE: This range curve demonstrates the distinction between mean range R_m (almost exactly equal to CSDA range) and extrapolated range R_e.

Figure 3: Intensity of mono-energetic protons in a beam as a function of integral pathlength,

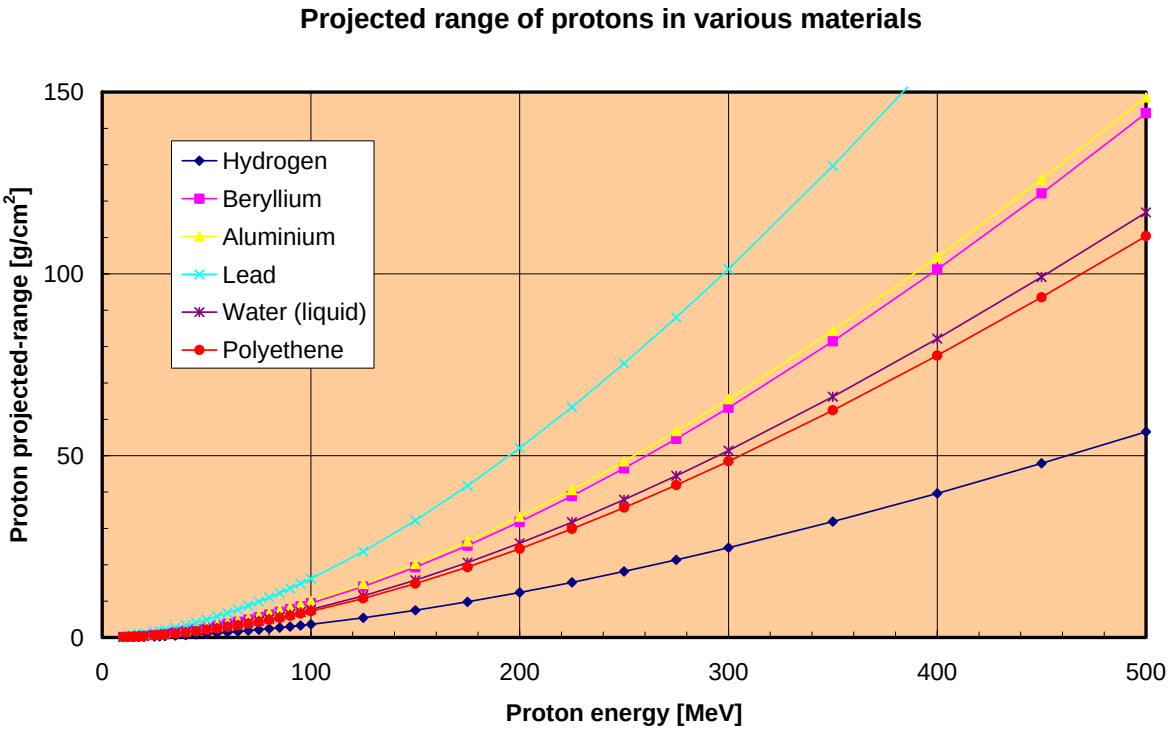

Figure 4: Projected range of protons in example low- and high-Z materials as a function of proton energy.

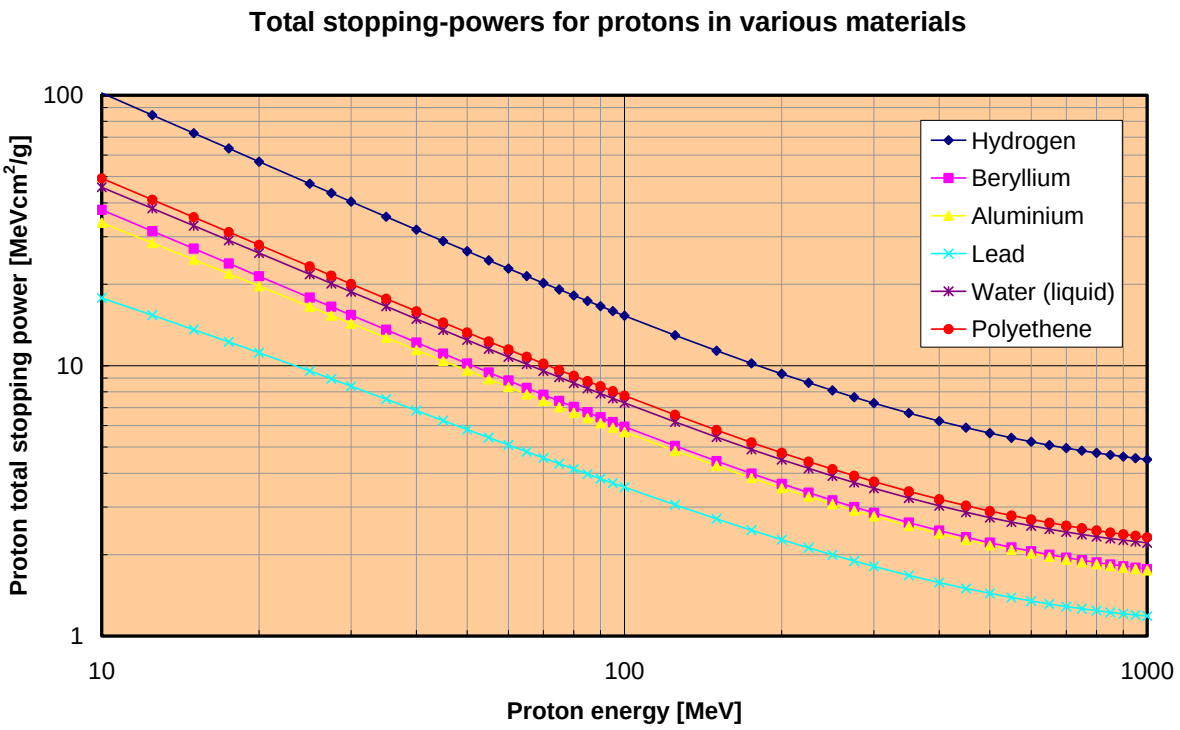

Figure 5: Total stopping powers for protons in example low- and high-Z materials.

The ranges and stopping powers for ions heavier than protons can be estimated based on the following approximate formulae:

$$S_i(E_i) = z_i^2 S_p\left(E_i \frac{M_p}{M_i}\right)$$
$$R_i(E_i) = \frac{M_i}{M_p z_i^2} R_p\left(E_i \frac{M_p}{M_i}\right) \quad \textbf{(2)}$$

where:

$S_i(E)$	= stopping power for ion with energy E;
$S_p(E)$	= stopping power for proton with energy E;
$R_i(E)$	= range of ion with energy E;
$R_p(E)$	= range of proton with energy E;
z_i	= charge number of ion;
M_i	= mass of ion;
M_p	= mass of proton.

In addition to interactions with electrons, there is however a small, but not negligible, chance of protons and other ions interacting with atomic nuclei, causing excitation and fragmentation of the nucleus or the emission of secondary neutrons, protons, α-particles and other light nuclear fragments, as well as γ-rays. The probability of such processes taking place depends on the charge, mass and energy of the incoming particle, and on the properties of the target material. The fragments and secondaries produced in this manner are hazards that cannot be ignored in some circumstances such as manned

missions or applications sensitive to single-event processes. Secondary neutrons produced in spacecraft materials contribute significantly to the radiation exposure to astronauts on large structures such as the Shuttle and Space Station, and can significantly enhance background rates in some sensitive scientific equipment. The secondary neutron flux produced by cosmic radiation and solar event particle interactions in planetary atmospheres or the surfaces of solar system bodies can also be important when considering radiation exposure for manned interplanetary missions, or enhanced background in specialised instrumentation such as radiation monitors.

The reader should note that in addition to being more efficient at slowing down ions through ionisation, low-Z materials produce fewer secondary products. Hydrogen is the optimum material on a mass basis, but is rarely practical. However, polythene is used extensively on the ISS.

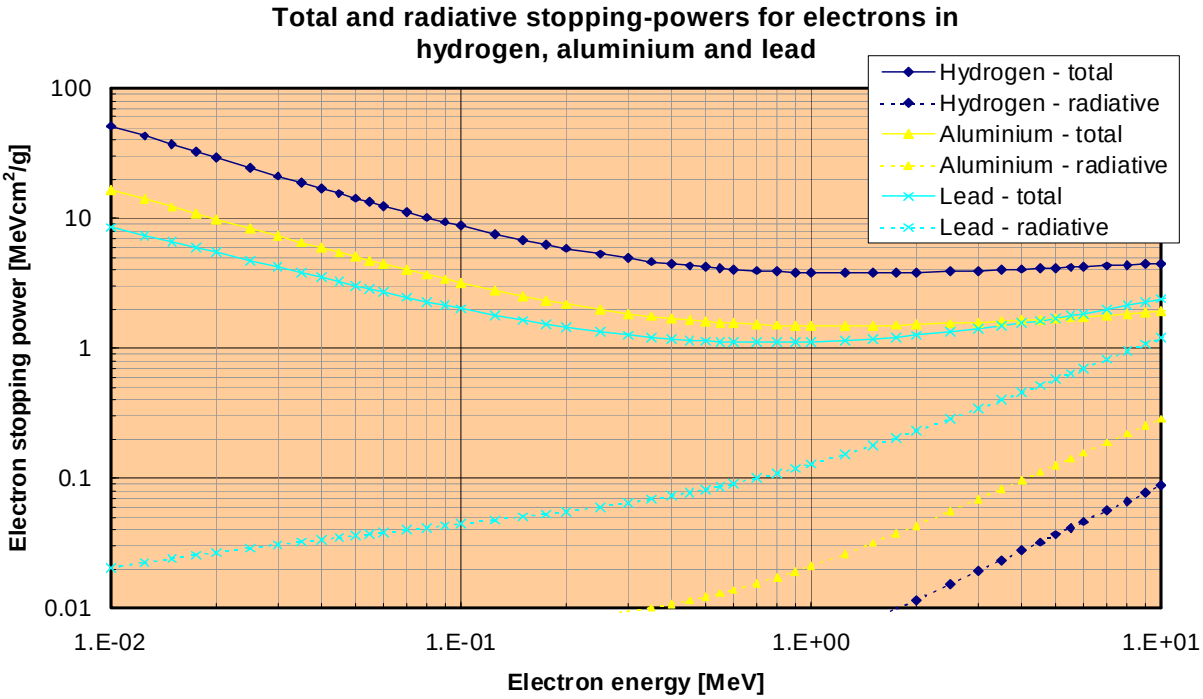

Figure 6: Stopping power for electrons from collisions with atomic electrons and bremsstrahlung production, and from bremsstrahlung production alone.

5.2.4. Electromagnetic radiation – bremsstrahlung

As electrons slow down in material, they generate "braking radiation," or bremsstrahlung, photons with a distribution of photon energies and directions. These photons subsequently interact through a number of processes (Rayleigh scattering, photoelectric effect, Compton effect and pair-production), resulting in the loss or scattering of the incident photon, and for the three latter processes, the production of electrons or positrons that can induce further ionisation or bremsstrahlung.

Photons generated by electron bremsstrahlung are the main concern from a space radiation perspective although ambient X-rays and gamma rays can also affect sensitive scientific payloads. Bremsstrahlung production allows energetic electrons to deposit energy significantly beyond the range of electrons in materials due to the longer average ranges of the photons.

The fraction of energy loss by bremsstrahlung production is highly dependent upon the material, varying as the square of the atomic number. Figure 6 shows the stopping power for electrons from collisions with atomic electrons and bremsstrahlung

production, and from bremsstrahlung production alone (the latter is identified as the *radiative stopping power* in the figure). It can be seen that for energetic electrons in higher-Z material, such as aluminium and especially lead, a greater fraction of energy loss occurs by the bremsstrahlung process than for low-Z materials.

5.3. Ionising dose enhancement

It is important to realise that simply adding more shielding does not always lead to reduced dose at the sensitive target. Depending on the radiation environment and on the local spacecraft and instrument geometry, there are cases where this can rather lead to more secondary particles or to undesirable changes in the incident particle energy spectrum, hence actually enhancing the dose. In particular, the high-energy cosmic rays are difficult to shield against, and nuclear interactions in the shield give rise to a significant multiplicity of secondary particles, the lower-energy charged particles producing more ionisation than the original cosmic ray. Additionally, dose enhancement can be seen at boundaries between high-Z and low-Z materials. This implies paying special attention in optimising the shielding structures.

5.4. Material selection

Higher-Z materials are more effective at shielding electrons as more electrons are scattered than in lower-Z materials. However, bremsstrahlung photon production increases with increasing Z number. As indicated above, it is therefore possible to create ‘sandwich’ composite shields, which balance the benefits of electron stopping power of high-Z materials along with the lower bremsstrahlung production of lower-Z materials.

To shield against electrons, the first layer facing space is a low-Z material that attenuates the high-energy electrons whilst minimising bremsstrahlung production, while the next, high-Z layer scatters lower-energy electrons and attenuates any bremsstrahlung created by earlier interactions. For X-rays, the shield is reversed (high-Z material first) to attenuate photons and then absorb secondary electrons in the lower-Z material.

Although there are occasions where such sandwich shields are desirable, the standard engineering approach is to calculate the shield thickness that achieves the required dose attenuation in aluminium and if possible to realise the shield in aluminium. Where housing issues arise the general approach is to convert the thickness of aluminium into that of a higher-Z material. As has been discussed previously higher-Z materials are more effective at attenuating electrons although they produce bremsstrahlung more effectively. It is important, when applying sector shielding analysis (which approximates all materials to aluminium), to ensure the result is still conservative. More accurate results imply considering such effects using, for example, Monte Carlo coupled electron-photon simulation codes..

5.5. Equipment design practice

5.5.1. Overview

The most common starting-point for equipment radiation effects and shielding analysis is the:

- ionising dose-depth curve;
- information on NIEL as a function of depth;
- LET spectrum (or for protons-induced SEEs, the proton flux) as a function of shielding.

A first-cut at the shielding analysis can be made by determining the dose or particle flux corresponding to the most lightly shielded part of the subsystem under evaluation. If the dose is tolerable then clearly no further analysis is performed. However, the identification of a problem implies a more extensive analysis of shielding be performed, possibly including a sector-analysis or even 3-D radiation transport simulation of the whole or a part of the spacecraft (see Clause 5.6).

5.5.2. The importance of layout

When optimising the configuration of equipment in a spacecraft, it is important that the designer always attempts to put equipment boxes containing the more sensitive devices in protected locations; to surround them with structures containing less sensitive materials. The ultimate aim of this design practice is to use "built-in" shielding such that the need for "add-on" shielding is minimised. Layout therefore has a fundamental importance in the design of a radiation-tolerant spacecraft. Considerations include, for example:

- If the spacecraft is spin-stabilised, the solar array is wrapped-around at least part of the spacecraft providing the equivalent of 3 to 4 mm of aluminium. This is a significant addition (possibly 30 kg) to the built-in shielding provided by platforms, box covers and circuit boards.
- Microelectronics in the centre of a stack of printed circuit boards can be exposed to only one-tenth of the dose received by the same circuits on the uppermost board of a stack. Similarly, equipment boxes near the edge of a platform receive greater dose than those near the centre.
- Many equipment boxes designed by European industry are made up of sections milled out of solid aluminium with certain parts milled very thin as a weight-saving measure. Such an absorber array gives less protection than the uniform sheet-metal enclosures more common in the USA. This is a case of the general rule that good built-in protection from radiation is a matter of total mass as well as efficient mass distribution. This same rule applies not only to box structures, but also to the arrangement of masses around a box containing sensitive devices.
- The mass of the spacecraft structure can be misleading when assessing radiation shielding. Often the mass is concentrated in struts, attachment points, mechanical connectors and stiffeners. The facings ("shims") of a carbon fibre honeycomb can be very thin (a few hundred micrometers), and the honeycomb structure can contain more mass but presents a smaller solid angle to interior objects.
- Other large subsystems, such as batteries, propellant tanks and apogee boost motor can provide significant shielding. Future missions can use lithium-ion battery technologies, which can make feasible the use of thin, large area cells that can also act as an absorber to the incident radiation.
- Clearly, all the above points are subject to other design issues such as spacecraft mass balance, thermal behaviour of subsystems and the overall spacecraft, and other threats to spacecraft operation such as from hypervelocity impact from debris or meteoroids.

5.5.3. Add-on shielding

5.5.3.1. Introduction

If built-in mass on the spacecraft cannot be arranged so as to protect all sensitive components, the solution can be to judiciously add some "add-on". Given the mass penalty from adding shielding, other options for protecting the component or subsystem should also be assessed from the point of view of impact on cost and system/mission performance.

The choices to be made when considering add-on shielding include:

- the elemental composition;
- the location;
- the method of attachment.

The question of material composition has been discussed earlier, and in the following sections, which consider shield location and method of attachment, the reader should bear in mind the possible use of high- or low-Z materials (or combinations of both) for the particular radiation environment.

Added shielding can be considered as either "local" or "whole box". If the array of devices to be shielded is small, we can save weight by enclosing the array in a compact shield rather than build the same thickness onto the outside of the equipment. This is the idea of "local" shielding: simply to obtain a given dose or particle flux reduction in a given volume for the minimum weight penalty. For instance, a single integrated circuit is best be protected by a blob of filled plastic applied directly to the package or by using thicker Kovar for the covers. This type of shield is called a "spot shield".

When adding shielding, it should be borne in mind that for the same thickness and mass of planar material added, the radiation dose/fluence from residual primary particles at a point behind the shield is reduced more if the shield is closer. This is as a result of the increased mean pathlength of the radiation as well as the increased solid angle subtended by the shield.

5.5.3.2. On-PCB shielding

5.5.3.2.1. Spot shielding

The simplest type of shield is one totally surrounding the device and lying close to it. Alumina-filled plastic has a good insulating power and can be given suitable mechanical strength to resist vibration. With ICs, shielding is sometimes performed in two parts: one above and one below the board. Screw-on fins have been designed for ICs, so screw-on shields can also be designed. The USAF has successfully procured CMOS devices with Kovar lids about twice the usual thickness.

A design of package incorporating radiation shielding was developed for the USAF [RDC.3] for the UK AMPTE satellite, tantalum spot-shielding was applied to the lids of certain CMOS circuits. Calculations of layered shield have shown that the dose in geosynchronous orbit can be reduced to 200 rad(Si) for 10 years.

5.5.3.2.2. Edge of board

Under the heading of "Efficient Use of Built-in Mass" comes the use of other active components on the same board. These, if arranged properly, can supply absorber mass in exactly the most critical direction - the line of view through the thin box walls. However, only the middle area of the board gets full benefit of this mode of shielding. On the other hand, if we put add-on shielding around the edge of the device area, the whole of the board gains full benefit.

5.5.3.2.3. Internal slabs

The types of shield so far described protect only one plane of a single component. If a whole plane or several planes are sensitive to radiation, then the region involved can be sandwiched between slabs of material. Such a slab is bolted onto the lower frame

element where the clearance with respect to the next board allows this. In certain cases, foam sheets can be inserted or potting compound can be poured into the module after fabrication. In extreme cases, an empty module - carrying only the add-on absorber- can be inserted.

5.5.3.3. Whole box shielding

5.5.3.3.1. Bolt-on slabs

The simplest way of adding mass to a box can appear to be by bolting a slab of plastic or metal to the outside. In fact, this is rarely convenient because:

- Suitable bolting can be unavailable on the outside of the box and
- The shield can foul other boxes or cables lying close to the sensitive box.

The latter difficulty can sometimes be dealt with by using a very dense material such as lead, tungsten or tantalum, but these can generate excessive bremsstrahlung if the low-energy electron fluxes from space impinge directly. As already mentioned, high-Z materials perform best once an initial few millimetres of lower-Z material (*e.g.* aluminium or polyethene) has removed these electrons so that bremsstrahlung generation is minimised.

5.5.3.3.2. Thickened walls

If the precise amount of shielding to be used is known at the beginning of the design, then box walls can be designed to the thickness over and above the thickness that meets the mechanical strength requirements. Many boxes are milled out of solid metal and hence this does not present mechanical difficulties. It has already been noted that, for radiation-sensitive boxes, thin areas of box wall are to be avoided. Such thin areas are sometimes produced when mechanically unnecessary material is milled away. As discussed, the thickening of a whole box is likely to be uneconomical in weight unless shielding of every component in the box is a requirement.

5.6. Shielding calculation methods and tools – Decision on using deterministic radiation calculations, detailed Monte Carlo simulations, or sector shielding analysis

Modelling of the effects of built-in or add-on shielding is strongly advisable, unless it can be shown by simple calculation that for the thinnest (worst-case) shielding condition, the radiation environment at component level is negligible, and the effects of secondary particle build-up can also be ignored.

The above sections show that the interaction processes of radiation in spacecraft materials can often be very complex and therefore non-trivial to quantify. A full treatment implies the solution of the Boltzmann transport equation (BTE). Deterministic methods apply numerical techniques to integrate the finite difference form of the Boltzmann equation. Although these are computationally efficient and accurate, deterministic methods are often limited to simulation of 1-D or 2-D geometries. Complex 3-D geometries are more often simulated using Monte Carlo solutions of the BTE, which involves simulating individual particle trajectories by the systematic sampling of probability distributions derived from cross-sections. Clause 5.7 provides a list of example radiation transport codes based on deterministic or Monte Carlo solutions to the BTE, applicable to coupled electron-gamma transport, coupled low-energy neutron-gamma transport, energetic nucleon-meson transport, or even comprehensive treatment of almost all hadronic and electromagnetic interactions of a wide variety of particles. The physics models which should be included in the simulation are identified in ECSS-E-ST-10-12C Table 6 as a function of source radiation and application.

Table 3: Description of physics models (part 1 of 4)

#	Primary Particle	Energy range	Target/geometry considerations	Application considerations	Physical processes treated
1	electrons	< a few 100s keV			Direct ionisation Multiple scattering
2	electrons	>100's keV <1.022 MeV	δ-rays important if their ranges are similar to or greater than geometry feature sizes bremsstrahlung increasingly important for high-Z materials (varies as Z^2)		Direct ionisation (including δ-ray electron production) Multiple scattering Bremsstrahlung production Transport of secondary electrons using above physics Transport of bremsstrahlung (photoelectric effect, Compton scattering)
3	electrons	>1.022 MeV	δ-rays important if their ranges are similar to or greater than geometry feature sizes Bremsstrahlung increasingly important for high-Z materials (varies as Z2)		Direct ionisation (including δ-ray electron production) Multiple scattering Bremsstrahlung Photoelectric effect Compton scattering Pair-production Annihilation
4	electrons			Important if angular distribution of photon spectrum is a requirement.	Rayleigh scattering
5	protons and other ions	up to a few 10's MeV/nuc			Direct ionisation Multiple scattering Elastic scattering

Table 3: Description of physics models (part 2 of 4)

#	Primary Particle	Energy range	Target/geometry considerations	Application considerations	Physical processes treated
6	protons and other ions	>10's MeV/nuc <200 MeV/nuc	Non-fissionable materials δ-rays important if their ranges are similar to or greater than geometry feature sizes, but typically electron transport can be ignored for TID calculations. Elastic scattering important when assessing energy deposition processes in microvolumes.		Direct ionisation (including δ-ray electron production) Multiple scattering *Elastic nuclear scattering* Nuclear spallation Nuclear pre-equilibrium Nuclear evaporation / break-up (light targets) Transport of secondary nucleons in the same manner
7	protons and other ions	>200 MeV/nuc	Non-fissionable materials δ-rays important if their ranges are similar to or greater than geometry feature sizes, but typically electron transport can be ignored for TID calculations. Elastic scattering important when assessing energy deposition processes in microvolumes. Charged pion decay and muon physics important if geometry feature sizes are many kilometres (*e.g.* atmospheric showers) but not for spacecraft.		Direct ionisation (including δ-ray electron production) Multiple scattering *Elastic nuclear scattering* Nuclear spallation Nuclear pre-equilibrium Nuclear evaporation / break-up (light targets) Transport of secondary nucleons in the same manner Secondary pion production and transport *Decay of charged pions to muons* *Muon transport (multiple scattering, ionisation, bremsstrahlung, pair-production and decay)*

Table 3: Description of physics models (part 3 of 4)

#	Primary Particle	Energy range	Target/geometry considerations	Application considerations	Physical processes treated
8	protons and other ions	>10's MeV/nuc		Applications where there is potential sensitivity to γ-ray flux (e.g. some types of radiation sensor)	As in row 6 + Photonuclear de-excitation Radioactive decay
9	protons and other ions		Fissionable materials		As rows 6, 7 and 8 (depending upon energy), but including nuclear fission physics
10	protons and		Geometry allows low-angle scattering of low-energy protons	X-ray telescopes using grazing incidence methods	Firsov scattering and accurate multiple scattering models

Table 3: Description of physics models (part 4 of 4)

#	Primary Particle	Energy range	Target/geometry considerations	Application considerations	Physical processes treated
11	high-energy neutrons	>10's MeV/nuc <200 MeV/nuc	Non-fissionable materials Elastic scattering important when assessing energy deposition processes in microvolumes.		Elastic nuclear scattering Nuclear spallation Nuclear pre-equilibrium Nuclear evaporation / break-up (light targets) Transport of secondary nucleons in the same manner
12	high-energy neutrons	>200 MeV/nuc	Non-fissionable materials Elastic scattering important when assessing energy deposition processes in microvolumes. Charged pion decay and muon physics important if geometry feature sizes are many kilometres (e.g. atmospheric showers) but not for spacecraft.		Elastic nuclear scattering Nuclear spallation Nuclear pre-equilibrium Nuclear evaporation / break-up (light targets) Transport of secondary nucleons in the same manner Secondary pion production and transport Decay of charged pions to muons Muon transport (multiple scattering, ionisation, bremsstrahlung, pair-production and decay)
13	low-energy neutrons	thermal to ~20 MeV	Radioactive decay important for applications where there is potential sensitivity to γ-ray flux (e.g. some types of radiation sensor)	Not important for TID calculations if charged ions are the primary particle. Important for SEEs	Elastic and inelastic scattering based on evaluated data for neutron-nuclear interactions. Generation of γ-rays Radioactive decay

Execution speed is the main limitation of Monte Carlo solutions to the Boltzmann equation, and radiation shielding engineering tools based on Monte Carlo techniques have yet to be fully developed and accepted by the spacecraft community. Although the availability of low-cost, powerful computers is making the use of such codes increasingly popular (more so for specialised applications), shielding codes such as SHIELDOSE and SHIELDOSE-2 [RDC.4] are more generally used for ionising radiation dose predictions. These tools employ pre-calculated data from Monte Carlo simulations to determine the dose behind 1-D aluminium shields of varying thickness (finite-slab, semi-infinite slab and spherical shields – see ECSS-E-ST-10-12C Table 6-2) for a user-provided electron or proton spectrum. A key limitation of SHIELDOSE and SHIELDOSE-2 is that they can determine the dose-versus-depth curve only for aluminium shields. A common approximation is to convert the actual material shielding to the equivalent in g/cm^2 of aluminium (*i.e.* based on the ratio of the actual mass density of the material to that of aluminium). Alternatively, tools such as MULASSIS [RDC.5] can be employed, which uses Geant4 to determine the ionising and non-ionising dose-depth curves, or particle fluence-versus-depth for 1-D shielding characteristics for any shield material.

In order to calculate the total ionising dose (TID) for a location within a more complex geometry, a sector shielding analysis (also known as sectoring analysis) can be performed using a separate tool [RDC.6][RDC.7]. In this technique, ray-tracing is performed for a large number (N) of rays emanating from a point in a computer geometry representing the complete spacecraft or subsystem. The intersections with the boundaries in the spacecraft structure are found and the total shield thickness along the ray computed (t_i). The elemental solid angles around each ray, Ω_i, are used to weight the interpolated dose values from the 4π dose-depth curve at the value of t_i. The dose is then determined from the sum for all rays and solid angles:

$$\text{Dose} = \sum_{i=1}^{N} \frac{\Omega_i}{4\pi} D(t_i) \qquad \textbf{(3)}$$

were $D(t)$ represents the dose-depth function. The above equation assumes that:

$$\sum_{i=1}^{N} \Omega_i = 4\pi \qquad \textbf{(4)}$$

i.e. there is no over-sampling of the solid angle elements.[2] Usually these elements are defined according to a mesh in spherical polar coordinates (θ,ϕ), or a mesh in rectangular coordinates on the faces of a cube that surrounds the point at which the dose is to be measured.

In the above description of sectoring analysis, the ray is assumed to always travel in a straight path from the originating point - this is the so-called SLANT technique shown in

Figure 7, where the path-length thickness (used to determine the dose) can be oblique with respect to any surface. This is more applicable to radiation that propagates in near straight-line paths such as protons, other ions and gamma rays. For electrons, which are affected more by multiple scattering, dose estimates can be based on the NORM technique, where the shielding thickness is calculated from the normal distance across the material encountered by the ray (Figure 7).

[2] Quite often it is advantageous to over-sample, *i.e.* sample more than one ray from each solid angle element, Ω_i. Obviously, this introduces an additional normalisation factor into equations **(3)** and **(4)**.

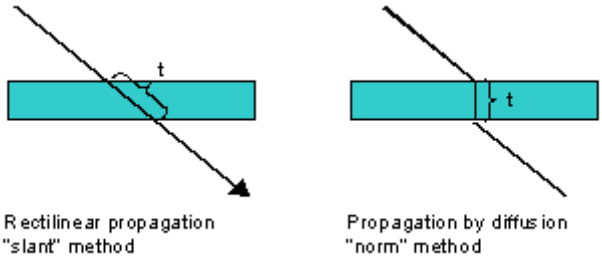

Figure 7: NORM and SLANT techniques for sector based analysis.

Note that for complex shielding structures, ray propagation using the NORM technique can, in some circumstances, lead to longer pathlengths being taken through the geometry (see Figure 8).

One should be careful to select dose-depth information for an appropriate geometry (whether solid sphere, spherical shell, finite planar shield – see ECSS-E-ST-10-12C Table 6-2) for use in combination with the NORM or SLANT methods. Above all, however, a description of the calculation techniques (whether NORM or SLANT method was used, the number rays sampled), together with dose-depth geometry type, should be provided with any results.

Although the above description of sectoring analysis is in the context of TID calculations, the same approach is applicable to calculating particle fluence at a location within the spacecraft, or indeed non-ionising energy loss. Furthermore, the sector shielding analysis process can also give graphical information on the directions in which a location is poorly shielded, and indeed a full distribution of shielding thickness.

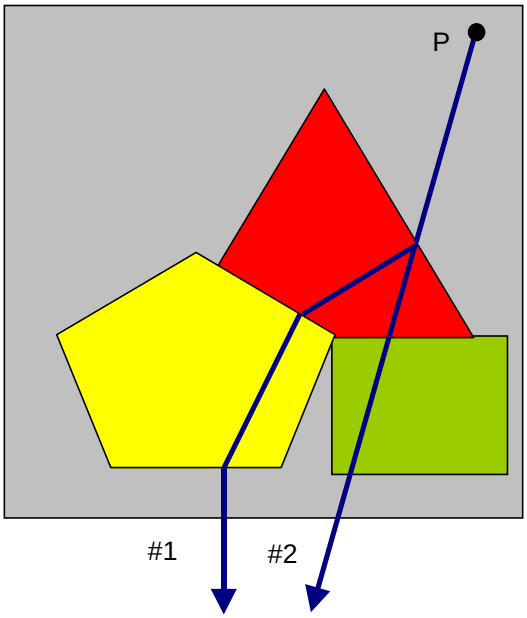

Figure 8: Example showing the NORM technique (ray #1) leading to a longer pathlength than the SLANT technique (ray #2)

Table 4: Example radiation transport simulation programs which are applicable to shielding and effects analysis.

Code name	Type	Application	Originator
CEPXS/ONELD	1-D deterministic	e-γ	Sandia and Los Alamos National Laboratories [RDC.8]
BRYNTRN	1-D deterministic	baryon nuclear/EM	NASA Langley Research Center [RDC.9]
ITS	1-D, 2-D or 3-D Monte Carlo	e-γ >1 keV	Sandia National Laboratory [RDC.10]
EGS	3-D Monte Carlo	e-γ	SLAC [RDC.11]
LHI/HETC	3-D Monte Carlo	nucleon-pion-muon (light ions for LHI) nuclear/EM >15 MeV/nuc	Oak Ridge National Laboratory / SAIC [RDC.12]
MORSE	3-D (biassed) Monte Carlo	n-γ, thermal to ~15 MeV	Oak Ridge National Laboratory [RDC.13]
MCNP	3-D Monte Carlo	n-e-γ, thermal to ~20 MeV	Los Alamos National Laboratory [RDC.14]
MICAP	3-D Monte Carlo	n-γ, thermal to ~20 MeV	Oak Ridge National Laboratory [RDC.15]
Geant4	3-D Monte Carlo toolkit	leptons, nucleons, mesons, photons nuclear/EM	Geant4 Collaboration [RDC.16][RDC.7]
MULASSIS	1-D Monte Carlo (derived from the Geant4 toolkit)	leptons, nucleons, mesons, photons nuclear/EM	QinetiQ / ESA [RDC.5][RDC.17]
SSAT	3-D Sectoring tool (derived from the Geant4 toolkit)	None – ray-tracing only	QinetiQ / ESA / Rhea [RDC.17]
GRAS	3-D Monte Carlo (derived from the Geant4 toolkit)	leptons, nucleons, mesons, photons nuclear/EM	Rhea / ESA [RDC.18]
MCNPX	3-D Monte Carlo	leptons, nucleons, mesons, photons nuclear/EM	Los Alamos National Laboratory [RDC.19]
FLUKA	3-D Monte Carlo	leptons, nucleons, mesons, photons nuclear/EM	INFN/CERN [RDC.20]
Integrated Radiation Transport Suite – IRTS	3-D Monte Carlo	leptons, nucleons, mesons, photons nuclear/EM	QinetiQ [RDC.21]
GEANT3/GCALOR	3-D Monte Carlo	leptons, nucleons, mesons, photons nuclear/EM	CERN/ORNL [RDC.22]
HERMES	3-D Monte Carlo	leptons, nucleons, mesons, photons nuclear/EM	Institut für Kernphysik Forschungszentrum Jülich GmbH [RDC.23]
NOVICE	3-D Monte Carlo		Experimental and Mathematical Physics Consultants, Gaithersburg, USA [RDC.24]

An important point to bear in mind when performing sector analysis is that it is not always appropriate to consider that the external environment is isotropic (uniform in all directions). This is a particular problem at low altitudes where there are very strong east-west and pitch-angle anisotropies. Gravity-gradient stabilisation on LDEF, for example, and a similar attitude control on the Space Station mean that different parts of these spacecraft are exposed to very different environments. Therefore it is important to emphasise that it makes almost no sense to perform a sectoring shielding analysis unless the anisotropy is accounted for at the same time.

Although computationally efficient, sector shielding analysis is an approximation as it ignores angular scattering of particles (which is particularly important for electrons), and the true angular distribution of secondary radiation is not explicitly treated. In addition, the technique involves treating all spacecraft materials as being the equivalent of one material type and therefore is not suitable for quantifying graded shielding or dose-enhancement effects. More complex models such as detailed Monte Carlo simulation tools described above are more appropriate, although the cost and time taken to perform such simulations should be assessed first.

5.7. Example detailed radiation transport and shielding codes

If undertaken, the physics simulation should be at a sufficient level of detail in order to ensure accurate treatment of the production of secondary particles which can affect the component, system or human, as well as the attenuation and scattering of the primary radiation (see Table 3).

Table 4 lists of some of the radiation transport simulation programs which can be used for the analysis of space radiation effects. These all provide a solution to the Boltzmann transport equation (whereas SHIELDOSE and SHIELDOSE-2 use tabulations derived from such simulation codes). Some of the codes treat only selected particle species (such as electron/positron/γ-ray simulations, or coupled neutron/γ-ray simulations). More recently, coupled suites of radiation codes have been used to follow all interaction-products, *e.g.* from high-energy nuclear interactions to the Compton scattering of nuclear de-excitation γ-rays. Examples of these include MCNPX and Geant3. Geant4 is a further example, although rather than being a combination of programs, it has been written from the outset as a toolkit to simulate comprehensively a wide range of interaction processes over an energy range of PeV to 100's eV (and even thermal energies for neutrons).

5.8. Uncertainties

Typically, 3-D Monte Carlo calculations of dose and flux/fluence estimates for electron environments has systematic uncertainties no better than 20 %, decreasing to 5-10 % for more precise calculations (high-fidelity geometries, comparisons of more than one Monte Carlo code to tune run parameters such as particle energy-cuts). For proton environments, dose estimates can be accurate to about 20 %, but errors in secondary particle fluxes from nuclear interactions, as well as quantities directly associated with these interactions (spallation rates and induced radioactivity) can be of a factor of two.

Mangeret has compared predictions of TID calculated using sector-shielding analysis and 3-D Monte Carlo for geostationary-orbit and geostationary-transfer (*i.e.* electron-dominated) environments [RDC.25]. The results indicate that if either shell sphere dose-depth information is combined with the NORM ray tracing techniques, or the solid sphere case is combined with the SLANT technique, the results for TID tend to agree within ±30 % with Monte-Carlo calculation. Using the shell sphere case with the SLANT technique gave rise to large underestimates of the doses in the cases studied and so this combination should be avoided. It is important to note that the results from detailed Monte Carlo calculations themselves also contain systematic errors already discussed.

Geometries considered within sector-shielding or detailed radiation transport calculations are often pessimistic, omitting large fractions of the overall spacecraft mass which represent numerous small items. This introduces hidden margin into the shielding predictions.

Uncertainties from using simple shielding calculations based on aluminium, and ignoring potential dose enhancements from local high-Z materials in electron environments can be more than a factor 20. Account should be taken of local material (e.g. packaging) (in)consistency between test, application and simulation conditions.

5.9. References

[RDC.1] NIST stopping power and range tables for electrons, protons, and helium ions: http://physics.nist.gov/PhysRefData/Star/Text/contents.html.

[RDC.2] H A Bethe and J Ashkin, "Passage of radiation through matter," in *Experimental Nuclear Physics*, **Vol 1**, Editor E Segrè, Published by Wiley, New York, 1959.

[RDC.3] A P Shmidt *et al*, "Microcircuit packages incorporating radiation shields for use in spacecraft electronics," Proc Int Soc for Testing and Failure Analysis (ISTFA), October 1985

[RDC.4] S M Seltzer, "Updated calculations for routine space-shielding radiation dose estimates: SHIELDOSE-2," NISTIR 5477, Dec 1994.

[RDC.5] F Lei, P R Truscott, C S Dyer, B Quaghebeur, D Heynderickx, P Nieminen, H Evans, E Daly, "MULASSIS: A Geant4 based multi-layered shielding simulation tool," *IEEE Trans Nucl Sci*, **49**, No 6, pp2788-2793, Dec 2002.

[RDC.6] ESABASE Reference Manual, ESABASE/GEN-UM-061, Issue 2, March 1994.

[RDC.7] Pete Truscott, Fan Lei, Clive Dyer, Colin Ferguson, Rudolfo Gurriaran, Petterii Nieminen, Eamonn Daly, John Apostolakis, Simone Giani, Maria Grazia Pia, Laszlo Urban, Michel Maire, "Geant4 – a new Monte Carlo toolkit for simulating radiation shielding and effects," IEEE NSREC 2000 Workshop Record, IEEE 00TH8527, 147-152, 2000.

[RDC.8] L J Lorence, Jr, W E Nelson, J E Morel, "Results guide to CEPXS/ONELD: A one-dimensional coupled electron-photon discrete ordinates code package, version 1.0," Sandia National Laboratories, 1990.

[RDC.9] J W Wilson, L W Townsend, J E Nealy, Y Sang Chun, B S Hong, W W Buck, S L Lamkin, B D Ganapol, K Khan, F A Cicinotta, "BRYNTRN: A Baryon Transport Model," NASA TP-2887, 1989.

[RDC.10] J A Halblieb, R P Kensek, T A Mehlhorn, G D Valdez, S M Seltzer, M J Berger, "ITS Version 3.0: The Integrated Tiger Series of coupled electron/photon Monte Carlo transport codes," SAND91-1634, Sandia National Laboratories, 1992.

[RDC.11] W R Nelson, H Hirayama, D W D Rogers, "The EGS4 code system," Stanford Linear Accelerator Report, SLAC-265, 1985.

[RDC.12] T W Armstrong, B L Colborn, Nucl Inst Meth., 169, pp161-172, 1980.

[RDC.13] M B Emmett, "The MORSE Monte Carlo radiation transport code system," Oak Ridge National Laboratory report ORNL-4972, 1975.

[RDC.14] J F Briesmeister, Ed., "MCNP - A General Monte Carlo N-Particle Transport Code, Version 4C," LA-13709-M, 2000.

[RDC.15] J O Johnson and T A Gabriel, "A User's Guide to MICAP: A Monte Carlo Ionization Chamber Analysis Package," ORNL/TM-10340, 1988.

[RDC.16] S Agostinelli *et al*, "Geant4 – a simulation toolkit," *Nucl Instrum Meth Phys Res*, **A506**, p250-303, 2003.

[RDC.17] http://reat.space.qinetiq.com, 2007.

[RDC.18] G Santin, V Ivanchenko, H Evans, P Nieminen, and E Daly, "GRAS: a general-purpose 3-D Modular Simulation tool for space environment effects analysis," *IEEE Trans Nucl Sci*, **52**, no 6, pp2294–2299, 2005.

[RDC.19] L S Waters, ed., "MCNPX User's Manual, Version 2.4.0," LA-CP-02-408, 2002.

[RDC.20] A Fasso, A Ferrari, J Ranft, P R Sala, "FLUKA: Status and Prospective for Hadronic Applications," Proceedings of the Monte

Carlo 2000 Conference, Lisbon, October 23-26, pp955-960, 2000, A Kling, F Barao, M Nakagawa, L Tavora, P Vaz, Eds, Springer-Verlag Berlin.

[RDC.21] N Hammond, C Comber, C S Dyer, P R Truscott, and A J Sims, "Calculation of radiation effects on gamma-ray scintillation detectors," Proceedings of RADECS 91, IEEE 91TH0400-2, pp553-557, 1991.

[RDC.22] R Brun, F Druyant, M Marie, A C McPherson, and P Zanarinin, "GEANT3," CERN DD/EE/84-1, Revised 1987 and subsequently.

[RDC.23] P Cloth *et al*, "A Monte Carlo Program System for Beam-Materials Interaction Studies," JUL-2203, NEA-1265/02, 1988.

[RDC.24] T M Jordan, "An adjoint charged particle transport method," *IEEE Trans Nucl Sci*, **23**, p1857, 1976.

[RDC.25] Renaud Mangeret, "Environment (mission) analysis and specification," presented at the RADECS 2003 Short Course "Radiation engineering methods for space applications," 15th September 2003, Noordwijk, The Netherlands.

6 Total ionising dose

6.1. Introduction

Total ionising dose (TID) degradation in microelectronics results from the build up of charge in insulating layers, and has a cumulative effect on electronics, resulting in a gradual loss of performance and eventual failure. TID also affects optical components such as cover glasses and fibre optics, and passive materials such as plastics.

6.2. Definition

TID is defined as the amount of energy deposited by ionisation or excitation in a material per unit mass of material.

$$D = \frac{dE}{dm} \quad \textbf{(5)}$$

The International System unit is the gray: 1 Gy = 1 J/kg, although the rad (radiation absorbed dose) is still frequently used; 1 rad = 1 cGy.

Since the dose is dependent on the target material, the dose is expressed in rad(material) or Gy(material). The dose is generally provided in rad(Si).

6.3. Technologies sensitive to total ionising dose

In semiconductor devices, ionisation produces electron-hole pairs within the semiconductor and insulators (such as oxides). Some of this charge is trapped in insulators or leads to the formation of interface states at the semiconductor/insulator surface. In MOS structures, the trapped charge causes a shift in the gate threshold voltage. Since the trapped charge resulting from ionisation is positive, n-type MOSFETs experience a reduction in threshold voltage and not always is completely switch off when no external bias is applied. Conversely, p-type MOSFETs experience a increase in threshold voltage and become harder to drive.

Mobility (which affects switching speed and drive current) is also degraded. In addition to the gate oxide, ionisation also affects the field oxide, which is used for isolation in MOS integrated circuits.

This results in extremely large leakage currents if the threshold shifts are large enough to cause inversion. Field oxide failure is an important failure mode for many commercial CMOS devices.

In bipolar devices, trapped charges at oxide layers cause two effects. The traps increase surface recombination, decreasing the gain of bipolar transistors. If the trap density is high enough, an inversion layer can be created in p-doped regions that increases the surface area of the junction. This also affects transistor gain, and can cause substantial increases in leakage current.

Bipolar technologies also suffer from an effect referred to as ELDRS (enhanced low-dose-rate susceptibility) where device electrical parameters can degrade more (per unit radiation dose) in a low dose-rate environment such as the natural space environment. Since laboratory radiation tests are often performed at high dose rates, there is a danger that using such laboratory data can result in underestimating the degradation observed in flight. Conversely, MOS semiconductors benefit from annealing during and after irradiation, and therefore per unit TID, suffer less damage when irradiated at lower dose rates. It is therefore important that component test data are selected carefully.

In optical materials, long-term ionisation effects appear primarily as an increase in optical absorption. These usually are manifestations of charge trapping at a pre-existing defect, so the absorption rate is a strong function of the initial material properties. For example, fused quartz generally colours less than alkali glasses from a given ionising dose.

In quartz crystal used for precision oscillators or filters, long-term ionisation effects can produce significant resonant frequency shifts. Again, there is a strong dependence upon the type of material used. Natural quartz shows the largest frequency shift for a given ionising dose; synthetic quartz shows less, and swept synthetic quartz even less. In these cases, selection of the quartz crystal growth method can minimise the potential effect.

The devices and materials of concern and the most serious radiation induced effects are:

- ***MOS devices*** – threshold voltage shift, decrease in drive current and switching speed, increase in leakage current.
- ***Bipolar transistors*** – hFE degradation, especially at low collector current; leakage current.
- ***Junction field effects transistors*** (JFETs) – enhanced source-drain leakage current.
- ***Analogue microcircuits*** – offset voltage, offset current and bias-current changes, gain degradation.
- ***Digital microcircuits*** – enhanced transistor leakage, or logic failure due to decrease in gain (bipolar devices) or changes in threshold voltage and switching speed (CMOS).
- ***CCDs*** – increased dark currents, some effects on CTE, effects on MOS transistor circuits (as described above).
- ***APS*** – changes to MOS-based circuitry or integer (as described above), including changes in pixel amplifier gain.
- ***Micro-electromechanical devices***, MEMS – Gradual change in response due to build-up of charge in any dielectric located near to the micro-electromechanical parts, resulting in deflection of the moving part. Also, amplifiers and digital microelectronics also on the chip can be susceptible to TID as discussed above.
- ***Quartz resonant crystals*** – frequency shifts.
- ***Optical materials*** – increased absorption, variations in absorption spectrum (coloration).
- ***External polymeric surfaces*** – mechanical degradation, changes in dielectric properties.

The components most sensitive to TID are active electronic devices such as transistors and integrated circuits (ICs). Their sensitivity thresholds typically range from 10 Gy(Si) (*i.e.* 1 krad(Si)) to 10 kGy(Si) (1 Mrad(Si)) depending on the technologies used.

6.4. Total ionising dose calculation

Provided that the particle intensity and spectrum does not change significantly travelling through the material, TID can be determined from the charged particle fluence at the surface of the material, and the electronic stopping power of the particle based on the approximate formula:

$$D = \frac{1}{\rho}\int_{E_1}^{E_2} \psi(E)\frac{dE}{dx}(E)dE \qquad \textbf{(6)}$$

where ρ is the mass density of the material, $\psi(E)$ is the differential energy spectrum defined between E_1 and E_2, and dE/dx is the stopping power in units of energy loss per unit particle pathlength. The reader is referred to 5 on radiation shielding for example stopping powers for electrons, protons and heavier ions in common materials.

The use of high atomic-number (Z) materials close to the location of a TID sensitive component can lead to dose enhancement effects (see 5) and therefore it is important to take care when accounting for such effects in shielding calculations when estimating the TID where there are significant changes in material Z.

6.5. Uncertainties

Uncertainties in TID predictions tend to be dominated by (and incorporated into) the shielding calculation, including issues of dose enhancements from local packaging materials (see Clause 5.8).

7
Displacement damage

7.1. Introduction

Displacement damage (DD) is a cumulative radiation damage effect which results from damage to the crystalline structure of semiconductors and some optical materials by energetic particle collisions. DD is predominantly an issue for semiconductors which rely on minority carrier current flow, such as opto-electronics, bipolar devices, solar cells, *etc*.

7.2. Definition

Particles traversing crystalline materials can deposit sufficient energy in a collision with an atom to displace the atom from its lattice position creating an instertitial. The empty position left by the atom is referred to as a vacancy. Interstitials and vacancies are mobile and can cluster together or react with impurities in the lattice structure creating stable defect centres. Radiation induced defect centres are the cause of numerous component parameter degradation effects.

Displacement damage is also referred to as *non-ionising dose dam*age as it arises from particles losing energy, not by way of ionisation, but by elastic/inelastic collisions with nuclei in the target material.

Displacement damage is normally expressed as either:

- Displacement damage equivalent particle fluence (DDEF) for mono-energetic spectra, *e.g.* damage induced as a function of fluence from 10 MeV protons, 1 MeV neutrons or 1 MeV electrons, identified by DDEF(particle, energy, material);
- The non-ionising energy loss (NIEL) dose[3] or (total) non-ionising dose ((T)NID), *i.e.* the energy deposition in a material per unit mass by radiation through displacements, rather than excitation/ionisation.

7.3. Physical processes and modelling

An incident high-energy particle is able to displace an atom in matter, if the energy imparted to the atom is greater than a threshold energy. The displaced atom is referred to as a *primary knock on atom*. Once sufficient energy is transferred, the displaced primary knock on atom moves through the lattice and comes to rest in a normally unoccupied position. The position left by the atom is called a vacancy and the displaced atom is the interstitial. Protons, electrons, neutrons and heavy ions are particles capable of producing displacement.

[3] Whilst NIEL dose refers to energy deposition due to DD per unit mass of material, NIEL, NIEL rate or NIEL coefficient is the energy loss by a particle per unit pathlength due to DD (in the same way that "stopping power" refers to energy loss by a particle per unit pathlength due to ionisation and excitation.)

The primary mechanism for electrons displacing an atom in matter is by Coulomb elastic scattering. This is also true for low-energy protons, but at higher energies (above ~10 MeV) the mechanism involves nuclear elastic scattering and nuclear inelastic reaction. Low-energy neutrons displace atoms primarily by elastic nuclear scattering (but at energies above ~20 MeV inelastic collisions start to dominate). The lower mass of electrons makes them less efficient at imparting momentum to atoms, and therefore, per unit fluence, they generally produce fewer displacements than protons or neutrons, γ-ray photons induce displacements as a result of secondary electrons, but the NIEL (non-ionising energy loss) of these electrons is low and the displacement damage produced at typical γ doses is very small. Therefore, the results of γ-ray irradiation are valuable for determining TID susceptibility but reveal no useful information on the susceptibility of a device to displacement damage effects.

There are uncertainties involved in estimating the number of displacements induced by a particle traversing matter. One can calculate this employing TNID, which is the averaged non-ionising energy loss per unit mass of material that goes into displacement. Some approximate models have been developed such as that due to Kinchin and Pease [RDE.1] which gives the number of displacements $G_d(Q)$ (Equation **(7)**) as a function of the energy imparted to the primary recoil atom (Figure 9).

$$\begin{aligned} G_d(Q) &= 0 && \text{for } 0 < Q < T_d \\ G_d(Q) &= 1 && \text{for } T_d < Q < 2T_d \\ G_d(Q) &= \frac{Q}{2T_d} && \text{for } 2T_d < Q < T_i \\ G_d(Q) &= \frac{T_i}{2T_d} && \text{for } Q > T_i \end{aligned} \qquad \textbf{(7)}$$

where:

Q = energy imparted to the primary recoil atom;

T_d = threshold energy to create a defect;

T_i = ionisation threshold energy.

We notice from this model that the number of displacements for a given unit length N_d is related to the NIEL by equation **(8)**:

$$NIEL = \left.\frac{dE}{dx}\right)_{displacement} = 2 \cdot T_d \cdot N_d \qquad \textbf{(8)}$$

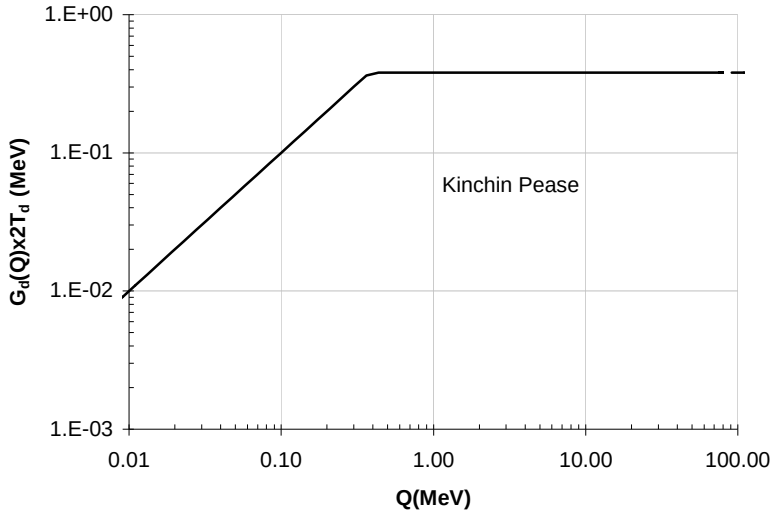

Figure 9: Variation of the number of displacements with imparted energy from Kinchin and Pease.

Seitz [RDE.2] estimated that the threshold energy is equal to about four times the sublimation energy (25 eV for silicon). Actual values range from a few electron-volts to tens of electron-volts. The measured experimental threshold energy values have large uncertainties that in turn result in uncertain NIEL values.

NIEL is given by equation **(9)**:

$$NIEL = \left.\frac{dE}{dx}\right)_{displacement} = 2 \cdot T_d \cdot \eta \cdot \int_{T_d}^{Q_{\max}} \frac{d\sigma}{dQ}(Q) \cdot G_d(Q) \cdot dQ \qquad \textbf{(9)}$$

where:

T_d	= threshold energy;
η	= atomic density (atoms/cm^3);
$G_d(Q)$	= Kinchin Pease formula;
$d\sigma/dQ$	= differential cross section phenomenon that induces a defect.

In the case of electrons, the Coulomb scattering equation states that:

$$\frac{d\sigma}{dQ}(Q) = \left.\frac{d\sigma}{dQ}\right)_{Coulombic} \qquad \textbf{(10)}$$

In the case of protons the elastic nuclear scattering and the inelastic scattering to be added to the Coulomb scattering is:

$$\frac{d\sigma}{dQ}(Q) = \left.\frac{d\sigma}{dQ}\right)_{Coulombic} + \left.\frac{d\sigma}{dQ}\right)_{elastic\ \ nuclear} + \left.\frac{d\sigma}{dQ}\right)_{nuclear\ \ reaction} \qquad \textbf{(11)}$$

For electrons the differential Coulomb scattering can be approximated by the Rutherford formula. For protons the Rutherford formula is valid for energies lower than ~10 MeV. Above ~10 MeV the contribution from nuclear elastic scattering becomes significant. The contribution from nuclear elastic scattering cannot simply be added to the Coulomb interaction contribution because of quantum mechanical interference. For this reason it is recommended to solve the Klein Gordon equation obtaining the quantum oscillation at high scattering angle, or to use experimental data. For energies greater than 100 MeV, it is important to take into account the nuclear reaction phenomenon. The intra-nuclear cascade model followed by the evaporation stage can model this.

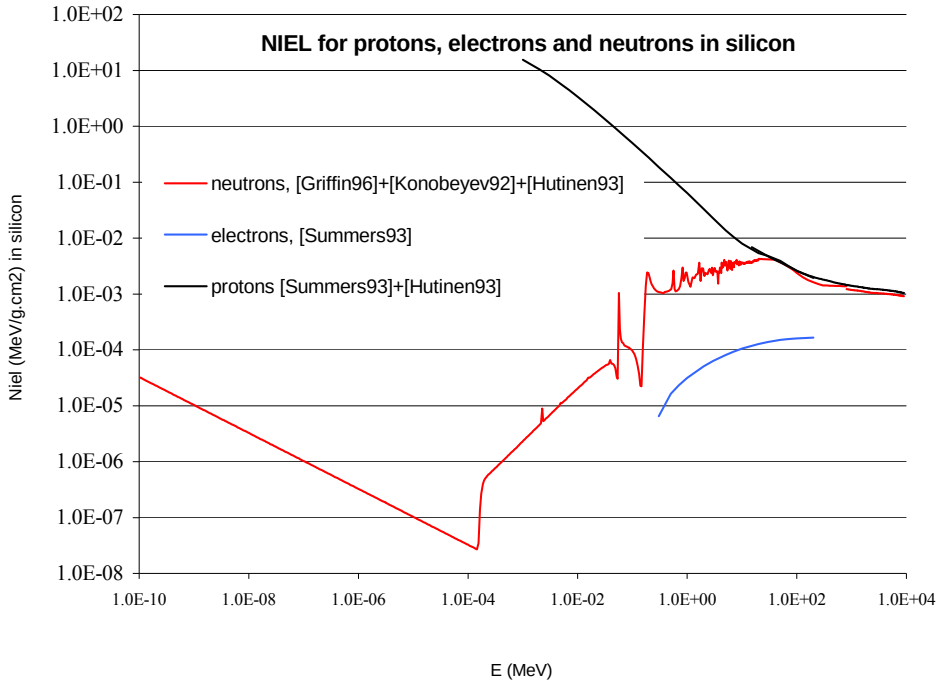

Figure 10: NIEL rates for protons, electrons and neutrons in silicon.

Figure 10 illustrates that for protons, due to a decrease of differential elastic scattering cross section versus the recoil energy, the NIEL rate (or NIEL coefficient) curve decreases. On the other hand for electrons the curve increases because, at low energy, even if the elastic scattering cross section increases rapidly, electrons have great difficulties generating defects due to their very small mass when compared to the target atom's mass.

At low energy, protons induce many more displacements than neutrons because in the case of protons the Coulomb elastic scattering cross section increases rapidly with the decrease of the energy but for neutrons the elastic nuclear scattering cross section remains relatively uniform.

At high energy, the effect of protons and neutrons is similar because in the case of protons the Coulomb barrier potential becomes less significant. Protons hit the atoms of the target like neutrons and the numbers of defects generated by each kind of particle are very close.

Caution should be applied when predicting component degradation based on the NIEL concept, especially for gallium arsenide devices. Figure 11 (see [RDE.3]) shows the calculated NIEL in GaAs as a function of proton energy, and the degradation observed in GaAs LEDs, solar cells and multiquantum-well laser diodes [RDE.7]. Whilst the trend in the degradation of the components is consistent with the NIEL dose in the low-energy regime, a range of results are observed at high proton energies depending upon

the device type. Some approach the predictions based on all non-ionising interactions which deposit energy (labelled "NIEL (Total)" in the graph), whereas components like the LED minority-carrier lifetime appear to follow the elastic component of NIEL. The difference in degradation can be due to the different dependence of the components on bulk material properties (such as minority-carrier lifetimes), which correlate with the elastic component of NIEL, and those more strongly affected by changes in the depletion region (recombination and generation), which correlate better with total NIEL [RDE.3].

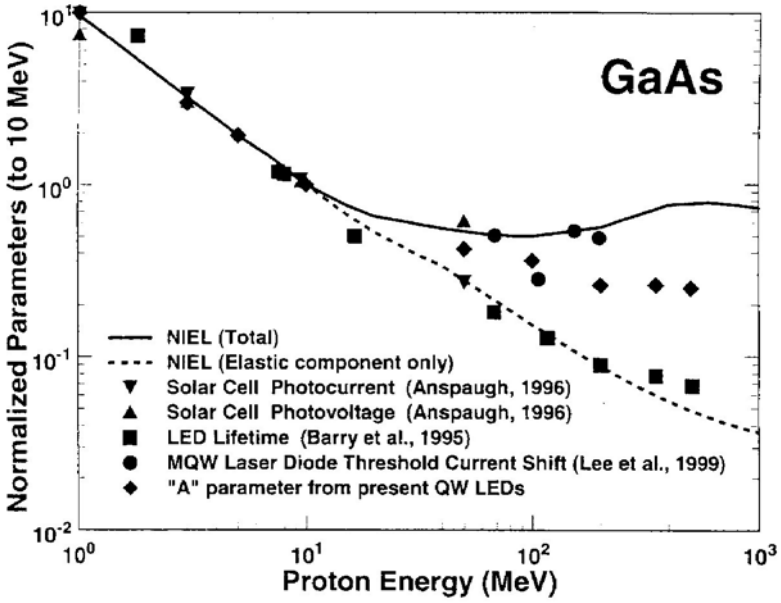

NOTE: All data normalised to the value at 10 MeV.

Figure 11: Comparison of proton damage coefficients measured in different optoelectronic devices with the calculated NIEL

Software is available for calculating NIEL. For protons, one can use PSTAR or SRIM, but these codes are only valid below 10 MeV because they only take into account the Coulomb elastic scattering.

7.4. Technologies susceptible to displacement damage

7.4.1. Overview

As already mentioned in previous sections, irradiation can produce lattice defects in crystalline materials degrading the electrical or optical performance of the material. Defects in semiconductors can be electronically active as illustrated in Figure 12. The electrically active defects in the band gap as illustrated in Figure 12, define five processes that can affect the electrical parameters of components. Generation occurs when valence band electrons with sufficient thermal energy jump to a defect in the band gap and are subsequently emitted to the conduction band creating an electron hole pair. Generation occurs via alternate emission of electrons and holes (to the conduction and valence bands, respectively) creating electron-hole pairs. The recombination process affects the minority carrier lifetime as a carrier is captured by a trap and is recombined at the trap with a carrier of the opposite sign. Trapping of carriers occurs when carriers are trapped in defects and re-emitted after a certain time period resulting in carrier removal and reducing mobility. This process affects parameters such as CCD *charge*

transfer efficiency. Compensation occurs due to radiation induced deep level defects as carriers of the opposite sign introduced by the defects remove majority carriers. Majority carrier reduction affects parameters such as resistivity.

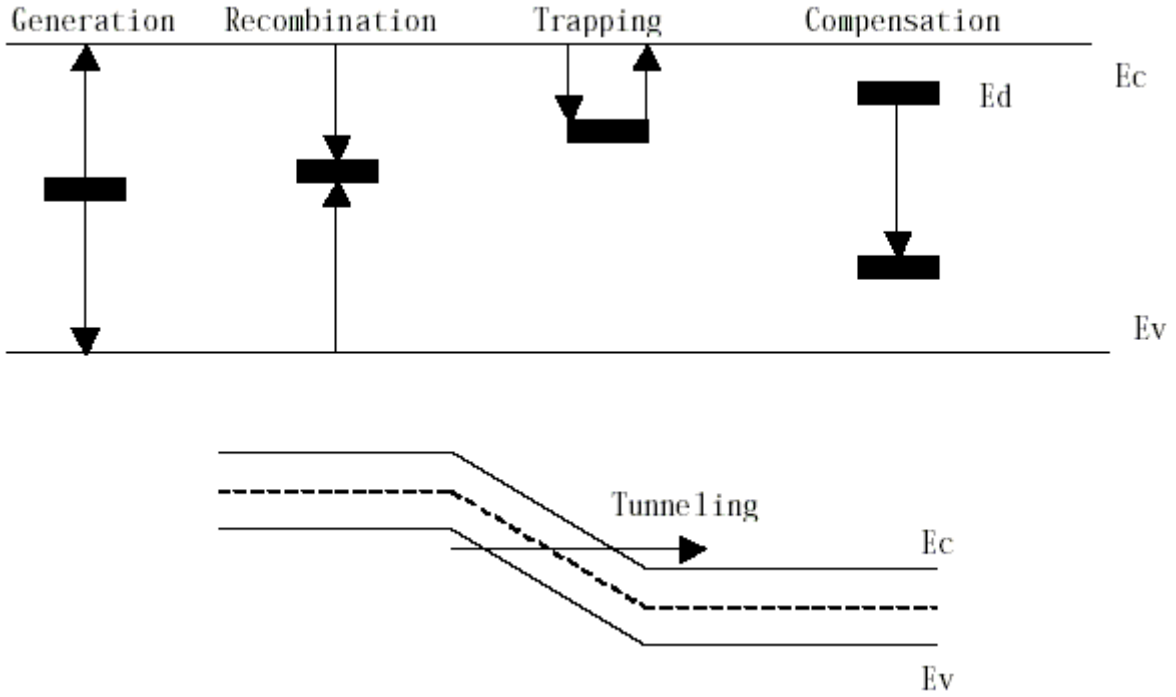

Figure 12: Five electric effects due to defects in the semiconductor band gap [RDE.4]

7.4.2 identifies technologies susceptible to displacement damage and describes key parameters affected. The following list of technologies and devices is not complete and is only meant as a brief guideline.

7.4.2. Bipolar

The effect of displacement damage in bipolar devices is to increase recombination of minority carriers and hence reduce their lifetime. The effect of reduced minority-carrier lifetime is a reduction of device gain (β). It is worth mentioning that both ionising effects and displacement damage contribute to gain degradation of bipolar devices.

In general PNP devices are more sensitive to displacement damage than NPN devices. Also employing low power devices with high collector current is recommended.

The degradation effects seen in discrete bipolar devices are also valid for bipolar integrated circuits (*i.e.* comparator, op-amp, voltage regulator).

7.4.3. Charge-coupled devices (CCD)

The active volume of a CCD, where charge is collected and transferred between adjacent device pixels is located in the bulk Si below the gate oxide layer. Radiation-induced defect centres in the active volume can affect the performance of a CCD by trapping charge as it is transferred or by introducing excess charge.

The following parameters are affected:

- **Charge transfer efficiency (CTE)**: CTE is degraded as radiation-induced defects trap charge in the active volume of the CCD. The trapped charge is eventually released with a time constant depending on the energy state of the

trap. CTE degradation is seen as a streaking effect in the direction for which charge is shifted.

- **Increased dark current**: Radiation-induced defects generate charge in the bulk Si. This excess charge is seen as an increased average dark current at the output of the CCD.
- **Increased hot spots**: Defect induced charge generation in some pixels can be significant and much higher than the average dark current. These pixels can be stable and in applications often masked (flagged by software as 'bad' pixels). Very bright hot spots can be generated by field enhanced emission mechanisms.
- **Increased bright columns**: In some cases defect induced dark current can saturate a pixel with a time constant comparable to or faster than the device readout times. In such cases, as charge is shifted in a column, all information (charge) in pixels above the damaged pixel is lost rendering part of the (or the entire) column unusable.
- **Random telegraph signals (RTS):** In contrast to stable hot spots, some pixels exhibit two- or multi-level dark current values varying with time. Switching time between different dark current levels can vary from seconds at room temperature to hours as the temperature is reduced. Due to their random behaviour it is often difficult to characterise pixels exhibiting RTS effects.

7.4.4. Active pixel sensors (APS)

Active Pixel Sensors are manufactured employing CMOS technology. The light collecting and signal readout mechanism differs from that of the CCD, in particular APS pixels are read out directly rather than involving charge transfer through a line of pixels. Hence, degradation effects such as CTE are not observed in APS devices. However, other parameter degradation effects are similar to ones observed for CCDs.

The following parameters are affected:

- **Increased dark current**: Radiation-induced defects generate charge in the bulk material. This excess charge is seen as an increased average dark current at the output of the APS.
- **Increased hot spots**: Defect induced charge generation in some pixels can be significant and much higher than the average dark current. These pixels can be stable and in applications often masked (flagged by software as 'bad' pixels). Very bright hot spots can be generated by field enhanced emission mechanisms.
- **Random telegraph signals (RTS):** In contrast to stable *hot spots*, some pixels exhibit two- or multi-level dark current levels varying with time. Switching time between different dark current levels can vary from seconds at room temperature to hours as the temperature is reduced. Due to their random behaviour it is often difficult to characterize pixels exhibiting RTS effects.
- **Responsivity:** The responsivity of the APS device can decrease due to a decrease in the minority carrier lifetime. However, this effect can also be contributed to total ionising dose effects.

7.4.5. Photodiodes

Radiation induced defects in the photodiode semiconductor can act as recombination/generation centres. These defect centres affect photodiode parameters by trapping electrons effectively reducing the carrier lifetime resulting in a degradation of the photocurrent. Another effect of the defect centres is to generate unwanted excess current contributing and increasing the device dark current.

Parameter Degradation:

- reduced photo current;
- increased dark current.

7.4.6. Laser diodes

Radiation-induced defects in semiconductor lasers can act as recombination and trap centres. These defects increase the non-radiative recombination rates in the semiconductor, trapping exited electrons. The creation of non-radiative centres reduces the carrier lifetime thus competing with the radiative process. The net effect of increased non-radiative recombination centres is the reduction of laser diode output power. To maintain laser diode output power, higher current is injected, thus increasing the laser diode threshold current.

Parameter degradation:

- reduced output power;
- increased threshold current.

7.4.7. Light emitting diode (LED)

As for laser diodes, radiation-induced defects in the LED semiconductor result in a reduction of the minority-carrier lifetime. The radiation-induced defects compete for the same carriers as pre-existing radiative defects hence, reducing the output power of the LED. The effect of displacement in LEDs depends on the impurities employed in the device. Thus, parameter degradation due to displacement damage can vary between devices employing different manufacturing processes.

Parameter degradation:

- reduced output power.

7.4.8. Optocouplers

Generally an optocoupler consists of a light emitting diode in conjunction with a photodiode or a phototransistor. Parameter degradation of the optocoupler is simply the contribution of radiation damage to each part of the device. Depending on the individual components employed in an optocoupler, these devices can be very sensitive to displacement damage. There can be, in terms of irradiation behaviour, large device-to-device variations.

Parameter degradation:

- reduced current transfer ration (CTR).

7.4.9. Solar cells

The output power of solar cells is degraded when exposed to the space radiation environment. An important cause of this degradation is due to displacement damage effects caused by both protons and electrons. However, the displacement damage cross section for electrons is much lower than that of protons. The sensitivity of solar cells to non-ionising radiation depends on the device material (*i.e.* Si, GaAs, InP). Degradation processes in the solar cell is due to a minority carrier lifetime degradation and carrier removal.

Parameter degradation:

- Reduced cell short circuit current;
- Reduced open circuit voltage;
- Reduced maximum power.

7.4.10. Germanium detectors

Cryogenically cooled, high-purity germanium (HPGe) detectors, used as γ-ray detectors, are relatively sensitive to performance degradation induced by displacement damage. Indeed the large volumes (potentially 100s cm^3) and long charge collection paths makes the effects of TNID more apparent than for conventional semiconductors. The effects of radiation damage are [RDE.5][RDE.6]:

- A shift in the apparent energy of γ-rays, as the charge collection efficiency (CCE) decreases.
- Poorer energy resolution. This is due in part to the poorer statistics associated with the decreased number of charge carriers. However, as radiation damage increases for cylindrical detectors, the Gaussian peak associated mono-energetic γ-rays becomes increasingly asymmetric. This effect is due to the variation in amount of charge trapping depending upon whether the event is from a γ-ray interaction near the axis or near the surface of the detector (discussed below).
- Poorer timing characteristics, which can be essential for space-borne detectors incorporating complex veto shields and electronics.
- Changes in detector resolution with time when the bias is switched on (called "resolution transients").
- Complex performance variability as a function of temperature. If the temperature of the detector is increased slightly and then returned to liquid nitrogen temperatures, the resolution often decreases until the annealing temperature is sufficiently high so that positive annealing effects dominate.

Displacement damage in HPGe detectors tends to introduce complex structures of defects (rather than single defect sites) that act as hole traps. For p-type cylindrical detectors, the mean distances which holes travel to reach the axial contact are longer than for n-type cylindrical detectors, where the holes travel to the surface contact. As a result, the change in CCE in n-type HPGe detectors is less affected by displacement damage. In addition, for p-type detectors events which occur closer to the detector axis are less effected by hole traps and therefore lead to greater charge collection, whereas events nearer the surface result in less charge being collected. For n-type detectors the opposite effect occurs. In either case, averaged over a large number of interactions, the peak associated with mono-energetic γ-rays looks asymmetric and broader in a cylindrical germanium detector, depending upon the level of radiation damage suffered [RDE.6].

7.4.11. Glasses and optical components

Degradation of optical components is usually considered as a phenomenon arising from ionisation in which electrons produced can occupy traps to create colour centres in the materials. For many optical materials, there are already sufficient lattice defects from the manufacturing process and impurities that radiation-induced displacements have little effect on performance. Alkali halide crystals, however, are highly susceptible to radiation-induced displacements, but also as a result of radiolytic reactions.

7.5. Radiation damage assessment

7.5.1. Equivalent fluence calculation

Since the level of displacement damage observed per unit fluence is highly dependent upon particle energy and species, it is often convenient to convert the actual particle environment to the displacement damage equivalent fluence (DDEF) of mono-energetic protons or electrons. The decrease in performance of a component can then be predicted from tests performed on the component at those mono-energetic energies. Typically

10 MeV proton fluences or 1 MeV electron equivalent fluence is used, these are defined based on NIEL values for the considered material and radiation environment specification. If no valid NIEL values are available in the open literature, they are determined following methodologies presented by Jun *et al* or Messenger *et al* [RDE.8][RDE.9]. Such curves are calculated as a function of equivalent aluminium shielding thickness, based on particle (trapped protons and electrons, flare (solar) protons) flux spectrum estimated for a specified mission.

7.5.2. Calculation approach

Sector-shielding analysis allows estimation of the particle spectra and intensity at component die level, which can then be converted to the mono-energetic equivalent particle fluence, *e.g.* 10 MeV equivalent proton fluence (see Clause 6 of ECSS-E-ST-10-12C and Clause 5 of the present handbook).

7.5.3. 3-D Monte Carlo analysis

The 3-D Monte Carlo radiation transport analysis method can be used in order to get a more accurate estimate of the actual particle fluence and spectrum, and hence the mono-energetic equivalent proton fluence value at part level (see Clause 6 of ECSS-E-ST-10-12C and Clause 5 of the present handbook). If a Monte Carlo code is used, equivalent proton fluence value results should have an appropriate statistical uncertainty. There are also non-statistical uncertainties due to the limits of physical accuracy of the model.

7.5.4. Displacement damage testing

Once the equivalent proton fluence has been determined, testing is performed employing protons, neutrons or electrons depending on device type and radiation environment.

It is important to select particles with sufficient energies to allow the particles to traverse the sensitive part of the device.

Mono-energetic particle testing is allowed if it has been clearly demonstrated that there is a consistent one-to-one relationship between device degradation and NIEL, or if particle energy chosen for testing leads to a worst case degradation of the device under test. Existing data show this is usually true in the medium energy range but it is currently not formally demonstrated for every device type, in particular for highest proton energy (>200 MeV). If such information is unavailable, appropriate verification cannot be performed without multi-energetic irradiation testing with the choice of particle energy depending on device type and radiation environment of concern.

Tested parts should be manufactured with technology identical to the technology to be used for FM parts (except if technology changes are proven not to alter displacement damage hardness). The parts selected for testing should either be:

- not more than 4 years older than the date of the Equipment Radiation Analysis, or
- tested parts from the same diffusion lot as FM parts, whatever date code, **and** test biasing conditions are either for worst or equivalent to the application.

7.6. NIEL rates for different particles and materials

The following three tables list NIEL rates /coefficients for electrons, protons and neutrons in Si, respectively. Table 5 to Table 7 are based on information reported by Lindström [RDE.10]. For most applications involving protons and electrons worst-case data from Table 8 to Table 10 should be used.

Table 5: NIEL rates for electrons incident on Si (from Summers *et al* based on Si threshold of 21 eV [RDE.11])

E_{kin} [MeV]	NIEL coefficient [MeV·cm²/g]
0.3	6.48E-06
0.5	1.63E-05
0.7	2.32E-05
1	3.14E-05
2	5.07E-05
3	6.37E-05
5	8.11E-05
7	9.28E-05
10	0.000105
20	0.000127
30	0.000138
50	0.000150
70	0.000156
100	0.000160
200	0.000165

Table 6: NIEL rates for protons incident on Si (part 1 of 2). This is a subset of NIEL data from Huhtinen and Aarnio [RDE.12].

E_{kin} [MeV]	NIEL coefficient [MeV·cm²/g]
15	0.00688
25	0.00521
35	0.00433
45	0.00383
55	0.00349
65	0.00322
75	0.00299
85	0.00281
95	0.00266
105	0.00253
115	0.00245
125	0.00236
135	0.00229
145	0.00224
155	0.00219
165	0.00214
175	0.00209
185	0.00206
195	0.00203
205	0.00200
215	0.00197
225	0.00194
235	0.00192
245	0.00190
255	0.00188
265	0.00186
275	0.00185
285	0.00183
295	0.00181
305	0.00180
315	0.00179
325	0.00178
335	0.00176
345	0.00175
355	0.00174
365	0.00173
375	0.00172
385	0.00171
395	0.00170
405	0.00169
415	0.00167
425	0.00166
435	0.00165
445	0.00164
455	0.00163
465	0.00162
475	0.00161
485	0.00160
495	0.00159
505	0.00159
515	0.00158
525	0.00158
535	0.00157
545	0.00157
555	0.00156
565	0.00155
575	0.00155
585	0.00154
595	0.00154
605	0.00153
615	0.00152
625	0.00152
635	0.00152
645	0.00151
655	0.00151
665	0.00150
675	0.00150
685	0.00150
695	0.00149
705	0.00149
715	0.00148
815	0.00145
915	0.00142
1015	0.00139
1115	0.00137
1215	0.00136
1315	0.00134
1415	0.00133
1515	0.00131
1615	0.00130
1715	0.00129
1815	0.00128
1915	0.00127
2015	0.00126
2115	0.00125
2215	0.00124
2315	0.00123
2415	0.00123
2515	0.00122
2615	0.00122
2715	0.00122
2815	0.00122
2915	0.00121
3015	0.00121
3115	0.00120
3215	0.00120
3315	0.00120
3415	0.00120
3515	0.00119
3615	0.00119
3715	0.00119
3815	0.00118

Table 6: NIEL rates for protons incident on Si (part 2 of 2). This is a subset of NIEL data from Huhtinen and Aarnio [RDE.12].

E_{kin} [MeV]	NIEL coefficient [MeV·cm²/g]
3915	0.00118
4015	0.00118
4115	0.00117
4215	0.00117
4315	0.00117
4415	0.00117
4515	0.00116
4615	0.00116
4715	0.00116
4815	0.00115
4915	0.00115
5015	0.00115
5115	0.00114
5215	0.00114
5315	0.00114
5415	0.00114
5515	0.00113
5615	0.00113
5715	0.00113
5815	0.00112
5915	0.00112
6015	0.00112
6115	0.00111
6215	0.00111
6315	0.00111
6415	0.00111

E_{kin} [MeV]	NIEL coefficient [MeV·cm²/g]
6515	0.00110
6615	0.00110
6715	0.00110
6815	0.00110
6915	0.00109
7015	0.00109
7115	0.00109
7215	0.00108
7315	0.00108
7415	0.00108
7515	0.00108
7615	0.00107
7715	0.00107
7815	0.00107
7915	0.00106
8015	0.00106
8115	0.00106
8215	0.00106
8315	0.00105
8415	0.00105
8515	0.00105
8615	0.00105
8715	0.00104
8815	0.00104
9005	0.00104

Table 7: NIEL rates for neutrons incident on Si (part 1 of 2). This is a subset of NIEL from Griffin *et al* [RDE.13].

E_{kin} [MeV]	NIEL coefficient [MeV·cm²/g]
1.025E-10	3.21E-05
1.750E-10	2.46E-05
2.900E-10	1.91E-05
5.125E-10	1.43E-05
8.200E-10	1.13E-05
1.313E-09	8.96E-06
2.250E-09	6.84E-06
3.900E-09	5.20E-06
6.450E-09	4.04E-06
1.025E-08	3.21E-06
1.750E-08	2.45E-06
2.900E-08	1.91E-06
5.125E-08	1.43E-06
8.200E-08	1.13E-06
1.313E-07	8.96E-07
2.250E-07	6.85E-07
3.900E-07	5.20E-07
6.450E-07	4.04E-07
1.025E-06	3.21E-07
1.750E-06	2.45E-07
2.900E-06	1.91E-07
5.125E-06	1.44E-07
8.200E-06	1.14E-07
1.313E-05	8.96E-08
2.250E-05	6.85E-08
3.900E-05	5.19E-08
6.450E-05	4.04E-08
1.025E-04	3.21E-08
1.750E-04	2.68E-07
2.900E-04	7.10E-07
5.125E-04	1.22E-06
8.200E-04	1.91E-06
1.313E-03	3.01E-06
2.250E-03	8.97E-06
3.900E-03	8.53E-06
6.450E-03	1.37E-05
1.025E-02	2.09E-05
1.750E-02	3.33E-05
2.900E-02	4.89E-05
5.125E-02	3.31E-05
8.200E-02	1.12E-04
0.1313	3.72E-05
0.2250	1.49E-03
0.3900	1.08E-03
0.6450	1.13E-03
1.050	1.63E-03
2.050	2.08E-03
3.050	2.60E-03
4.050	2.91E-03
5.050	3.28E-03
6.050	3.39E-03
7.050	3.61E-03
8.050	3.68E-03
9.050	3.82E-03
10.05	3.59E-03
11.05	3.54E-03
12.05	3.63E-03
13.05	3.79E-03
14.05	3.64E-03
15.05	3.61E-03
19.95	4.02E-03

Table 7: NIEL rates for neutrons incident on Si (part 2 of 3). These data are from Konobeyev *et al* [RDE.14].

E_{kin} [MeV]	NIEL coefficient [MeV·cm²/g]
20	0.00422
25	0.00417
30	0.00416
40	0.00410
50	0.00368
60	0.00335
70	0.00305
80	0.00281
90	0.00258
100	0.00238
130	0.00198
160	0.00176
200	0.00161
250	0.00149
300	0.00142
350	0.00141
400	0.00140
450	0.00140
500	0.00139
600	0.00138
700	0.00138
800	0.00137

Table 7: NIEL rates for neutrons incident on Si (part 3 of 3). This is a subset of NIEL from Huhtinen and Aarnio [RDE.12].

E_{kin} [MeV]	NIEL coefficient [MeV·cm²/g]
805	1.22E-03
905	1.20E-03
1005	1.18E-03
1105	1.16E-03
1205	1.16E-03
1305	1.15E-03
1405	1.13E-03
1515	1.12E-03
1645	1.10E-03
1795	1.09E-03
1955	1.07E-03
2105	1.06E-03
2265	1.05E-03
2415	1.04E-03
2545	1.04E-03
2665	1.04E-03
2795	1.04E-03
2915	1.03E-03
3045	1.03E-03
3165	1.03E-03
3295	1.02E-03
3415	1.02E-03
3545	1.02E-03
3665	1.02E-03
3795	1.01E-03
3915	1.01E-03
4035	1.01E-03
4135	1.01E-03
4235	1.00E-03
4335	1.00E-03
4435	1.00E-03
4535	9.98E-04
4635	9.96E-04
4735	9.94E-04
4835	9.92E-04
4935	9.89E-04
5035	9.87E-04
5135	9.85E-04
5235	9.83E-04
5335	9.81E-04
5435	9.79E-04
5535	9.77E-04
5635	9.75E-04
5735	9.73E-04
5835	9.71E-04
5935	9.69E-04
6035	9.67E-04
6135	9.65E-04
6235	9.63E-04
6335	9.61E-04
6435	9.59E-04
6535	9.57E-04
6635	9.55E-04
6735	9.53E-04
6835	9.51E-04
6935	9.49E-04
7035	9.47E-04
7135	9.45E-04
7255	9.43E-04
7385	9.40E-04
7515	9.37E-04
7635	9.35E-04
7765	9.33E-04
7885	9.30E-04
8015	9.28E-04
8135	9.26E-04
8265	9.23E-04
8385	9.21E-04
8515	9.18E-04
8635	9.16E-04
8995	9.09E-04

Table 8: NIEL rates for electrons in Si and GaAs (Akkerman *et al* [RDE.15])

E_{kin} [MeV]	Si NIEL coefficient [MeV·cm²/g]	GaAs NIEL coefficient [MeV·cm²/g]
0.2	4.56E-06	1.77E-06
0.4	1.28E-05	7.52E-06
0.6	2.02E-05	1.37E-05
0.8	2.66E-05	1.92E-05
1	3.21E-05	2.40E-05
2	5.22E-05	4.10E-05
4	7.58E-05	5.93E-05
6	9.05E-05	7.04E-05
8	1.01E-04	7.84E-05
10	1.09E-04	8.94E-05
20	1.34E-04	1.06E-04
40	1.54E-04	1.29E-04
60	1.62E-04	1.42E-04
80	1.67E-04	1.52E-04
100	1.69E-04	1.58E-04
150	1.73E-04	1.73E-04
200	1.73E-04	1.73E-04

Table 9: NIEL rates for protons in Si

E_{kin} [MeV]	Si NIEL coefficient – Akkerman *et al* [RDE.15] [MeV·cm²/g]	Si NIEL coefficient – Summers *et al* [RDE.11] [MeV·cm²/g]	*Si NIEL coefficient – worst-case [MeV·cm²/g]*
1		0.0638	***0.0638***
2		0.0329	***0.0329***
3	0.0273	0.0224	***0.0273***
5	0.0167	0.0138	***0.0167***
10	0.00962	0.00789	***0.00962***
20	0.0068	0.00536	***0.0068***
30	0.00563	0.00478	***0.00563***
40	0.00418	0.00444	***0.00444***
50	0.00349	0.00388	***0.00388***
60	0.00289	0.0035	***0.0035***
80	0.0022	0.00289	***0.00289***
100	0.00188	0.00260	***0.00260***
120	0.00151	0.00222	***0.00222***
150	0.00146	0.0021	***0.0021***
180	0.00149	0.002	***0.002***
200	0.00151	0.00194	***0.00194***
220	0.0015		

Results from Summers *et al* assume an Si threshold energy of 21 eV.

Table 10: NIEL rates for protons in GaAs.

E_{kin} [MeV]	GaAs NIEL coefficient – Akkerman *et al* [RDE.15] [MeV·cm²/g]	GaAs NIEL coefficient – Summers *et al*[RDE.11] [MeV·cm²/g]	*GaAs NIEL coefficient – worst-case [MeV·cm²/g]*
1		0.054	***0.054***
2		0.0289	***0.0289***
3		0.0199	***0.0199***
5	0.0108	0.0125	***0.0125***
10	0.00628	0.00659	***0.00659***
20	0.00438	0.0047	***0.0047***
30	0.0043	0.0040	***0.0043***
40	0.00422	0.0038	***0.0422***
50	0.00416	0.0037	***0.00416***
60	0.00403	0.00365	***0.00403***
80	0.00386	0.0036	***0.00386***
100	0.0037	0.0035	***0.0037***
120	0.0038	0.0036	***0.0038***
150	0.0038	0.00365	***0.0038***
180	0.0038	0.0037	***0.0038***
200	0.004	0.0039	***0.004***
220	0.0041		***0.0041***

7.7. Uncertainties

Predictions for TNID are subject to the same uncertainties associated with the shielding calculation used to determine the particle flux/fluence at the device or equipment (see Clause 5.8). In addition, comparisons of NIEL coefficients generated through Monte Carlo simulations of radiation interaction in semiconductors indicate there are variations in these values of the order of 10 % for neutrons, and potentially ~50 % for protons high-energy protons (see Table 9).

In this Standard the policy has been followed that no additional margin is applied for uncertainties in NIEL if the worst-case NIEL coefficients in Table 9 and Table 10 are used.

A greater uncertainty can lie in the principle of the NIEL hypothesis, *i.e.* that it is possible to equate damage to a semiconductor due to different particles at different energies through a NIEL coefficient calculated on the basis of only the initial interaction process (see Clause 7.3).

7.8. References

[RDE.1] G H Kinchin, and R S Pease, "The displacement of atoms in solids by radiation," *Reports on Progress in Physics*, **18**, pp1-51, 1955.

[RDE.2] F Seitz, and J S Koehler, "Displacement of atoms during radiation," *Solid State Physics*, **2**, pp305-448, 1956.

[RDE.3] Robert J Walters, Scott R Messenger, Geoffrey P Summers, Edward A Burke, Shyam M Khanna, Diego Estan, Lorne S Erhardt, Hui Chun Liu, Mae Gao, Margaret Buchanan, Anthony J SpringThorpe, Alain Houdaya and Cosmo Carlone, "Correlation of proton radiation damage in InGaAs-GaAs quantum-well light-emitting diodes," *IEEE Trans Nucl Sci*, **48**, No 6 pp1773-1777, 2001.

[RDE.4] J R Srour "Displacement Damage effects in Electronic Materials, Devices, and Integrated Circuits", Tutorial Short Course Notes

presented at 1988 IEEE Nuclear and Space Radiation Effects Conference, 11 July 1988.

[RDE.5] M Koenen, J Brückner, M Körfer, I Taylor, M Wänke, "Radiation damage in large-volume n-and p-type high-purity germanium detectors irradiated by 1.5 GeV protons," IEEE Conference Record 94CH35762, pp201-205, 1994.

[RDE.6] M Koenen, J Brückner, U Fabian, H Kruse, M Wänke, A N F Schoeder, R Starr, L G Evans, J I Trombka, D M Drake, P A J Englert, and J Dempsey, "Analysis of radiation damaged HPGe detectors with a new algorithm," *IEEE Trans Nucl Sci*, **43**, No 3, pp1570-1575, 1996.

[RDE.7] Robert J Walters, Scott R Messenger, Geoffrey P Summers, Edward A Burke, Shyam M Khanna, Diego Estan, Lorne S Erhardt, Hui Chun Liu, Mae Gao, Margaret Buchanan, Anthony J SpringThorpe, Alain Houdaya and Cosmo Carlone, "Correlation of proton radiation damage in InGaAs-GaAs quantum-well light-emitting diodes," *IEEE Trans Nucl Sci*, **48**, No 6, pp1773-1777, 2001.

[RDE.8] Insoo Jun, Michael A Xapsos, Scott R Messenger, Edward A Burke, Robert J Walters, Geoff P Summers, and Thomas Jordan, "Proton nonionising energy loss (NIEL) for device applications," *IEEE Trans Nucl Sci*, **50**, No 6, pp1924-1928, 2003.

[RDE.9] Scott R Messenger, Edward A Burke, Michael A Xapsos, Geoffrey P Summers, Robert J Walters, Insoo Jun, and Thomas Jordan, "NIEL for heavy ions: an analytical approach," *IEEE Trans Nucl Sci*, **50**, No 6, pp1919-1923, 2003.

[RDE.10] Gunnar Lindström's NIEL web-site http://sesam.desy.de/members/gunnar/Si-dfuncs.html, 2007.

[RDE.11] G P Summers, E A Burke, P Shapiro, S R Messenger, R J Walters, "Damage correlations in semiconductors exposed to gamma, electron and proton radiations," *IEEE Trans Nucl Sci*, **40**, No 6, pp1372-1379, 1993.

[RDE.12] M Huhtinen and P A Aarnio, "Pion-induced displacement damage in silicon devices," *Nucl Instrum Meth Phys Res*, **A335** pp580-582, 1993 and private communication.

[RDE.13] P J Griffin *et al*, Sandia National Laboratory report SAND92-0094, 1993 and private communication.

[RDE.14] A Yu Konobeyev, Yu A Korovin and V N Sosnin, "Neutron displacement cross-sections for structural materials below 800 MeV," *J Nucl Mat*, **186**, pp117-130, 1992.

[RDE.15] A Akkerman, J Barak, M B Chadwick, J Levinson, M Murat, and Y Lifshitz, "Updated NIEL calculations for estimating the damage induced by particles and γ-rays in Si and GaAs," *Rad Phys Chem*, **62**, pp301-310, 2001.

8
Single event effects

8.1. Introduction

Energetic ions passing through integrated circuits semiconductors produce a trail of ionisation which induces a variety of physical phenomena known as single event effects (SEE). These failures result from the charge deposited by a single particle crossing a sensitive region in the device and are a function of the amount of charge collected at the sensitive node(s).

Energetic protons and neutrons can also produce SEEs in devices by means of nuclear reactions (presently, the maximum stopping power or protons is too low to induce an event by direct ionisation). From the collision, the incident proton or neutron transfers part of its energy to a recoil atom (elastic/inelastic collision or spallation mechanism). The probability of such reactions are low (approximately 10^{-5} for most devices of interest), however fluxes of protons can be very high in the inner proton belt or during solar particle events, and this mechanism can dominate the SEE rates in many situations for modern devices that have a low LET threshold. The recoiling nucleus deposits energy in the same way as a heavy ion but has a very short range (see Figure 13). In addition, other reaction products, such as α-particles, can add to the energy deposition.

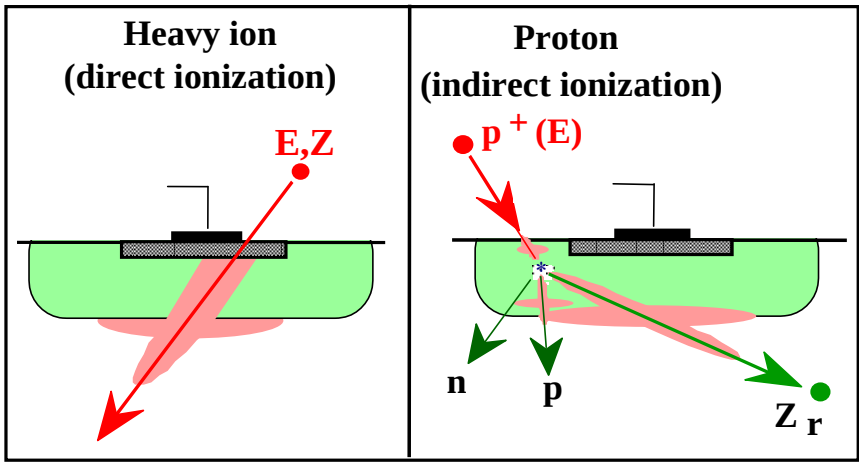

Figure 13: SEE initial mechanisms by direct ionisation (for heavy ions) and nuclear interactions (for protons and neutrons).

SEE phenomena can be divided into two sub-groups:

- Those which are or can be destructive, such as single event latch-up (SEL), single event snapback (SESB), single event dielectric rupture (SEDR), single event gate rupture (SEGR), and single event breakdown (SEB).
- Non-destructive single event effects, such as single event transient (SET), single event disturb (SED), single event upset (SEU), multiple-cell upset (MCU), single-word multiple-bit upset (SMU), single event functional interrupt (SEFI), and single event hard error (SEHE).

8.2. Modelling

8.2.1. Overview

There are three important parameters to model the SEE response of a device. These are described in the following sections.

8.2.2. Notion of LET (for heavy ions)

The amount of energy deposited in the track per unit pathlength is called the ***linear energy transfer*** (LET) and for SEE analysis is typically measured in MeV·cm^2/mg. LET is a function of the particle type and energy, and can be approximated to the particle stopping power (in energy loss per unit linear pathlength).

$$\begin{cases} LET(x) \cong \frac{1}{\rho}\frac{dE}{dx}(x) & 0 \le x \le r \\ LET(x) = 0 & \text{otherwise} \end{cases} \quad \textbf{(12)}$$

where r is the range of the particle, and ρ the density of the target material (2.32 g/cm^3 for silicon). The deposited energy over a distance d (in micrometres) can therefore be calculated using the formula:

$$E_{dep} = LET \times d \times 0.232 \quad \textbf{(13)}$$

where E_{dep} is in MeV, and LET is defined in units of MeV·cm^2/mg. This relation is valid if the LET is constant over the distance d (*i.e.* for long-range ions).

Different ions with the same incident LET do not always produce the same charge distribution along the track and different charge is collected particularly in small devices. Therefore the LET concept breaks down for very small sensitive devices and high-energy particles.

8.2.3. Concept of cross section

The ***cross section*** is the probability of a SEE occurring and is experimentally measured as the number of events recorded per unit fluence (Figure 14). SEE cross sections for ions heavier than protons are usually expressed as a function of LET, and as a function of energy for protons and neutrons. Strictly speaking, cross sections of some mechanisms are also dependent on the angle of incident of the particle.

$$\sigma_{ion}(LET) = \frac{Number\ of\ events}{Ion\ fluence} \quad \text{or} \quad \sigma_{nucleon}(E) = \frac{Number\ of\ events}{Proton\ or\ neutron\ fluence} \quad \textbf{(14)}$$

For ions, cross section measures the LET-dependent sensitive area of the chip. For SEEs produced by nuclear interactions, the interpretation is not so clear, since the cross section incorporates the probability of a nucleon-nuclear interaction, and the probability that the nuclear recoil and other nuclear fragments results in sufficient charge density in the correct places of the semiconductor to induce an event.

Cross section is usually expressed in units of cm²/device for SEEs in general, but for SEUs, MCUs, and SMUs, cm²/bit is often used.

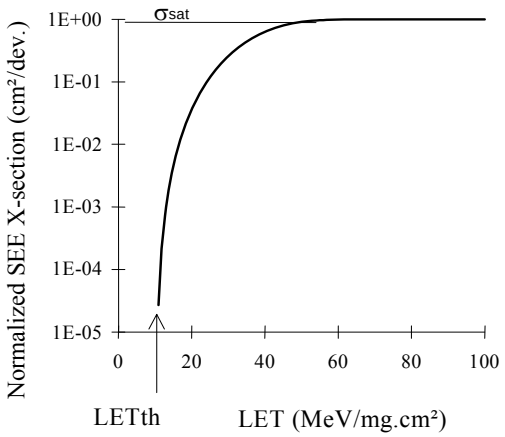

Figure 14: Example of SEE cross section versus LET.

8.2.4. Concept of sensitive volume, critical charge and effective LET

The ***critical charge***, Q_C is the minimum amount of charge collected at a sensitive node due to a charged particle strike that results in SEE. Qc is proportional to the critical energy, E_C deposited in the sensitive volume of the device. In the case of silicon, Q_C (in pC) is deduced from E_C (in MeV) by the expression:

$$Q_C = \frac{E_C}{22.5} \quad \textbf{(15)}$$

The ***sensitive volume*** (SV), sometimes referred to as the ***sensitive node*** is often modelled as a rectangular parallelepiped from which deposited charge can be collected in such a manner as to produce SEE. The lateral dimensions of the SV can be calculated from the saturation cross section, σ_{sat} (sensitive surface in cm²/bit) and the thickness is often assumed to be of the order of 2µm (funnelling and diffusion are ignored). 2 µm is an approximate value for the thickness of sensitive volumes. It is a historical value based on single event upset studies, but for recent and highly integrated technologies with small geometries, and for new SEE mechanisms, is not always valid. However, it is possible to get a more precise estimation of the actual geometry of the sensitive volume with reasonable physical meanings, from experimental measurements. For instance, variation of the SEE sensitivity with angle of incidence (the "tilt angle") can bring some useful information on the thickness of the sensitive volume [RDF.1]. Some recent studies also propose experimental methods to measure this parameter [RDF.2][RDF.3][RDF.4].

For devices exhibiting sensitive volumes with a large aspect ratio (large horizontal dimensions when compared to the vertical one), one can define the concept of ***effective LET*** as following

$$LET_{eff}(\theta) = \frac{LET(\theta = 0)}{\cos\theta} \quad \textbf{(16)}$$

8.3. Technologies susceptible to single event effects

Technologies which are susceptible to single event effects are identified in ECSS-E-ST-10-12C Table 10. Note that this table is based on what is presently know about the

current major technologies, and should not be considered to be an exhaustive list. It is important to consider the SEE probability and effects on any technologies identified in this table, and intended for use on spacecraft and planetary-mission systems.

8.4. Test methods

8.4.1. Overview

Three specifications are widely used and recognised for single event testing:

- EIA/JEDEC standard (EIA/JESD57), "Test procedures for the measurement of single event effects in semiconductor devices from heavy ion irradiation," December 1996 [RDF.5].
- ESA/SCC Basic specification 25100, "Single event effects test method and guidelines," October 1996 [RDF.6].
- JEDEC JSDC89, "Measurement and reporting of alpha particles and terrestrial cosmic ray-induced soft errors in semiconductor devices," August 2001, 2005 update in draft [RDF.7].

The goal of SEE testing is to determine the model parameters capable of predicting the space environment (cross section plot versus heavy ion LET, or proton or neutron energy). The approach is to expose an operating device to a known particle beam (LET or energy parameter) and observe the device response (event counting).

The radiation environment in space widely varies in composition and energy characteristics and is largely omnidirectional. Therefore, SEE testing cannot be appropriately performed without the use of an accelerator which can be operated with a variety of particle species and energies.

Ground-based measurements are at best an approximation of the space environment. For galactic cosmic rays, relatively low energy heavy ions are used at accelerators to predict the response to much higher energy particles (but having the same LET). For protons testing, it cannot be done without a very high energy generator.

A typical experiment set-up can be divided in two groups:

- the beam delivery and dosimetry, and
- the device testing equipment including harness and device-under-test (DUT) position/tilt monitoring.

8.4.2. Heavy ion beam testing

It is important that a standard beam for SEE testing is contaminant-free, well defined in terms of energy and species (to accurately determine LET), spatially uniform over the surface of the die where flux levels can be varied between 10^2 to 10^5 ions/(cm^2s). Particles of interest produce LET values which are used to determine the SEE threshold and saturated value and have range long enough to allow the incident ion to penetrate the sensitive volume of the circuit without suffering significant energy loss across this region. The establishment of these characteristics implies a specific beam dosimetry system that:

- measures the flux and fluence of the selected beam (real-time counting of the particles) typically by means of a scintillator/photo-multiplier assembly, Si surface barrier detector (SBD) or parallel plate avalanche counter (PPAC);
- permits energy calibration before the operation (usually SBDs are used).

For heavy ion irradiation, the components are de-lided in order to be tested because of the ions' short range.

8.4.3. Proton and neutron beam testing

The important parameters for proton SEE testing are:

- the particle energy and resolution;
- the proton flux (typically 10^5-10^8 particles/cm^{2}s).

The flux is also important for neutrons, but due to the fact that most energetic neutrons are produced either as a general spallation reaction of protons in a high-Z material, or from specific energetic reactions of protons (*e.g.* ^{7}Li(p,n) and ^{9}Be(d,n)), the energy of these sources is not as well defined and several orders of magnitude lower in flux than for protons.

Considering the very high energy of protons generated by cyclotrons (up to 600 MeV), it is possible to use beams in air. The energy of particles is often modified by interposition of attenuators of different materials with calibrated thicknesses. The final energy on the target is calculated by taking into account the energy loss in the attenuators and in the layer of air through which the particle has passed. Neutrons suffer negligible attenuation in air, but can be scattered out of the proton beam by equipment and dense materials up-stream.

For protons, the LET of the recoil nucleus is not accessible, so, the problem is reduced to the characteristics of the primary proton beam. The parameter used during the tests is no longer the LET, but the energy of the incident proton or neutron. Then, the irradiations are commonly performed with the beam at normal incidence but modern devices can show angular dependence (some experiments have shown that cross section can vary by almost an order of magnitude with angle of incidence [RDF.8][RDF.9].

An important consideration for protons is total ionising dose damage. Some measurements show an increase in SEU susceptibility of up to two orders-of-magnitude as a result of TID effects from proton irradiation.

8.4.4. Experimental measurement of SEE sensitivity

The part is exposed to the beam while under normal operating bias at room temperature. A test system is used to operate the component and to detect functional anomalies.

SEE testing consists of irradiating a device with a specified particle beam of known energy and flux, in such a way that the number of events can be detected as a function of the beam fluence. The cross section is the number of events per unit fluence and is corrected to include tilted beams (θ is the incidence angle of the beam with respect to the perpendicular of the chip). In this case, the SEE sensitivity is described as (in the case of heavy ions):

$$\sigma = \frac{N}{\Phi \cos\theta} \qquad \textbf{(17)}$$

where:

σ = cross section of device (cm^2/device);

N = number of SEEs per device;

Φ = fluence to produce N events (particles/cm^2);

θ = angle of incidence.

To plot σ as a function of LET, the energy transfer can be varied by changing the ion species, the energy or the incidence angle of the beam. In this latter condition, the *effective LET* scales with the LET at normal incidence (see equation **(16)**. These two relations are considered as correct if the device sensitive volume is thin compared to the lateral dimensions, so that there is little change in the ion's LET. Furthermore, there are

some SEE mechanisms such as single event latch-up and single event snapback where the concept of effective LET is not valid.

8.4.5. Influence of testing conditions

8.4.5.1. Overview

The irradiation and test conditions strongly affect the device response to SEE. Therefore the following are the factors to be taken into consideration:

- particle energy (and hence ionisation track structure and range);
- angle of incidence;
- temperature of the device under test;
- total ionising dose received;
- data pattern stored – the susceptibility of memory devices to SEUs varies with the specific pattern of ones and zeros held in the memory;
- operational mode;
- clock rate, including whether static or dynamic test is performed;
- electrical bias (low bias conditions are worse for single event upsets, but generally better for latch-up and burnout);
- current-limiting conditions;
- reset conditions, duty factor;
- fractional portion of chip tested.

Examples of effect of some of these parameters are explained below, whilst further details can be found in [RDF.8], [RDF.9], [RDF.10], [RDF.11], [RDF.12], [RDF.13] and [RDF.14].

8.4.5.2. Energy and track structure dependence

The validity of the use of relatively low-energy ion-beam facilities to simulate the deposition of charge from a space particle is determined by the LET parameter. This assumption is accurate under restricted conditions. Significant differences can arise because:

- LET is usually approximated to the stopping power of the particle, *i.e.* the energy loss by the particle per unit pathlength rather than the energy deposited per unit pathlength.
- LET is an average value and does not account for statistical variations in energy deposition. In addition, track structure appears to play an important part in the dynamics of charge collection during a single event transient.

Up to now, no clear track structure/energy dependence has been observed on most of the tested devices. If any difference appears, the low energy measurement is always conservative.

8.4.5.3. Angle effect on device response

The device response is by means of the effective LET of the ion which is changed by varying its angle of entry into the device. Even though the charge deposited within the sensitive region scales with $sec\theta$, the transient amplitude is not always scaling with the same factor. The physical feature of the sensitive volume can also lead to data that deviate from the inverse cosine law (non-validity of the relation LET_{eff} = LET(0°)/$cos\theta$). There can also be azimuth angle dependencies (see Figure 15) [RDF.10]. Therefore, from an experimental point of view, it is important that the number of beams used to acquire the sensitivity curve provides an overlap of data from one ion species to the next.

This effect can also be observed with protons in the case of devices with small sensitive volumes and grazing angle incidence beams.

8.4.5.4. Pattern influence

In many cases, a test pattern dependence is observed on integrated memories. It can be due to the existence of a preferential state, showing up differences in sensitivity between 0 to 1 and 1 to 0 transitions. In the case of DRAM, only the cells with discharged capacitors are sensitive to SEU.

It is therefore advisable to use several test patterns.

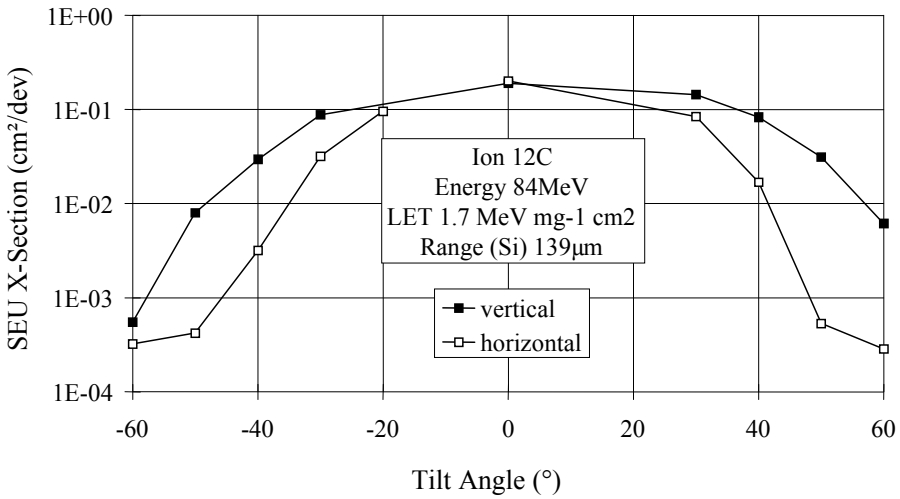

Figure 15: Tilt-angle dependence for the SP44100 4Mbits DRAM SEU sensitivity for two azimuth angles.

8.5. Hardness assurance

8.5.1. Rate prediction

The method used to analyse the need for SEE risk reduction depends on the possibility of calculating a SEE rate. When SEE error rate calculations are technically possible (*e.g.* case of single event upset and single event transient, single event latch-up), they are obtained by combining the experimental sensitivity curve with the appropriate environment parameters.

8.5.2. Prediction of SEE rates for ions

When an ion crosses a device it leaves a dense plasma of electron hole pairs along its path. When the charges are generated close to a sensitive node of a circuit, a p-n junction of a transistor for example, these charges are collected and, if of sufficient magnitude, are able to generate soft errors.

The upset rate calculation depends on the paths available in the charge collection region (the sensitive volume). Ordinarily, this region is assumed to be a rectangular parallelepiped (RPP). It leads to two different SEE rate calculations: the RPP model and IRPP model.

The principle for the RPP model is very simple: the energy deposited (E_{dep}) by an incident ion in the sensitive volume is estimated and if E_{dep} is greater than the threshold energy, the upset occurs. As incident ions are very energetic, they have very long ranges

compared with typical device feature sizes and one can assume that their slowing down is continuous and linear. In that case, the deposited energy E_{dep}, can be expressed simply as:

$$E_{dep} = \rho \cdot LET \cdot d \tag{18}$$

The ion is characterised by its LET. An upset occurs when the incident ion has a LET greater than the threshold LET (LET_{th}). To calculate the upset rate, the LET spectrum of the incident particles is evaluated. It leads to a very simple formula due to **Bradford** where the upset rate is expressed as a function of the incident LET spectrum and the pathlength distribution (such as the examples shown in Figure 16 and Figure 17):

$$N = \frac{A}{4}\int_{LET_{Min}}^{LET_{Max}} \frac{d\Phi}{d(LET)}(LET) \cdot P_{CL}(> D(LET)) \cdot d(LET) \tag{19}$$

Bradford formula for RPP

$$A = 2 \cdot (lw + lh + hw) \tag{20}$$

where:

A = total surface area of the SV;

l, w and h = length, width and height of the SV;

$d\Phi/d(LET)$ = differential ion flux spectrum expressed as a function of LET (shortened to "differential LET spectrum") integrated over 4π steradians;

$P_{CL}(>D(LET))$ = integral chord length distribution, *i.e.* the probability of particles travelling through the sensitive region with a pathlength greater than D.

LET_{Min} = minimum LET to upset the cell (also referred to as the LET threshold);

LET_{Max} = maximum LET of the incident distribution (~10^5 MeV·cm²/g).

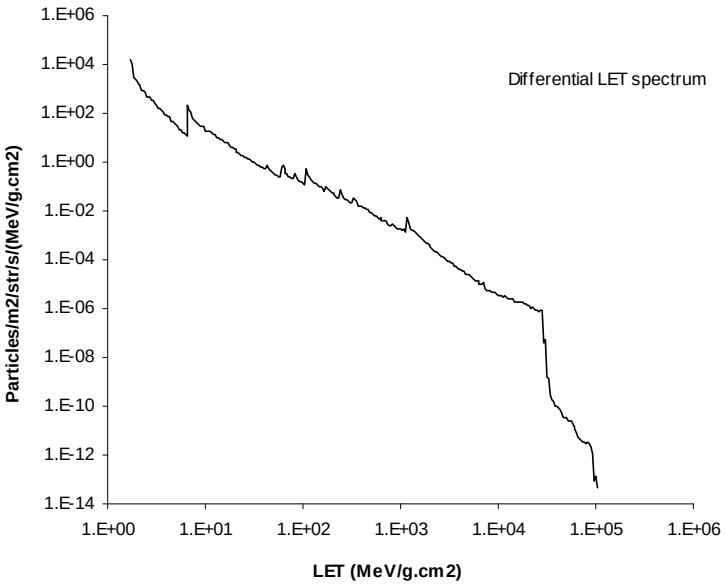

Figure 16: Example differential LET spectrum.

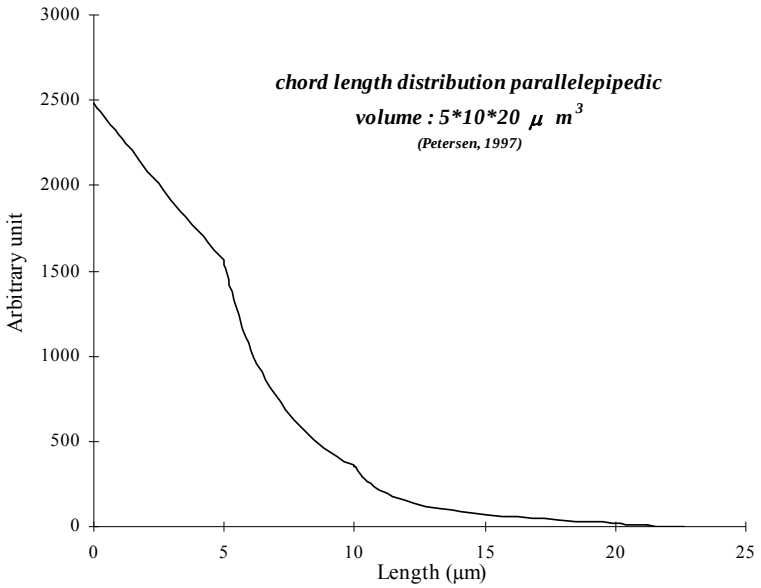

Figure 17: Example integral chord length distribution for isotropic particle environment.

Equation **(19)** is the Bradford formula used in the CREME model [RDF.15]. Some other similar expressions exist that use the differential chord length distribution and the integral LET spectrum as in Equation **(21)** and equation (22) respectively due to Pickel and Blandford and Adams [RDF.16][RDF.17][RDF.18].

$$N = \frac{A}{4}\int_{D_{Min}}^{D_{Max}} \Phi(>LET(D)) \cdot \frac{dP_{CL}}{dD}(D) \cdot dD \qquad \textbf{(21)}$$

$$N = \frac{A}{4}\frac{E_C}{\rho}\int_{LET_{Min}}^{LET_{Max}} \frac{1}{LET^2} \cdot \Phi(>LET) \cdot \frac{dP_{CL}}{d(D(LET))} \cdot D(LET) \cdot d(LET) \qquad \textbf{(22)}$$

But all these RPP model expressions make the same assumption. The LET threshold of each SV is considered equal to a unique value. Petersen pointed out that sensitivity variations across the device cannot be properly accounted for, if the LET spectrum is not folded with the experimental cross section curves [RDF.1].

In reality the critical LETs of the sensitive nodes are not the same but form a distribution that can be fitted by a Weibull function. To take into account the variation of sensitivity by integrating over a distribution of upset rates corresponding to the variation of cross section versus LET, the Integrated RPP approach (IRPP) is used.

$$N = \frac{A}{4S}\int_{LET_{i,Min}}^{LET_{i,Max}} \left\{ \frac{d\sigma_{ion}}{d(LET)}(LET_i) \int_{\frac{h}{D_{Max}}LET_i}^{LET_{Max}} \frac{d\Phi}{d(LET)}(LET) \cdot P_{CL}(>D(LET)) d(LET) \right\} d(LET_i) \qquad \textbf{(23)}$$

Integrated rectangular parallelepiped (IRPP) equation

$$S = l \cdot w \qquad \textbf{(24)}$$

where:

$d\Phi/d(LET)$ = differential LET spectrum integrated over 4π steradians;

$P_{CL}(>D(LET))$ = integral chord length distribution;

$d\sigma_{ion}/d(LET)$ = differential upset cross section;

A = total surface area of the sensitive volume;

S = surface area of the sensitive volume in the plane of the semiconductor die;

l, w and h = length, width and height of the sensitive volume;

D_{Max} = maximum length that can be encountered in the SV;

LET_{Max} = maximum LET of the LET spectrum;

$LET_{i,Min}$ = lower bin limit in the differential upset cross section $d\sigma_{ion}/d(LET)$;

$LET_{i,Max}$ = upper bin limit in the differential upset cross section $d\sigma_{ion}/d(LET)$.

8.5.3. Improvements

Improvements to the calculation method can be made, taking into account the following issues:

- Sensitive volumes are not simply rectangular parallelepipeds.
- Both sensitive volume dimensions and critical charge vary along the cross section curve. The real behaviour can be a mix of inter-cell and intra-cell variations (only the critical charge distribution is taken into account in the IRPP method).
- It is questionable as to whether there is a true saturation over the measured effective LET range, and therefore whether σ_{sat} can be precisely determined.
- Much better heavy-ion upset rate predictions can be achieved using realistic sensitive thickness data (see Figure 18).

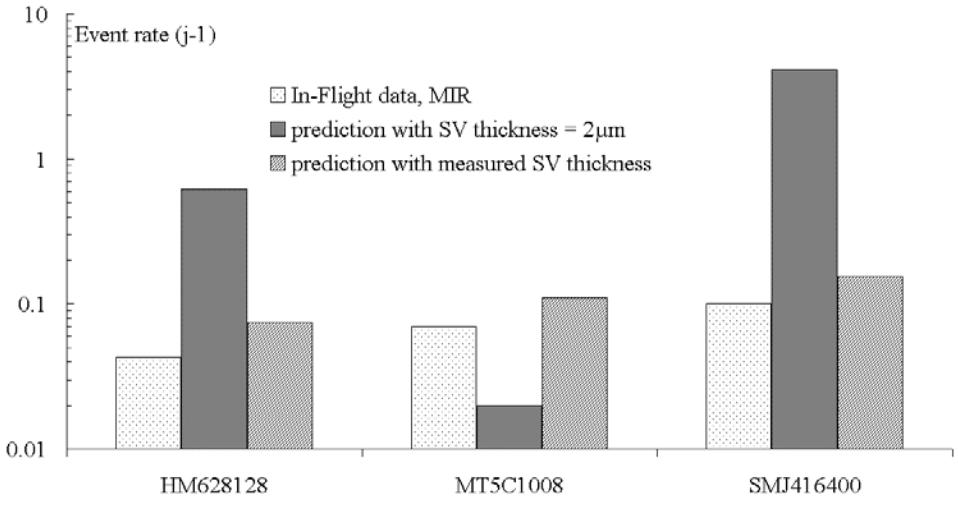

Figure 18: Accuracy of predictions when compared with in-flight MIR data.

8.5.4. Method synthesis

- Input

  Cross section experimental curve giving at least LET threshold and saturation cross section, or Weibull function parameters if known.

  LET spectra for cosmic rays and heavy ions from solar flares as given in the radiation environment specification.

- Task

  Estimate of device sensitive volume.

  Use integration method for calculation of error rate, taking into account the whole cross section curve.

- Output

  Heavy ion contribution to error rate.

8.5.5. Prediction of SEE rates of protons and neutrons

Protons and neutrons rely on indirect ionisation processes (*i.e.* following nuclear interaction) and therefore the pathlength distribution through a sensitive volume is less meaningful for standard methods of calculating cross section. Instead the SEE rate is determined from the environment proton or neutron fluxes and SEE cross sections:

$$N = \int_{E_{Min}}^{E_{Max}} \frac{d\Phi}{dE}(E) \cdot \sigma_{nucleon}(E) dE \qquad \textbf{(25)}$$

where:

$d\Phi/dE$ = differential proton or neutron flux spectrum as a function of energy integrated over 4π steradians;

E_{Min} = minimum energy of the differential energy neutron spectrum;

E_{Max} = maximum energy of the differential energy spectrum;

$\sigma_{nucleon}(E)$ = proton or neutron SEE cross section as a function of energy.

Strictly speaking, there is also a dependence on the angle of incidence, therefore:

$$N = \int_{E_{Min}}^{E_{Max}} \left\{ \int_0^{\pi} \frac{\partial \Phi}{\partial E \partial \theta}(E,\theta) \cdot \sigma_{nucleon}(E,\theta) \cdot \sin\theta d\theta \right\} dE \qquad \textbf{(26)}$$

(of course assuming no azimuthal angle dependence).

Rather than explicitly including angular dependence of the SEE cross section, a more practical solution is to define $\sigma_{max}(E)$ as the value of $\sigma(E,\theta)$ at the angle θ where the cross section maximises for that energy. Likewise, if the incident proton or neutron flux is anisotropic and cannot be approximated to an isotropic flux, $d\Phi/dE$ can be approximated to the angle-averaged incident flux if used in conjunction with the maximum cross section data, $\sigma_{max}(E)$.

SEE rates can also be approximately determined from proton- or neutron-induced energy deposition spectra and cross sections obtained from ion-beam irradiations:

$$N = \frac{S_{sample}}{S} \int_{E_{Min}}^{E_{Max}} \frac{d\Phi}{dE}(E) \left\{ \int_{\varepsilon_C}^{\varepsilon_{Max}} \sigma_{ion}\left(\frac{\varepsilon}{\rho h}\right) \frac{dP}{d\varepsilon}(E,\varepsilon) d\varepsilon \right\} dE \qquad \textbf{(27)}$$

where:

$dP/d\varepsilon(E,\varepsilon)$ = differential energy deposition spectrum for protons/neutrons of energy E depositing energy ε within the sensitive volume;

ε_C = critical or threshold energy deposition for inducing SEE;

ε_{Max} = maximum energy deposition defined for energy deposition spectrum;

$\sigma_{ion}(LET)$ = SEE cross section for ions as a function of LET for normally incident ions;

h = height of sensitive volume;

ρ = mass density of semiconductor;

s_{sample} = area of cell sampled by proton/neutron simulation to obtain energy deposition spectrum.

Other parameters are as defined for the previous equations.

The energy spectrum can be estimated from, for example, simulation of monoenergetic protons or neutrons on a representation of the sensitive volume, the dimensions for which have been determined from ion-beam irradiations. It is important that the radiation transport simulation includes nucleon-nuclear interaction models as well as models for ionisation by nuclei and light charged particles.

This method of calculation is less accurate compared with direct use of experimentally-determined proton or neutron cross sections, and shows error levels of factors of three to ten. Therefore, it is recommended that this be used to help provide an initial assessment, and if the SEE rates (including errors) are shown to be significant for the mission, then proton/neutron irradiation of the devices should be performed.

8.5.6. Method synthesis

- Input

  Cross section experimental curve giving saturation cross section and 2 other cross section/energy points in the proton energy range 10-200 MeV, or from thermal energies to 200 MeV for neutrons.

  When the heavy ion cross-section experimental curve exists, proton cross section curve can be simulated by adapted tools (to be agreed by the project before use) and correlated with experimental data [RDF.19] [RDF.20][RDF.21][RDF.22].

  Integral or differential energy spectra for protons or neutrons as given in the radiation environment specification.

- Task

  Use integration method for calculation of error rate, taking into account the whole cross section curve and the limited range of protons inside devices.

- Output

  The proton or neutron contribution to error rate.

8.5.7. Calculation toolkit

The CREME software is most commonly used to evaluate upset rates. SPACERAD, OMERE and SPENVIS (which are based on CREME-86) are also widely used. OMERE and SPENVIS also include the ISO standard cosmic ray environment.

Calculation of chord length distribution can be performed by Monte Carlo simulation, or in the case of rectangular parallelepiped volumes by the analytical expression given by Luke and Buehler [RDF.23]. Energy deposition spectra for equation **(27)** can be generated using codes such as Geant4, FLUKA, and MCNPX [RDC.16][RDF.25][RDC.19][RDC.20].

8.5.8. Applicable derating and mitigating techniques

For SEE phenomena such as single event burnout and gate rupture, error or failure rate cannot be quantified along the lines discussed above, so instead radiation assurance is based on derating of maximum operation values.

The derating and mitigation techniques are defined in ECSS-Q-ST-60-15.

8.5.9. Analysis at system level

In the case of single event transient or single event disturb, the component response is highly dependent on electrical test conditions in terms of power supply, charge, frequency, *etc*. For this reason, it is very difficult to define a set of test conditions that is applicable to multiple applications and is not too severe. For the same reason, it is extremely difficult to find applicable experimental data.

Therefore, it is preferable to perform a SET/SED effects analysis in order to determine the effects of SET/SED on equipment performance. In this case, test are not necessary, the estimation of the component behaviour is based on state-of-the-art knowledge for all families. It consists of propagating a standard perturbation signal in the final electrical design to study its influence at system level.

8.6. Destructive SEE

8.6.1. Single event latch-up (SEL) and single event snapback (SESB)

8.6.1.1. Definition

A ***single event latch-up*** is a potentially destructive triggering of a parasitic PNPN thyristor structure in a device (Figure 19). When a latch-up occurs, the current increases and if the power supply is maintained, the device can be destroyed by thermal effect. The use of a current monitoring and a power control circuit allows the power to be shut down quickly after the latch-up is detected in order to protect the device against thermal destruction.

Single event snapback is very similar to a latch-up (*i.e.* it is another high-current mode SEE), but occurs within a single MOS transistor structure. A single high-energy particle can trigger snapback if the field across the drain region is sufficiently high. Snapback occurs when the parasitic bipolar transistor that exists between the drain and source of a MOS transistor amplifies avalanche current that results from the heavy ion. This results in a very high current between the drain and source region of the transistor, with subsequent localised heating.

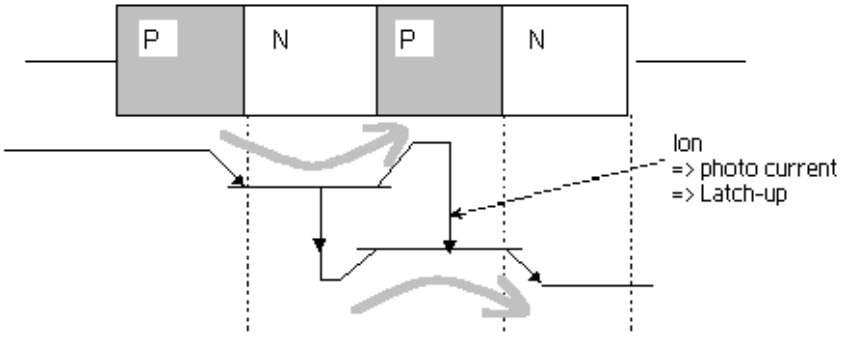

Figure 19: Diagram illustrating parasitic bipolar transistors and current flow associated with single event latch-up.

8.6.1.2. Sensitive devices

- **SEL:** To date, only CMOS, BiCMOS devices have been found to be sensitive to SEL. Complementary bipolar components can also be sensitive (because of the intrinsic PNPN structure) but their integration level is too low and the critical charge for latch-up is too high compared to LET values for heavy ions.
- **SESB:** N-channel MOSFET structures, SOI devices.

8.6.1.3. Modelling

See clause 8.2.

8.6.1.4. Test method

The device is electrically exercised while being irradiated (static or dynamic) with a protection system against thermal destruction [RDF.28]. In static mode the component is put on a stable state and its power supply is monitored (current and level).

A whole characterisation consists of testing the latch-up response of a component using several ions with LET values from nearly 0 MeV·cm²/mg to the maximum level identified in ECSS-E-ST-10-12C Clause 9.4.1.4. In addition, testing using protons are also performed for energies from the minimum threshold (determined by shielding and packaging conditions) to the maximum identified in ECSS-E-ST-10-12C Clause 9.4.1.5. Because of the importance of charge collected by diffusion in the triggering of the SEL event, long-range beams are preferable [RDF.29]. For the same reason, it is advised to consider with caution the use of tilted beams.

Latch-up response can be affected by bias conditions and temperature [RDF.30]. In order to be conservative, the device should be operated at maximum power supply and maximum temperature conditions expected for the final application.

A latch-up is detected when the current exceeds a threshold value defined by de-rating the standard current value [RDF.28]. Dynamic mode is used when the SEL test is associated to SEU or SET testing. In this case, the power supply is monitored while the component is activated. Moreover, in complex circuits, many latch-up paths can occur leading to different current increase levels. In this case, small current variations (micro-latches) are not always detected and therefore a 'simple' functional testing of the device is sometimes performed to ensure that latch-up is detected.

The result of such a test is confirmation that the device is not sensitive to latch-up up to the particle fluence of the test, or latch-up cross section curves versus heavy ion LET values, or proton or neutron energy values. When calculating the SEL cross section, it is important to take into account the dead time introduced by the power supply cycling.

The same characterisation method is used for SESB. It can be difficult to separate a SESB from a SEL. The main differences are:

- SESB is a much more localised effect and therefore draws less power than SEL.
- SESB is temperature independent, whereas SEL has a positive temperature coefficient.
- SEL condition can be removed only with power off while SESB condition can be removed by turning the channel region on and lowering the drain bias.

8.6.1.5. Hardness Assurance

The methods are defined in ECSS-Q-ST-60-15 and applicable documents therein.

8.6.1.6. Prediction issues in case of SEL

Contrary to SEU, SEL cross section versus LET plots of complex devices exhibit a gradual sensitivity increase near threshold and no clear saturation. There are two main reasons for such a behaviour. At first, several SEL paths can occur in complex devices linked to different regions within the device. Therefore, the final plot sums the different contributions. Secondly, depending on the ion characteristic and strike location, different parts of the parasitic thyristor are responsible for the induced SEL (anode or cathode [RDF.31]). This is consistent with the typical slow onset of the threshold part of the curve. Thirdly, the major contribution from diffusion is at the origin of the absence of saturation for higher LETs. These observations indicate that one should not consider a constant sensitive volume for the latch-up event and poses a problem regarding how to deal with SEL when making prediction calculations for complex devices.

8.6.2. Single event gate rupture (SEGR) and single event dielectric rupture (SEDR)

8.6.2.1. Definition

A ***single event gate rupture*** is the formation of a conducting path in the gate oxide due to a high field generated by high current (see Figure 20) Single event dielectric rupture is a similar phenomenon but applies to ionisation in dielectrics generally, such as used in the antifuses of FPGAs. The charges created by the heavy ion crossing the semiconductor are collected and propagate up to the insulator interface making the electric field accross the dielectric exceed a critical value (breakdown voltage).

Unlike latch-up, there is no way to avoid a SEGR becoming destructive. The only way to protect a component against single event gate or dielectric rupture is to use it with electrical conditions that do not allow the SEGR/SEDR to occur (*i.e.* derating).

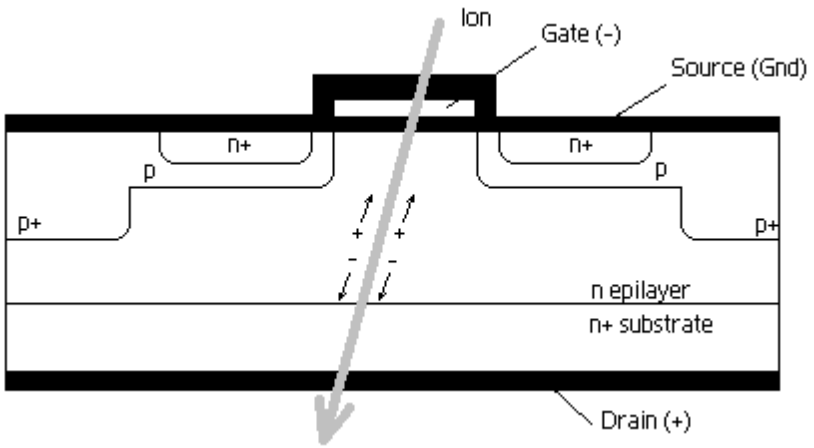

Figure 20: Charge deposition and collection processes associated with single event gate rupture in a power MosFET.

8.6.2.2. Sensitive devices

N and P-channel power MOSFETs [RDF.32][RDF.33], non-volatile NMOS structures [RDF.34], high-density memories and ICs [RDF.35], linear devices [RDF.36], capacitors with very thin gate oxide [RDF.37].

8.6.2.3. Modelling

For this type of event the effective LET concept is not valid (the sensitivity decreases with LET).

8.6.2.4. Test method

Actually, the main objective of the evaluation of a device's response to SEGR or SEDR is not measuring the LET-dependent cross-section curve but rather defining the critical conditions for an SEGR/SEDR to occur. In the case of SEGR in MOSFETs, the test method consists of monitoring the drain and gate voltages and their current while the device is being irradiated. Several supply conditions (V_{DS}/V_{GS}) are applied in order to find the electrical conditions that produce or avoid an SEGR [RDF.38].

The methods are defined in ECSS-Q-ST-60-15 and applicable documents therein.

8.6.2.5. Hardness Assurance

The methods are defined in ECSS-Q-ST-60-15 and applicable documents therein.

8.6.3. Single event burnout (SEB)

8.6.3.1. Definition

A ***single event burnout*** is the destructive triggering of a vertical n-channel transistor accompanied by regenerative feedback (see Figure 21). This occurs in a power MOSFET biased in the OFF state (*i.e.*, blocking a high drain-source voltage) when a heavy ion passing through deposits enough charge to turn the device on. This happens with high current condition.

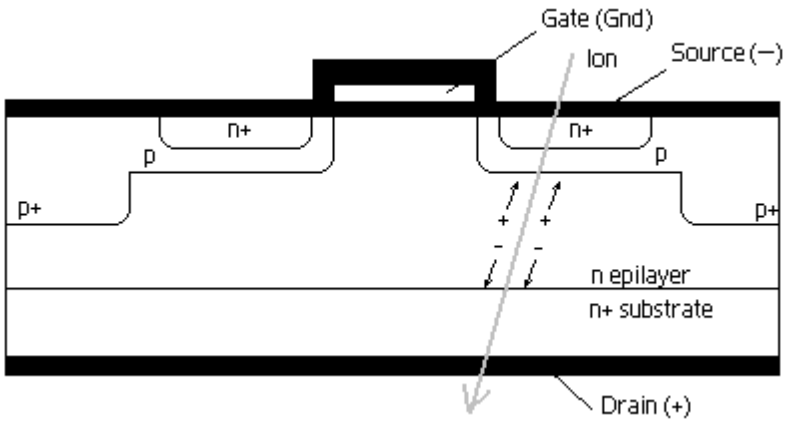

Figure 21: Charge deposition and collection processes associated with single event burn out.

8.6.3.2. Sensitive devices

BJTs, N-channel Power MOSFETs, IGBTs.

8.6.3.3. Modelling

See Clause 8.2. The effective LET concept is not valid (vertical geometry) [RDF.33].

8.6.3.4. Test method

The methods are defined in ECSS-Q-ST-60-15 and applicable documents therein.

8.6.3.5. Hardness Assurance

The methods are defined in ECSS-Q-ST-60-15 and applicable documents therein

8.7. Non-destructive SEE

8.7.1. Single event upset (SEU)

8.7.1.1. Definition

Single event upset is a single bit flip induced in a digital element either by direct ionisation from a traversing particle or by a recoiling nucleus emitted from a nuclear reaction. This event induces no damage to the basic element which can be rewritten with the right value.

8.7.1.2. Sensitive devices

SEUs occur in both memory circuits and VLSI logic devices. Most of the technologies are sensitive to this phenomenon (Si CMOS and bipolar, SOI and GaAs).

8.7.1.3. Modelling

See Clause 8.2.

A particle strike in or near the drain of the OFF transistor(s) in a 4- or 6-transistors basic SRAM cell causes the latch to switch to the opposite state. Changes to either ‘1’ or ‘0’ state are possible. As the basic SRAM cell structure is based on the continuous regeneration of the state of the stored information (using a feedback loop), any perturbation of a critical level and duration causes the cell to regenerate in the other stable state [RDF.40].

In the case of DRAMs, a particle strike in or near either the storage capacitor or the source of the access transistor provokes what is usually referred to as ‘1 to 0’ errors. This mechanism prevails over the other error sources. However, ‘0 to 1’ transitions are also observed and attributed to the source/drain shunt of the access transistor [RDF.40].

8.7.1.4. Test method

The part is exposed to the beam and a test system operates the component in order to check for the integrity of the stored information. Several test patterns are run to measure the sensitivity for both bit flip polarities (0 to 1 or 1 to 0 transitions) [RDF.40]. The testing can be performed while the device is exercised in static or dynamic mode [RDF.13]. A ‘low’ bias level is the worst case for SEU response (lower critical charge and therefore LET threshold) [RDF.14].

8.7.1.5. Hardness assurance

On orbit predictions can be performed as described in Clauses 8.5.2 to 8.5.7.

The rate unit is “number of events per day and per device or bit.”

8.7.2. Multiple-cell upset (MCU) and single word multiple-bit upset (SMU)

8.7.2.1. Definitions

Multiple-cell upsets (MCUs) occur when two or more bits (physically adjacent or not) become corrupted by a single particle, or its secondary particles from nuclear interactions. These erroneous bits can appear to be physically adjacent (clusters of

errors) or in the case of SMUs, logically related (word/bit line errors in a DRAM, several corrupted bits within a common word) depending on the location of the interaction, *i.e.* whether it is within the memory array or the control circuitry area [RDF.41][RDF.42]. Multiple Bit Upsets (MBU) refers to the basic principle of one particle or interaction event causing one upset. Other acronyms refer to the functional anomaly (for instance a SMU can be the anomaly signature of a SEFI in which case it is a SEE but not a true MBU).

8.7.2.2. Devices susceptible to MCU

Circuits sensitive to charge collection by diffusion, or charge sharing from a single ion are susceptible to MCUs. This type of phenomenon is primarily of concern for high levels of integration. Several MBU/SMU error modes are observed in DRAM/SDRAM circuits due to their complex operation modes. SMUs are particularly troublesome because traditional error detection codes (EDAC) can fail to correct this sort of event.

8.7.2.3. Modelling

In the case of MCUs/SMUs caused by a single particle striking physically adjacent cell, different mechanisms are involved [RDF.43]:

- diffusion of charge to adjacent nodes;
- charge transfer between adjacent cells due to a shunt effect. The ion track acts as a conductive path and a current conduit is formed between the two structures. Excess charge, not generated by the ion, can move through this conduit leading to more collected than deposited charge;
- charge collected from an ion track intersecting a number of cells.

As device geometry shrinks (smaller volumes and spacing between cells), the device feature size approaches ion track dimensions. Therefore multiple bits upsets are very sensitive to the angle of incidence and the characteristics of the particle (LET, energy, range) emphasising the limitation of standard characterisations using low energy ions. Moreover, the basic assumption of a rectangular parallelepiped sensitive volume does not take into account coupling phenomena and its validity is questionable for grazing angles. The bias condition is also an important parameter (state of the neighbouring cells).

In the case of 'logical' MCUs (*i.e.* SMUs), the following failure modes can be described in DRAMs. For example, bit-line mode upsets can occur due to the collection of charges into a diffusion region which is electrically connected to the bit access lines while in a floating logic state, and that is during a read cycle (prior to or during the sensing operation). In this case, temporal characteristics of the strike in relation to the clocking signal are critical [RDF.44][RDF.45].

The use of redundant bit lines and a word redundancy array permits the replacement of defective word lines in the main array of the device. The decoding information of these redundant rows/columns can be stored in latch circuits and, therefore, their integrity can be corrupted under exposure to ionising radiation.

An erroneous state of the address decoder can lead to unknown data being stored in the cells during a refresh/read cycle.

Depending on the device architecture and failure mode, the bits affected can reside in the same digital word, leading to a SMU.

8.7.2.4. Test

MCUs/SMUs can be detected with the standard SEU test approach. However, the use of a physical-to-logical map is mandatory to investigate physical MCUs (this mapping can be realised by means of a laser experiment). As many parameters influence the MCU device response (energy, LET, angle, bias, *etc.*), a full set of measurements should be performed to characterise a device [RDF.46][RDF.47]. For instance, the notion of threshold LET doesn't apply in this case as studies have shown that the critical angle to induce MCU increases with decreasing LET.

The timing conditions are very important to evaluate the sensitivity to word/bit line errors, including the representativeness of the refresh frequency to the final application (the highest specified frequency is the worst case). A testing limitation can arise for the test facility to accommodate the large number of errors to be recorded for each event (a complete row for instance).

Generally, the cross section of this class of event is small in comparison with those of memory elements, the cross section cannot be accurately measured without irradiating the device with a significant fluence. The analysis of the event signature is important to identify the impact on the system and the origin of the error.

8.7.2.5. Hardness assurance

On orbit predictions can be performed as described in Clauses 8.5.2 to 8.5.7.

The rate unit is “the number of events per day and per component or bit.”

8.7.3. Single event functional interrupt (SEFI)

8.7.3.1. Definition

A ***single event functional interrupt*** is caused by a single ion strike or nuclear interaction that leads to a temporary non-functionality (or interruption of normal operation) of the affected device. A SEFI is not accompanied by a high current condition and can last as long as the power is maintained (persistent SEFI) or a reset is sent to resume the normal operation.

8.7.3.2. Susceptible components

Complex devices with embedded state machine/control sections as in the case of many modern memories (flash-EPROMs, EEPROM, DRAMs, SDRAMs), FPGAs, ADCs, Processors, DSPs [RDF.42][RDF.48][RDF.49].

SEFI remains loosely defined as many causes and signatures are observed depending on the circuit. As the complexity of devices becomes greater, new kinds of event are encountered that can be classified into the SEFI category.

8.7.3.3. Modelling

See Clause 8.2.

8.7.3.4. Test method

A SEFI characterisation is performed as for SEU characterisation. However, the SEFI occurrence can be operating-mode dependent. Furthermore, due to the complexity of the device susceptible to this class of event, it is important that the test application is able to exercise most of the internal functional sub-structures and parse the events based on their specific signatures and recovering modes [RDF.50].

Generally, the SEFI cross section is small in comparison with those of memory elements. As a SEFI results in the loss of functionality of the device, the fluence for the first event to occur is recorded (as a result, there is also significant statistical uncertainty for the measured cross section).

8.7.3.5. Hardness assurance

On orbit predictions can be performed as described in Clause 8.5.2 to 8.5.7.

The rate unit is the ‘number of events per day and per component or bit’.

Conditions for the device to recover proper operation (power supply cycling, reset, *etc.*).

8.7.4. Single event hard error (SEHE)

8.7.4.1. Definition

A ***single event hard error*** (also referred to as a ***"stuck" bit error*** or ***hard fault***) is an unalterable change of state that is associated with semi-permanent damage to a memory cell from a single ion track or nucleon-nuclear interaction. It's related to a micro-dose circuit effect.

8.7.4.2. Devices susceptible to SEHE

SEHE was first observed in resistive-load SRAM devices [RDF.54][RDF.55][RDF.56] but are also of concern for DRAMs. Evidence of such effects in 4Mb DRAMs can be found in [RDF.57]. In DRAMs, decreasing retention time effects observed after irradiation are also linked to this failure mode.

As the relative size of the ion track and device "sensitive" region is of primary importance, this failure mode can be of concern for future technologies as a result of the effects of scaling.

8.7.4.3. Modelling

This effect is induced by the local deposition of oxide charge by a heavy ion within the gate region, or in a narrow area of the bird's beak region in the case of LOCOS technologies [RDF.51][RDF.52][RDF.53]. This failure mode is attributed to high increase of the leakage current in the impacted transistor. This effect is dependent on ion track structure (and therefore the particle species and energy) that affects the interface trapped charge distribution responsible for the induced leakage current which produces an inversion layer.

As mentioned in the definition, stuck bits are semi-permanent errors that is to say that annealing is observed at ambient temperature as a result of recombination of the interface trapped holes with electrons crossing the Si/SiO_2 interface by tunnelling. The lifetime for the persistence of SEHE events therefore ranges from several hours to weeks.

8.7.4.4. Test method

Up to now, there's no testing procedure applicable to hard errors. However, the following comments can be considered in a future guideline.

A hard error is a single event phenomenon as one single ion is able to induce this failure mode. Therefore SEU standard testing procedures can be applied (the cross sections determined from the number of stuck bits for a received particle fluence). However, depending on the device type, stuck bits are detected with the test pattern used under exposure (DRAM) or with the complementary one (SRAM).

The cross section concept applies to this type of event (sensitive area). The notion of critical charge (LET threshold) is not relevant, and the variable to be taken into account in this case is the species/energy/incidence angle of the ion (with the ion's track wide enough to cover a significant region of the gate region).

The combined effects of total ionising dose and microdose has also to be taken into account. Actually, the addition of a certain level of total dose can reveal the degradation due to particle impacts (latent stuck bits).

In the case of DRAMs, the clock speed used for the refresh mode should affect the device response to SEHE.

8.7.4.5. Hardness assurance

For devices exhibiting a linear relationship between the number of SEHE events and the received fluence, a cross section versus LET curve can be measured. Therefore rates can be calculated using the same methods used for SEU [RDF.57]. However, it is important that studies on the angular dependence of device sensitivity are carried out.

8.7.5. Single event transient (SET) and single event disturb (SED)

8.7.5.1. Definition

A single event transient or single event disturb is a momentary voltage excursion (voltage spike) at a node in semiconductors [RDF.59]. The voltage spike is originally formed by the electric field separation of the charge generated by an ion passing through or near a circuit junction (obviously, the effect can similarly be induced by a nuclear-interaction event).

Depending the node where it has appeared, the spike propagates inside the circuit. Depending when and where it occurs, a local spike can have several consequences at the component level:

- The spike can be absorbed by local RC elements of the circuit and have no impact on the component behaviour.
- The spike can be propagated up to at least one output of the component.
- It can be converted to an SEU when the signal reaches a latch.

A non-captured SET that has propagated up to the circuit's output is characterised by its amplitude and its duration. Whether the spike propagates to the whole system depends on the RC equivalent circuit the output sees.

SET tends to refer to transients induced in linear circuits and therefore the name of single event disturb is used for an SET in digital devices or clocks. The signal perturbation is very short but can, in some cases, propagate through the whole system depending on where and when it occurs and how the numeric signal is used.

8.7.5.2. Sensitive devices

All linear circuits are known to be sensitive to SET (operational amplifiers, comparators, voltage regulators, pulse-width modulators, ADCs). Opto-electronics (CCD, IR arrays, opto-couplers, fibre-optic data links, *etc.*) are also very sensitive as the typical optical signal used in photo-detectors has a very low power. The electrical signal that represents a single bit is normally 100 to 1000 electrons and is easily corrupted by even lightly ionising particles that strike the detector.

SEDs can also disturb fully combinatorial logic devices (such as switches, bus line drivers, logic gates), clocks and PLLs, asynchronous control signals (ASIC, processors, memories, FPGAs). This phenomenon is particularly important for signals which are already in transition. Depending on the device and signal function, the consequence of a SET/SED can be very different:

- logic gates suffer a short perturbation in the output signal;
- switches, bus line drivers: commutation and short output signal perturbation;
- clocks and PLLs: short output signal perturbation, loss of one cycle, and change of frequency;
- asynchronous control signals: short output signal perturbation.

8.7.5.3. Modelling

See Clause 8.2.

8.7.5.4. Test method

The device is electrically and functionally exercised while being irradiated. Its output is monitored and compared to a reference response. SET/SED events are counted and registered. The SET/SED response is very dependent on electrical test conditions (*e.g.* power supply, charge, frequency) and it is therefore important to use existing data with care [RDF.60][RDF.61]. If convenient, SET and SED can be split in several categories depending on their impact at system level.

8.7.5.5. Hardness assurance

On orbit predictions can be performed as described in Clauses 8.5.2 to 8.5.7. Note that this implies a complete characterisation of the SET susceptibility as a function of the electrical test conditions (power supply, output load, frequency, *etc.*). In this case, the rate unit is the 'number of events per day and per component'. More often, a SET effects analysis is done in order to determine the impact of SET on the equipment performance. See Clause 8.5.9.

Hardening design rules exist in order to prevent the propagation at system level of the short perturbation of the output signal. They consist in choosing output equivalent charges high enough to filter the spike without changing the analogue function.

Any remaining SETs which have a strong impact at system level because they change the state of the sensitive component (*e.g.* parasitic commutation of a switch) are studied in the same way as SEU (test and rate calculation).

8.8. References

[RDF.1] E Petersen, "Single event analysis and prediction," IEEE Nuclear and Space Radiation Effects Conference, Short Course section III, 1997.

[RDF.2] C Inguimbert *et al*, "Using a carbon beam as a probe to extract the thickness of sensitive volumes," Proceedings of the 5th RADECS, pp180, 1999.

[RDF.3] P J McNulty. *et al*, "Modelling charge collection and single event upsets," *Nucl Instrum Meth Phys Res*, **B61**, pp52, 1991.

[RDF.4] A Chugg *et al*, "Probing the charge collection Sensitivity profile using a pico-second pulsed laser at a range of wavelengths," *IEEE Trans Nucl Sci*, **49**, No 6, pp2969, 2002.

[RDF.5] EIA/JEDEC standard (EIA/JESD57), "Test procedures for the measurement of single event effects in semiconductor devices from heavy ion irradiation," December 1996.

[RDF.6] ESA/SCC Basic specification 25100, "Single event effects test method and guidelines," October 1996.

[RDF.7] JEDEC JSDC89, "Measurement and reporting of alpha particles and terrestrial cosmic ray-induced soft errors in semiconductor devices," August 2001, 2005 update in draft.

[RDF.8] R A Reed *et al*, "Evidence for angular effects in proton-induced single-event upsets," *IEEE Trans Nucl Sci*, **49**, No 6, pp3038-3044, 2002.

[RDF.9] S D Kniffin *et al*, "Angular effects in proton-induced single-event upsets in silicon-on-sapphire and silicon-on-insulator devices," IEEE Radiation Effects Data Workshop, 22 July 2004 pp115–119, 2004.

[RDF.10] R Koga, "Single event effect ground test issues," *IEEE Trans Nucl Sci*, **43**, No 2, pp661, 1996.

[RDF.11] S M Guertin *et al*, "Angular dependence of DRAM upset susceptibility and implications for testing and analysis," *IEEE Trans Nucl Sci*, **47**, No 6, pp2380, 2000.

[RDF.12] W J Stapor, "Single event effects qualification", IEEE Nuclear and Space Radiation Effects Conference, Short Course, Section II, 1995.

[RDF.13] S Duzellier, and R Ecoffet, "Recent trends in single event effect ground testing," *IEEE Trans Nucl Sci*, **43**, No 2, pp671, 1996.

[RDF.14] F W Sexton "Measurement of single event phenomena in devices and ICs," IEEE Nuclear and Space Radiation Effects Conference, Short Course, Section III, 1992.

[RDF.15] J N Bradford "Geometrical analysis of soft errors and oxide damage produced by heavy cosmic rays and alpha particles," *IEEE Trans Nucl Sci*, **27**, pp942, Feb 1980.

[RDF.16] C Inguimbert, *et al*, "Study on SEE rate prediction: analysis of existing models", Rapport technique de synthèse, RTS 2/06224 DESP, June 2002.

[RDF.17] J C Pickel and J T Blandford, "Cosmic-ray induced errors in MOS devices," *IEEE Trans Nucl Sci*, **27**, No 2, pp1006, 1980.

[RDF.18] J H Adams, "Cosmic ray effects on microelectronics, Part IV," NRL memorandum report 5901, 1986.

[RDF.19] P J McNulty *et al*, "Proton induced spallation reactions", *Rad Phys Chem*, **A43**, No 1, pp139, 1993.

[RDF.20] P Calvel *et al.*, "An empirical model for predicting proton induced upset," *IEEE Trans Nucl Sci*, **43**, No 6, pp2827, 1996.

[RDF.21] C Inguimbert *et al.*, "Proton upset rate simulation by a Monte Carlo method," *IEEE Trans Nucl Sci*, **44**, No 6, pp2243, 1997.

[RDF.22] E L Petersen, "The relationship of proton and heavy ion upset thresholds," *IEEE Trans Nucl Sci*, **39**, pp1600, Oct 1992.

[RDF.23] K.L. Luke, M.G. Buehler, "An exact, closed-form expression of the integral chord-length distribution for the calculation of single-event upsetsinduced by cosmic rays", J. Appl. Phys. 64 (10), November 1988, p. 5132.

[RDF.24] S Agostinelli *et al*, "Geant4 – a simulation toolkit," *Nucl Instrum Meth Phys Res*, **A506**, p250-303, 2003

[RDF.25] P R Truscott, F Lei, C Dyer, C Ferguson, *et. al*, "Geant4 - a new Monte Carlo toolkit for simulating space radiation shielding and effects," IEEE Radiation Effects Data Workshop 2000, IEEE Proceedings 00TH8527, pp147-152, 2000.

[RDF.26] L S Waters, ed., "MCNPX User's Manual, Version 2.4.0," LA-CP-02-408, 2002.

[RDF.27] A Fasso, A Ferrari, J Ranft, P R Sala, "FLUKA: status and prospective for hadronic applications," Proceedings of the Monte Carlo 2000 Conference, Lisbon, October 23-26, pp 955-960, 2000, A Kling, F Barao, M Nakagawa, L Tavora, P Vaz, Eds, Springer-Verlag Berlin.

[RDF.28] EIA/JESD78 (IC Latch-up test, March 1997)

[RDF.29] A H Johnston, "The influence of VLSI technology evolution on radiation-induced latch-up in Space System," *IEEE Trans Nucl Sci*, **43**, No 2, pp505, 1996.

[RDF.30] A H Johnston *et al*, "The effect of temperature on single-particle latch-up," *IEEE Trans Nucl Sci*, **38**, pp1435, 1991.

[RDF.31] G Goto, H Takahashi, T Nakamura, "Modeling and analysis of transient latchup in double-well bulk CMOS," *IEEE Trans Electron Dev*, **ED33**, No 9, pp1341-1347, 1986.

[RDF.32] J L Titus *et al*, "Impact of oxide thickness on SEGR failure in vertical power MOSFETs: development of a semi-empirical expression," *IEEE Trans Nucl Sci*, **42**, No 6, pp1928, 1995.

[RDF.33] J L Titus *et al*, "Experimental study of single event gate rupture and burnout in vertical power MOSFET's," *IEEE Trans Nucl Sci*, **43**, No2, pp533, 1996.

[RDF.34] T F Wrobel *et al*, "On heavy ion induced hard-errors in dielectric structures," *IEEE Trans Nucl Sci*, **34**, No 6, pp1262, 1987.

[RDF.35] G Swift *et al*, "An experimental survey of heavy ion induced dielectric rupture in Actel field programmable gate arrays (FPGAs)," proceedings of the 3rd RADECS, pp425, 1995.

[RDF.36] G Lum *et al.*, "The impact of single event gate rupture in linear devices," *IEEE Trans Nucl Sci*, **47**, No 6, pp2373, 2000.

[RDF.37] L W Massengill *et al*, "Heavy-ion-induced breakdown in ultra-thin gate oxides and high-k dielectrics," *IEEE Trans Nucl Sci*, **48**, No 6, pp1904, 2001.

[RDF.38] MIL-STD-750-D Military Standard Test Methods for Semiconductor Devices, FSC 5961, February 28, 1995.

[RDF.39] D L Oberg *et al*, "Firsts non-destructive measurements of power MOSFET single event burnout cross sections," *IEEE Trans Nucl Sci*, **34**, No 6, pp1736, 1987.

[RDF.40] P E Dodd, "Basic mechanisms for single event effects", IEEE Nuclear and Space Radiation Effects Conference, Short Course, Section II, 1999.

[RDF.41] D Falguère *et al*, "In-flight Observations of the radiation environment and its effects on devices in the SAC-C polar orbit," presented at NSREC 2002.

[RDF.42] K A Label *et al*, "Anatomy of an in-flight anomaly: investigation of proton-induced SEE test results for stacked IBM DRAMs," *IEEE Trans Nucl Sci*, **45**, No 6, pp2898-2903, December 1998.

[RDF.43] S Buchner *et al*, "Investigation of single-ion multiple-bit upsets in memories on board a space experiment," Proc. 5th RADECS Conf., pp 558, 1999.

[RDF.44] S Duzellier *et al*, "Application of laser testing in study of SEE mechanisms In 16-Mbit Drams," *IEEE Trans Nucl Sci*, **47**, No 6, December 2000.

[RDF.45] A Makihara *et al*, "Analysis of single-ion multiple-bit upset in high-density DRAMs," *IEEE Trans Nucl Sci*, **47**, No 6, pp2400-2404, December 2000.

[RDF.46] C S Dyer *et al*, "Microdosimetry code simulation of charge-deposition spectra. Single event upset and multiple bits upsets," *IEEE Trans Nucl Sci*, **46**, No 6, pp1486, December 1999.

[RDF.47] O Musseau *et al*, "Analysis of multiple bit upsets (MBU) in a CMOS SRAM," *IEEE Trans Nucl Sci*, **43**, No.6, December 1996.

[RDF.48] R Koga et al, "Single event functional interrupt (SEFI) sensitivity in microcircuits," Proc. 4th RADECS Conf., pp311, 1997.

[RDF.49] L Hoffmann, R C DiBari, R Katz, L Cohn, "Radiation testing and characterisation of programmable logic devices," IEEE Nuclear and Space Radiation Effects Conference, Short Course, Section V, 2000.

[RDF.50] R Koga *et al*, "Permanent single event functional interrupts (SEFIs) in 128- and 256-Mb synchronous dynamic random access memories (SDRAMs)," *IEEE Trans Nucl Sci*, **48**, No 6, December 2001.

[RDF.51] J G Loquet *et al*, "Calculation of heavy ion induced leakage current in n-MOSFET," *IEEE Trans Nucl Sci*, Vol. **47**, December 2000.

[RDF.52] J G Loquet *et al*, "Simulation of heavy-ion-induced failure mode in n-MOS cells of ICs," *IEEE Trans Nucl Sci*, **48**, pp2278, December 2001.

[RDF.53] J P David *et al*, "Heavy ions induced latent stuck bits revealed by total dose irradiation in 4T cells SRAMs," Proc. 5th RADECS Conf., pp80, 1999.

[RDF.54] T R Oldham *et al*, "Total dose failure in advanced electronics from single ions," *IEEE Trans Nucl Sci*, **40**, No 6, pp1820-1830, 1993.

[RDF.55] C Dufour *et al*, "Heavy ion induced single hard errors on sub-micron memories," *IEEE Trans Nucl Sci*, **39**, No 6, pp1693-1697, 1992.

[RDF.56] R Koga, *et al.*, "On the suitability of non-hardened high density SRAMs for space application," *IEEE Trans Nucl Sci*, **38**, No 6, pp1507-1511, 1991.

[RDF.57] S Duzellier *et al.*, "Protons and Heavy ions induced stuck bits on large capacity DRAMs," Proc. 2nd RADECS Conf., pp468, 1993.

[RDF.58] L D Edmonds, "Ion-Induced Stuck bits in 1T/1C SDRAM cells", *IEEE Trans Nucl Sci*, **48**, No 6, pp1925-1930, December 2001.

[RDF.59] T L Turflinger, "Single-Event Effects in Analog and Mixed-Signal Integrated Circuits," *IEEE Trans Nucl Sci*, **43**, No 2, pp594, 1996.

[RDF.60] R Harboe-Sorensen *et al*, "Single event transient characterisation of analog IC's for ESA's satellites," Proceedings of the 5th RADECS Conference, pp573, 1999.

[RDF.61] C Poivey *et al*, "Development of a test methodology for single event transients (SETs) in linear devices," *IEEE Trans Nucl Sci*, **48**, No 6, pp2180, 2001.

[RDF.62] ECSS-Q-ST-60-15 "Space product assurance - EEE component radiation hardness assurance"

9
Radiation-induced sensor backgrounds

9.1. Introduction

In addition to the effects described in the previous sections, mission-specific flight hardware can suffer from enhanced background and degradation depending on the instrument function and design. Such issues are often encountered for space science missions, and are especially a problem for instruments which are themselves radiation detectors. The potential range of effects include enhanced backgrounds in sensors from direct ionisation or charging by incident particle radiation and secondaries, and delayed radiation effects particularly from the build-up of radioactivity in the materials of the spacecraft and instrument.

Assessment of potential effects involves examination of the range of mechanisms by which the primary and secondary radiation can deposit energy, or charge, or impart momentum to parts of a sensor in a manner which meets the criteria for the event to be accepted by the sensor electronics, or to induce sufficient drift in instrument performance.

This chapter provides a review of some of the possible effects for space science missions. The information is necessarily qualitative since the response of specific equipment depends very much on the instrument design. However, methods of quantifying effects, particularly proven simulation techniques, are discussed.

9.2. Background in ultraviolet, optical and infrared imaging sensors

Current imagers for ultraviolet, optical and near-infrared wavelengths often use CCDs. Furthermore, increasing use is being made of charge injection devices (CIDs) and CMOS active pixel sensors (APSs) as these do not suffer problems associated with charge transfer between pixels. At other wavelengths of the infrared spectrum, the principal sensor material types are InSb, InGaAs, GaAs/GaAlAs, HgCdTe, PtSi and extrinsic silicon (see Table 11) [RDG.1]. All are subject to transients from ionisation both from direct ionisation by charged particles and nuclear interactions, in an analogous process as for single event effects. These can produce changes to single pixels, or multiple pixels if charge overflows into neighbouring pixels, or if the particle impacts at an oblique angle or produces secondaries that travel close to the detector plane.

Table 11: Typical materials for UV, visible and IR sensors, with band-gap and electron-hole production energies (e-h production energy for MCT is based on Klein semi-empirical formula.

Material	Operating waveband	Bandgap [eV]	e-h production energy [eV]
Si	UV - SWIR LWIR	1.12	3.6
InSb	visible to MWIR	0.24	1.1
InGaAs	SWIR	0.73	3.2
HgCdTe (MCT)	SWIR - LWIR	0.19 (MWIR) 0.12 (LWIR)	1.3 (MWIR) 1.1 (LWIR)
GaAs/GaAlAs	LWIR	1.42 (GaAs)	4.6 (GaAs)
NOTE: See [RDG.2].			

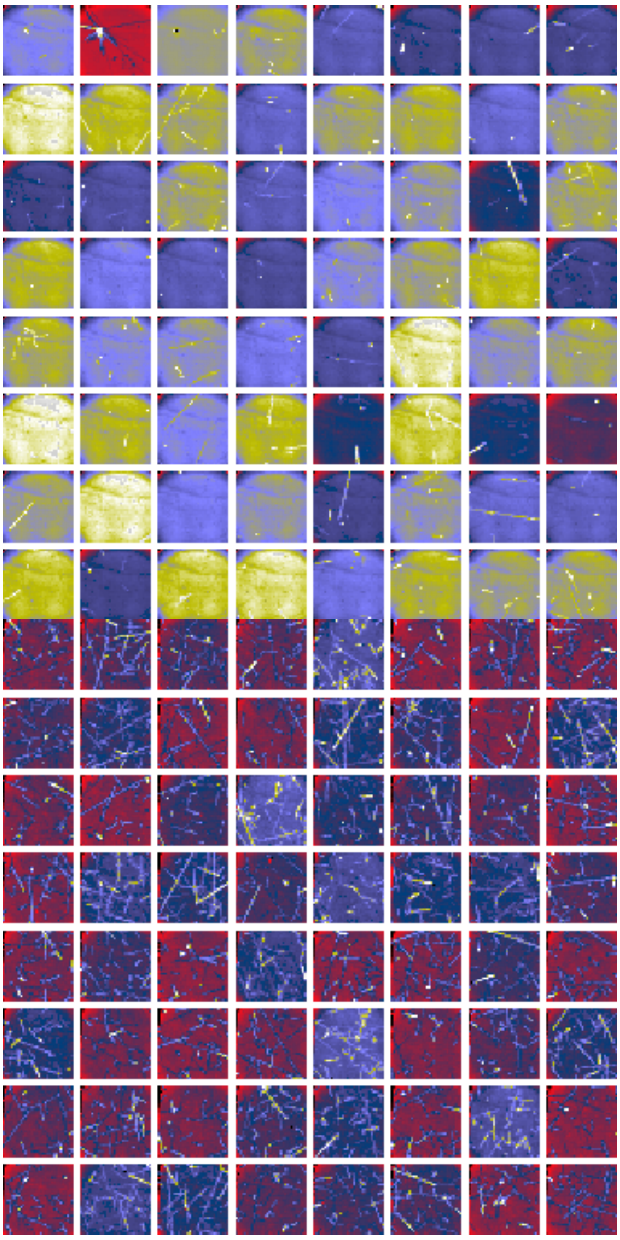

Courtesy of Marc Sauvage, CEA-Saclay

Figure 22: ISOCAM images for quiet conditions (top) and during solar flare event of November 1997.

Some experience of radiation-induced backgrounds in space-based InSb infrared detectors comes from ISO (see Figure 22). The ISO science window was open during the outer belt passage and as a result a degree of correlation was reported between detector glitches and energetic electron fluxes as observed by the GOES series of spacecraft in the geostationary orbit [RDG.3]. This was the case especially at the extremes of the science window, *i.e.* at ISO altitudes roughly comparable to that of GOES. In addition to incident electrons these effects can be due to electron bremsstrahlung in the outer structures of the spacecraft or instrument shielding.

Galactic cosmic ray effects also show up as a continuous particle track or “glitch” background. Due to the high energies involved, there is very little that can be done to exclude these effects, and increasing the shielding thickness can in fact be deleterious since more secondary particles (neutrons, protons, spallation products) are generated, thus potentially adding to the problem.

The number of electron-hole pairs released from an ionising particle in a pixel can be estimated from the energy deposition and energy used to produce a single electron-hole pair (see Table 11). The energy deposition spectrum from ions can be calculated based on the incident particle spectrum, the particle LETs (approximated using the stopping power) and the pathlength distribution through the detector – in essence the same principles used to estimate single event upset rates in microelectronics using tools such as CREME96 (discussed in Clause 8.5).

$$\frac{d\Psi}{d\varepsilon}(\varepsilon) = \frac{A}{4}\int_{E_{\min}}^{E_{\max}} \frac{d\Phi}{dE}(E) \cdot \frac{dP_{CL}}{dD}\left(\frac{\varepsilon}{LET(E)}\right) \cdot \frac{1}{LET(E)} dE$$

approximated to:

(28)

$$\frac{d\Psi}{d\varepsilon}(\varepsilon) = \frac{A}{4}\int_{E_{\min}}^{E_{\max}} \frac{d\Phi}{dE}(E) \cdot \frac{dP_{CL}}{dD}\left(\varepsilon\left\{\frac{dE}{dx}(E)\right\}^{-1}\right)\left\{\frac{dE}{dx}(E)\right\}^{-1} dE$$

where:

$d\Psi/d\varepsilon(\varepsilon)$ = energy deposition rate spectrum;

A = total surface area of the SV or detector;

$d\Phi/dE(E)$ = differential incident particle flux spectrum expressed as a function of energy, E;

$dP_{CL}/dD(D)$ = differential chord length distribution through the sensitive volume for an isotropic distribution;

$dE/dx(E)$ = stopping power for particles of energy E;

E_{min} = minimum energy for the incident particle spectrum;

E_{max} = maximum energy of the incident particle spectrum.

This expression assumes the incident particle spectrum on the detector is or can be approximated to a isotropic angular distribution. Furthermore, it is assumed that the change in the stopping power of the particle through the sensitive volume and any multiple scattering can be neglected.

If a higher fidelity analysis is performed, especially where the energy deposition spectrum from proton-nuclear interactions is calculated, more detailed radiation transport tools can be applied, although the event rate can be estimated based on the incident particle spectrum and the nuclear interaction cross section. Even for monoenergetic ions passing through a pixel, fluctuations in the number of electron-hole pairs occur between events as a result of:

- Differences in the path-length taken through the pixel for an omnidirectional source;
- Lateral spreading of charge;
- Energy-loss straggling (*i.e.* differences between events due to the stochastic nature of the energy-loss process).

Note that δ-ray electrons can carry part of the energy lost by the particle to the material away from the sensitive volume. Based on the energy lost by a minimum ionising proton, one can expect approximately 100 e-h pairs to be produced per micrometre, where as δ-ray production reduces this to ≈ 80 e-h pairs [RDG.1] (*i.e.* the energy is based on the energy *gained* by the material within the sensitive volume rather than the energy lost by the particle in the volume).

In addition to the above energy deposition processes, the definition of the sensitive volume is also affected by potential charge funnelling effects (see Clause 8.5).

For nucleon-nuclear collision-induced energy deposition, the complexity of the initial nuclear interaction and subsequent ionisation processes by the interaction products

make it simplest to apply radiation simulation tools such as Geant4, MCNPX, and FLUKA (see Table 4). However, if it is possible to define a response function for the energy deposition spectrum due to nuclear interaction by a particle of energy E, and provided that the dimensions of the detector volume are small compared with the ranges and mean-free paths of the incident particles, then:

$$\frac{d\Psi}{d\varepsilon}(\varepsilon) = \frac{MN_A}{W}\int_{E_{\min}}^{E_{\max}} \frac{d\Phi}{dE}(E)\cdot\sigma(E)\cdot\frac{dP}{d\varepsilon}(E,\varepsilon)dE \qquad \textbf{(29)}$$

where:

M = mass of sensitive volume;

N_A = Avogadro's constant;

W = atomic or molecular mass of the material making up the detector;

$\sigma(E)$ = nuclear-interaction cross-section for the material as a whole due to incident particles of energy E;

$dP/d\varepsilon(E,\varepsilon)$ = energy deposition rate spectrum (or response function) for incident particles of energy E, and energy deposition, ε;

(Other variables are as defined above).

9.3. Background in charged particle detectors

Charged particle detectors are used in space both for scientific purposes and for engineering-type radiation monitoring. Background in such instruments is caused mainly by primary and secondary particles entering the detector system from outside the view cone. This can be ameliorated to a certain extent by active or passive shielding around the detectors, by using coincidence or anti-coincidence techniques (or both), and generally by optimising the instrument configuration by Monte Carlo radiation transport simulations.

In simpler monitor-class instruments, a typical problem is the separation of energetic protons from electrons. Such cross-contamination often leads to one particle species being registered in an energy channel intended for the other particle.

The semiconductor and scintillating detectors used in charged particle instruments are obviously prone to the total dose and non-ionising dose effects described elsewhere in this document, and the electronics systems of such devices can experience SEE phenomena as any other instrumentation. In certain cases, it is the task of the charged particle instrument to provide a radiation alarm for the host spacecraft. For such critical applications, it is especially important that the system be designed to withstand the very environment it is monitoring.

9.4. Background in X-ray CCDs

Instruments such as EPIC and RGS on the ESA X-ray Multi-mirror Mission (XMM) spacecraft, and ASIC on the NASA Chandra X-ray telescope use concentric grazing incidence mirrors to focus X-rays onto CCD detectors. Obviously one issue associated with their use is displacement damage induced in the CCDs (see 7) particularly from low-angle scattering of low-energy (<1 MeV) protons through the mirrors. Consideration should be given to the efficiency of this process and to mitigation measures such as shielding the detectors during passage through radiation belts [RDG.4][RDG.5].

Other mechanisms by which background levels can be enhanced by the particle radiation environment are direct ionisation by primaries and secondaries [RDG.6]. Given that a 1 GeV near-minimum ionising proton loses approximately 10 keV within 30 μm of pathlength (depending upon stochastic variations between events), many directly ionising charged hadrons and nuclei can be ignored by the signal processing electronics, depending upon the depletion depth, the upper energy limit of the detector, and the amount of energy lost from the sensitive region by δ-ray production (see Clause 9.2). Note also that low-energy particles entering through the grazing incidence mirrors can contribute to this background. (See Clause 9.2 for further discussion on background in pixelated detectors from charged particles.)

Electromagnetic cascades from the very energetic hadrons and nuclei, and γ-rays from photo-nuclear de-excitation can result in background within the detector bandwidth through Compton scattering of γ-rays. Therefore, although the γ-ray photons can have energies outside the bandwidth of the detector, Compton processes can permit partial energy loss to the X-ray sensor. The event rate can be estimated from a detailed radiation transport simulation to calculate the secondary γ-ray spectrum and integrating the Klein-Nishina cross-section for Compton scattering events and the pathlength distribution for Compton electrons in the detector.

In addition, obviously a proportion of the induced photon spectrum lies within the sensor bandwidth. The intensity from this source depends upon the production rate in local materials and the "optical-depth" for the X-rays in these materials. The spectra is characteristic of the materials, and contain lines from K-, L-, M-shell, *etc.* atomic transitions – materials local to the detector should therefore be chosen carefully to minimise strong X-rays within the detector bandwidth.

Note that γ-rays from radioactive decay can also contribute to the above background sources, although studies performed for XMM suggest effects from cosmic-ray induced radioactivity is a factor of five lower than the prompt effects of electromagnetic showers from cosmic rays.

9.5. Radiation background in gamma-ray instruments

Astrophysical γ-ray detectors usually incorporate charged particle shields to veto ionisation effects in the central detector elements from charged particles. Detectors such as the Oriented Scintillator Spectrometer Experiment (OSSE) instrument on the NASA Compton Gamma Ray Observatory (CGRO), and SPI and IBIS on the ESA INTEGRAL mission use scintillation materials (such as sodium iodide and caesium iodide) or semiconductor materials (*e.g.* germanium and cadmium telluride) as the central detector. In addition, instruments incorporate active collimation detectors (usually based on scintillators) to improve the directional discrimination of the instrument [RDG.7][RDG.8]. Therefore ionisation events which do not trigger the veto shield, but deposit sufficient energy in the central detector contributes to the observed background. Such events include:

- Leakage of γ-rays through the collimator, which have been induced in the spacecraft structure, or as part of the albedo flux from the Earth's atmosphere (produced by cosmic-ray collisions). The γ-ray lines that appear in the instrument are characteristic of the materials in which they are induced.
- Elastic and inelastic neutron-nuclear interactions in the instrument resulting in energy deposition in the sensor. Again these neutrons can be secondaries from the spacecraft or atmospheric albedo. For thermal neutron radiative capture, for example, the response of the detector is the appearance of one or more γ-ray lines associated with the photo-nuclear de-excitation process, whereas the events are less well defined if the nucleus absorbs some of the neutron momentum.
- Radioactive decay following spallation in the instrument. $\beta^{\pm}$ and α decays have an effect if they occur in the active detector elements, whilst γ-rays associated

with these decays or other isomeric transition processes can be effective even if they originate in passive materials. Radioactivity induced in the active elements of the instrument therefore results in a superposition of discrete line spectra, corresponding to energy deposition from γ-rays, internal conversion electrons and α-particles, and continuous line spectra where decays also include $\beta^{\pm}$-emission.

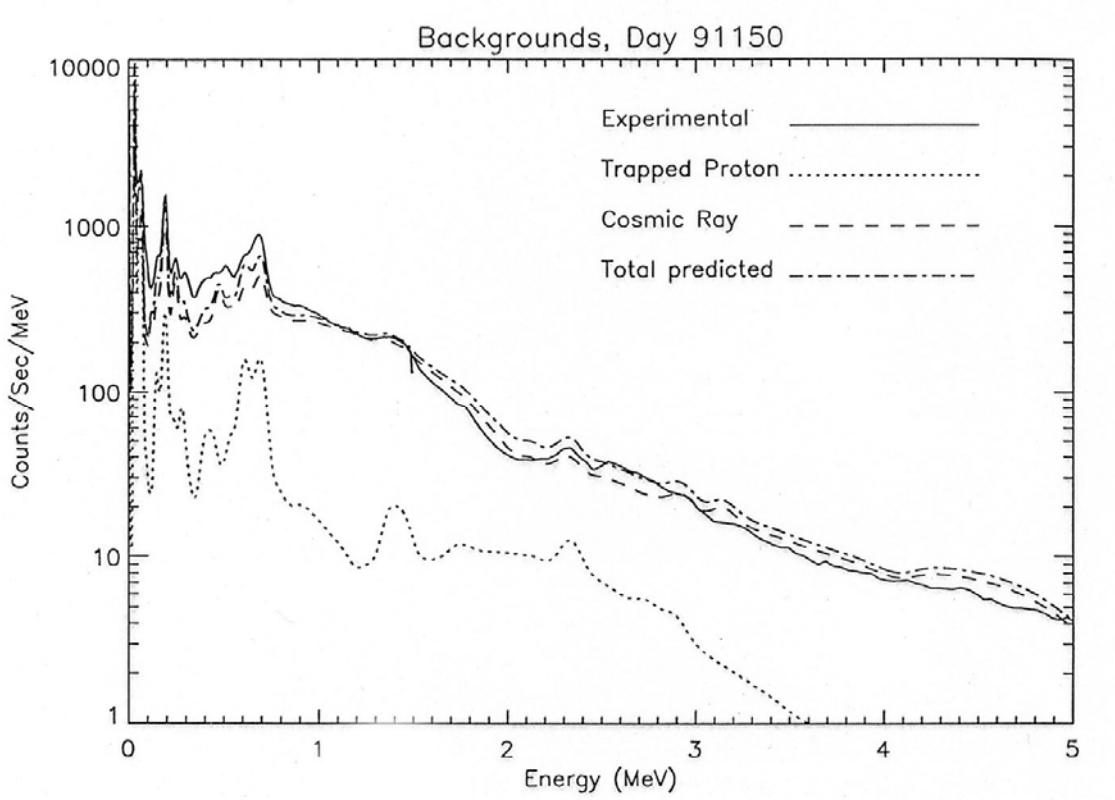

Figure 23: Predicted and measured background spectra observed in OSSE instrument on Compton Gamma-Ray Observatory 419 days after launch [RDG.10].

Figure 23 shows a spectrum with these features taken from the CGRO OSSE instrument 419 days after launch, compared with predicted backgrounds induced by trapped protons and cosmic radiation.

For cases where the dimensions of the detector volume are small compared with the ranges and mean-free paths of the incident particles, then the nuclear interaction rate within the detector can be approximated to the expression:

$$R_i(t) = \frac{MN_A}{W} \sum_j \int_{E_{j,\min}}^{E_{j,\max}} \frac{d\Phi_j}{dE}(E,t) \cdot \sigma_{j \to i}(E) dE \qquad \textbf{(30)}$$

where:

$R_i(t)$ = production rate for nuclide species i at time t;

M = mass of detector;

N_A = Avogadro's constant;

W = atomic or molecular mass of the material making up the detector;

$d\Phi_j/dE(E,t)$ = differential incident flux spectrum expressed as a function of energy, E and time, t for particle species j (these are both primary and secondary particles);

$\sigma_{j\to i}(E)$ = nuclear-interaction cross-section for the production of nuclide i in the detector material due to incident particle species j of energy E;

$E_{j,min}$ = minimum energy for the incident particle spectrum, j;

$E_{j,max}$ = maximum energy of the incident particle spectrum j.

More complex analytical expressions can be developed for cases where energy loss, secondary particle interactions or charged particle multiple scattering are significant. However, it is generally more straightforward to resort to detailed radiation transport simulation using codes such as Geant4, MCNPX and FLUKA.

The decay process itself can produce an important and complex non-linear relationship in time between the radioactivity and the source: for example short passages through the South Atlantic Anomaly can produce significant background levels that last much longer. One simplification which can be implemented for both analytical expressions and computer simulations is to assume that the shape of the incident particle spectra do not change significantly as a function of time, but only in overall intensity. The radioactivity from the decay of nuclides within the detector, which can be descendants of the direct spallation products calculated using equation **(30)**, can then be calculated based on an extension of recursive formulae of Bateman [RDG.9].

The resulting decay rates can then be convolved with response functions for the decay of radioactive nuclides within the detector, usually determined using radiation transport simulation codes.

Other γ-ray detectors such as COMPTEL are designed such that the event can remain unregistered if energy deposition does not occur in more than one location of the instrument. In the case of COMPTEL, the equivalent events can result from neutron interactions with nuclei in the first detector layer producing ionisation from recoil and γ-rays that also deposit energy in the second detector (calorimeter).

Aside from their primary purpose, γ-ray experiments such as COMPTEL can also be utilised to observe neutron emission from large solar flares. Background effects in this observation mode can be caused by nuclear events within the spacecraft, by internal radioactivity, or by albedo neutrons from the Earth's upper atmosphere that can be registered as solar neutrons.

Results from instruments such as CGRO highlight the need to simulate the effects of secondary particle production in the spacecraft structure - for CGRO this amplified activation levels by a factor of twenty. Therefore this effect cannot be appropriately simulated if detailed radiation transport simulation tools to treat hadron-nuclear and nuclear-nuclear interactions, photo-nuclear de-excitation and radioactive decay are not used, and indeed they have been successfully applied to background analysis [RDG.10].

The use of low atomic number (low-Z) materials near to the detector, especially inside the active collimator, is preferable than higher-Z materials (such as iron). This is because a wider range of long-lived spallation products can result from higher-Z elements. At the same time, instrument designers can wish to use graded shield (layers of materials where the Z is changed with depth) to suppress K-shell X-rays from other parts of the spacecraft/instrument.

In addition to enhanced background levels, semiconductor γ-ray detectors (*e.g.* high-purity germanium detectors) suffer from degraded resolution as a result of displacement damage in the semiconductor material. The effects of this, including the influence of temperature cycling on the clustering or removal of traps, are discussed further in Clause 8 of ECSS-E-ST-10-12C, and Clause 7.4.10 of the present handbook, on displacement damage.

9.6. Photomultipliers tubes and microchannel plates

Photomultiplier tubes (PMTs) have in the past been used for UV to near-IR photon detection. When used on combination with scintillation or Cerenkov materials they can also detect more energetic ionising radiations. PMTs comprise a vacuum tube containing a cathode with a high photoelectric yield, and a series of dynodes with high secondary electron yield, each dynode biased to a steadily increasing potential before the anode is reached. The potential gradient ensures amplification with the multiplication of the number of electrons so that a single particle can release typically 10^6 electrons which can be detected electronically.

Background events can be induced in a PMT by one or more of the following mechanisms:

- direct ionisation of the cathode or dynode by a particle producing secondary electrons;
- fluorescence, or more generally scintillation, in any optical components of the PMT (or instrument which are in line-of-sight of the photocathode) induced as a result of ionisation by an incident particle;
- Cerenkov radiation induced in any optical components of the PMT (or instrument) from particles above the Cerenkov threshold for the material.

Daly *et al* conclude that the background rates observed in the *Hipparcos* PMTs were largely as a result of Cerenkov and fluorescence processes [RDG.11] from radiation-belt electrons, magnetospheric electron events and solar proton events.

Microchannel plates (MCPs) are also used in a number of particle and X-ray detection systems and act by means of electron multiplication. X-rays, radiation-belt ions and electrons and low-energy particles can have their signal amplified by this device while retaining positional accuracy (the last of these can occur if the particle is accelerated prior to striking the MCP). MCPs comprise a large number of microscopic tubes, coated inside with a material of high secondary electron yield, and operated with a strong potential gradient between the front and back surfaces of the plate. The result is similar electron amplification to the PMT. Any form of particle or radiation that can produce secondary electrons in the MCP is a potential source of noise. Particles that pass through the walls of the instrument and strike near the front of a channel result in a current pulse that is indistinguishable from a valid count. Particles that strike part of the way along a channel produce a pulse which is smaller than a valid count (equivalent to the particle hitting a dynode rather than the photocathode in a PMT).

Some mitigation of the background in PMTs and MCPs can be effected by suitable adjustment to the threshold and there is a trade-off between detector efficiency and noise immunity. However, small pulses can still be counted if very frequent since pulse pile-up causes near-simultaneous pulses to be added together. As well as giving rise to false events, very high numbers of noise pulses can reduce the gain of the device:

- In an MCP the high-pulse rate causes excessive current to pass through the resistive coating of the channels, depressing the potential difference across the plate thereby lowering gain. Ultimately for an MCP, very high numbers of noise pulses and high current can cause overheating which damages the MCP.
- For a PMT, high count rates can produce space-charging around the anode, again lowering the effective potential difference of the anode.

An example of an instrument using MCPs is the Cold Ion Detector, flown on STRV-1a. This had the primary aim of detecting low-energy ions from the ambient environment and an on-board electric propulsion system. However, the instrument encountered noise as a result of both ions and electrons, during passages through the inner and outer belts [RDG.12]. In fact the instrument functioned very well as a radiation detector which was a bonus for investigators. For its primary purpose, the radiation noise can be subtracted but there was a resultant loss of dynamic range and sensitivity. This instrument was relatively exposed, being mounted outside of the spacecraft skin, so that the MCP was

shielded only by around 2 mm aluminium, giving it a minimum electron energy threshold of approximately 750 keV.

Radiation noise in MCPs is a strong constraint on observations made in the Chandra X-ray observatory [RDG.13]. Data acquisition is stopped during radiation belt passage to prevent damage to the High Resolution Camera. This results in about 25 % of the 63.5 hour orbit being unusable.

If shielding is introduced to minimise electron contamination of detector events, consideration should be given to optimising the shield performance using a combination of low-Z and high-Z material (*i.e.* graded shielding) as described in Clause 5.4.

9.7. Radiation-induced noise in gravity-wave detectors

Space-based gravity-wave interferometric experiments such as LISA attempt to measure the separation between free-floating masses on separate spacecraft using laser interferometry. The natural radiation environment can provide a source of noise from cosmic-ray primaries and secondaries by the following mechanisms:

- changing the charge on the free-floating mass, necessitating a method of discharging the test mass at intervals [RDG.14];
- acting as a source of energy to change thermal conditions for cryogenically cooled materials [RDG.15];
- changing the critical temperature of superconducting materials [RDG.16].

The key processes to quantify are therefore the energetic particles incident upon and lost by the free-floating mass, including potential δ-rays (*i.e.* energetic knock-on electrons from ionisation) and spallation or fragmentation products that are emitted near the surfaces of the mass and surrounding materials [RDG.17].

9.8. Other problems common to detectors

As mentioned above, detectors which use semiconductor materials are subject to radiation damage effects described in earlier chapters of this document (displacement damage and total ionising dose). It is also important to consider potential effects on the electronic systems processing the output from the detectors, *e.g.* that can degrade the noise performance of the front-end amplifier.

During major solar flares, or during passage through an environment that has otherwise very high fluxes of charged particles, the radiation detectors can be overwhelmed, leading to instrumental “dead time” that poses another difficulty. The relative extent of the dead time can be used to estimate the number of counts the instrument failed to detect and so calculate an estimate of the countrate had the detector been 100 % effective during the measurement. However, this solution becomes increasingly inaccurate for larger dead times.

9.9. References

[RDG.1] G R Hopkinson, “Radiation effects in 2D IR sensors,” Sira Ltd, A/9920/00/C104/GRH/001, 1997, Produced under European Space Agency contract number 11755/95/NL/NB.

[RDG.2] C A Klein, “Band gap dependence and related features of radiation ionisation energies in semiconductors,” *J Appl Phys*, **39**, pp 2020-2038, 1968.

[RDG.3] Ana Heras, "ISO/FIRST Glitches Working Group," Final Report, Issue 1, ftp://astro.estec.esa.nl:21/pub/aheras/iso_gwg/gwg_fr.pdf

[RDG.4] R Nartallo, E Daly, H Evans, P Nieminen, F Lei, P Truscott "Low-angle scattering of protons on the XMM-Newton optics and effects on the on-board CCD detectors," *IEEE Trans Nucl Sci*, **48**, No 6, pp1815-1821, 2001.

[RDG.5] A Rasmussen *et al.*, "Proton scattering off XMM optics: XMM Mirror and RGS grating samples," XMM Project Document, RGS-COL-CAL-99009, November 1999.

[RDG.6] C S Dyer, P R Truscott, H E Evans, C L Peerless, "The analysis of XMM instrument background induced by the radiation environment in the XMM orbit," Defence Research Agency Customer Report DRA/CIS(CIS2)/CR95032/1.0, 1995, Final report on work performed for ESTEC under contract number 10932/94/NL/RE.

[RDG.7] W N Johnson, R L Kinzer, J D Kurfess, M S Strickman, W R Purcell, D A Grabelsky, M P Ulmer, D A Hillis, G V Jung, and R A Cameron, *Ap J Supp*, **86**, pp693-712, 1993.

[RDG.8] A Parmar, C Winkler, P Barr, L Hansson, E Kuulkers, R Much, and A Orr, "The INTEGRAL mission," Proceedings SPIE 4851 X-ray and gamma-ray telescopes and instruments for astronomy, August 2002.

[RDG.9] P R Truscott, PhD Thesis, University of London, 1996.

[RDG.10] C S Dyer, P R Truscott, H E Evans, N Hammond, C Comber, and S Battersby, "Calculations and observations of induced radioactivity in spaceborne materials," I*EEE Trans Nucl Sci*, **41**, No 3, pp438-444, June 1994.

[RDG.11] E J Daly, F van Leeuwen, H D R Evans, and M A C Perryman, "Radiation belt and transient solar magnetospheric effects on Hipparcos radiation background," *IEEE Trans Nucl Sci*, **41**, No 6, pp2376-2382, 1994.

[RDG.12] R H A Iles, A N Fazakerley, A D Johnstone, N P Meredith, and P Buehler, "The relativistic electron response in the outer radiation belt during magnetic storms," European Geophysical Society 2002, *Annales Geophysicae*, **20**, pp957–965, 2002.

[RDG.13] http://cxc.harvard.edu/proposer/POG/html/TVIS.html.

[RDG.14] T Sumner, H Araújo, and P Wass, "Space Science Simulations Using Geant4 – LISA/LISAPF Application," University of London Imperial College of Science, Technology and Medicine Report, WP210-RP-ICL-001 issued under QinetiQ Contract CU009-0000028631 (ESA SEPTIMESS Project), 2005.

[RDG.15] A L Vampola, R D Jiminez, and J E Cox, "Heat loads due to the space particle environment," *J Spacecraft and Rockets*, **26**, pp474-476, 1989.

[RDG.16] G P Summers, D B Chrisey, W G Maisch, G H Stauss, E A Burke, M Nasatasi, and J R Tesmer, "Electron and proton radiation effects on high temperature superconductor $YBa_2Cu_3O_{7-8}$," *IEEE Trans Nucl Sci*, **36**, pp1840, 1989.

[RDG.17] P Wass, H Araújo, T Sumner, "Simulation of test mass charging in the LISA Pathfinder Mission," University of London Imperial College of Science, Technology and Medicine Technical Note, WP600-TN-ICL-001 v1.1 issued under QinetiQ Contract CU009-0000028631 (ESA SEPTIMESS Project), March 2004.

10
Effects in biological material

10.1. Introduction

In this clause the effects of space radiation are discussed with respect to biological systems and, in particular, astronauts. The effects that ionising radiation produces in living matter result from energy transferred from radiation into ionisations (and excitations) of the molecules of which a cell is made. The primary effects start with the transfer of energy by physical interactions modifying the electronic configuration of atoms and molecules. Subsequently the altered molecules interact by chemical and later enzymatic reactions and interfere with the regulatory processes within the cell (Figure 24). Among the molecular hierarchy in the cell the DNA (deoxyribonucleic acid) plays an important role in cell proliferation, but many other molecular structures are also essential for the integrity of the cell.

Radiobiological effects in man are divided into two different types:

- stochastic effects, where the probability of manifestation, rather than their magnitude, is a function of dose, and
- deterministic effects, where the severity of the effect depends – also in a probabilistic manner – on dose, with a lower threshold dose below which no response occurs.

Sequelae of radiation exposure can be classified as either early or late effects. Early effects are those symptoms which occur within 60 days of exposure, whereas late effects usually become manifest many months or years later. The parameters that measure radiobiological effects, and the different types of effects are discussed in this clause.

10.2. Quantities used in radiation protection work

10.2.1. Overview

Specific radiation measurements are used to characterize the radiation fields for the description of their impacts on man. One set of specific quantities is used as a measure of the health risk associated with an exposure to ionising radiation and another set of specific quantities is used to measure in practice the radiation exposure. The quantities for radiation protection can therefore divided in protection quantities and operational quantities

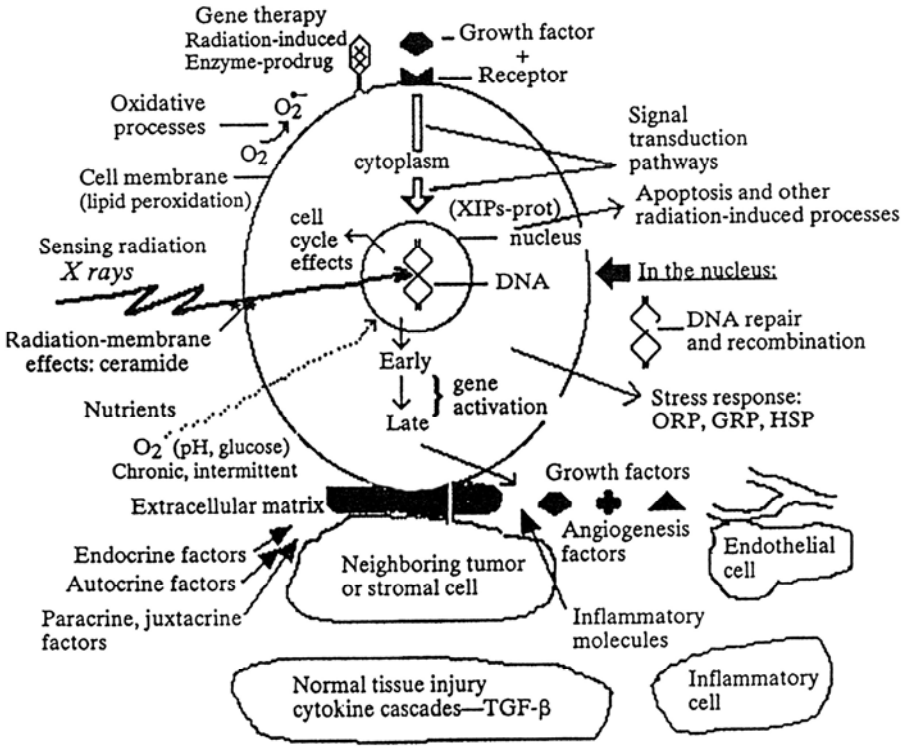

Figure 24: Effects of radiation on cells.

10.2.2. Protection quantities

Protection quantities are defined by the International Commission on Radiobiological Protection (ICRP), and relate the basic physical parameters to biological systems. The main protection quantities are the *mean organ absorbed dose*, D_T, the *organ equivalent dose*, H_T, and the *effective dose*, E.

The ***mean organ absorbed dose*** is given by:

$$D_T = \frac{\varepsilon_T}{m_T} \tag{31}$$

where

m_T = mass of the organ;

ε_T = total energy imparted in a tissue or organ.

For the description of the biological effects the knowledge of the absorbed dose is insufficient. Experiments show that different radiations are able to produce the same type of effect, but the magnitude of the effect per unit absorbed dose is different. In order to quantitatively allow for findings the **relative biological effectiveness** (RBE) was introduced.

The ***RBE*** is defined as the inverse ratio of the absorbed dose from one radiation type to that of a reference radiation (usually ^{60}Co or 200-250 keV X-rays) that to produces the same degree of effect. For a given type of radiation, the RBE depends upon the tissue, the cell, the biological effect under investigation, the total dose, and the dose rate.

A large number of RBE values in a wide variety of biological systems have been determined. The values range between 0.35 up to 200 depending on the biological endpoint and the radiation type [RDH.1]. Biological endpoints important for radiation protection against stochastic effects are tumour induction, life shortening, cell transformation and chromosome aberrations. In addition to the fact that only a small amount of data from

experiments in human subjects exist, only a very small fraction of these empirical data are relevant to low dose and dose rate conditions.

To account for the different biological efficiencies of different types of ionising radiation, the ***quality factor***, Q, was introduced. This factor depends not only on appropriate biological data, but reflects a judgement concerning the importance of the biological endpoints and how their empirical RBE values should be weighted. For most protection purposes RBE values observed at the lowest absorbed dose should guide the selection of values of Q.

The biological effectiveness of a given absorbed dose is dependent on the microscopic distribution of altered molecules, *i.e.* on the distribution of energy deposition – in space as well as time. This distribution is described by the number and the nature of charged particles that traverse an infinitesimal volume located at the point of interest and deliver the dose. This flux or fluence rate can refer to directly ionising radiation (*i.e.* charged particles) or indirectly ionising radiation (*e.g.* photons, neutrons, etc.). The linear energy transfer (LET) is used as the quantity that describes the energy deposition in the material by a charged particle per unit distance travelled in a medium. The dependence of RBE on LET leads to the relationship of the Q to LET that is applied to weight radiations of different radiation quality. Q is specified as a function of the unrestricted linear energy loss, LET, of charged particles in water. ICRP-26 [RDH.2] recommended a quality factor ranging from unity for an LET <3.5 keV/µm to twenty for LET >175 keV/µm.

In the 1990 recommendations of the International Commission on Radiological Protection (ICRP) [RDH.3] the quality factor Q was replaced by the ***radiation weighting factor***, w_R, which is applied to the mean absorbed dose over the organ or tissue of interest. The difference between Q and w_R is that w_R is more directly related to relative biological effectiveness and is only indirectly related to LET whereas Q is a direct function of LET. Values of w_R are specified for most, but not all, different radiation types and energies as given in ECSS-E-ST-10-12C Table 11-1.

The recommendations of 'NCRP 1993' [RDH.4] are mostly in line with that of ICRP concerning w_R, the only difference being the w_R for protons, which is set to 2 instead of 5 in the ICRP recommendation. This is of special interest where protons play a significant role in the radiation exposure, which is especially the case in space and in civil air traffic. In this standard we recommend that the ICRP values should be used.

This radiation weighting factor allows the *equivalent dose* and the *effective dose* to be defined. The ***equivalent dose***, H_T, in a tissue or organ, which is exposed to several radiation types, is the sum of each contribution of the absorbed dose from the different radiation types multiplied by its own value of w_R. This product correlates better to the observed biological effects than the purely physical quantity absorbed dose. The equivalent dose is measured in units of sievert, Sv (1 Sv = 1 Jkg^{-1} (=100 rem)).

$$H_T = \sum w_R \cdot D_{T;R} \qquad \textbf{(32)}$$

The weighted sum of dose equivalents of various tissues, the ***effective dose***, E, is calculated using tissue weighting factors (see ECSS-E-ST-10-12C Table 11-2), which take into account the varying sensitivity of the organs with respect to stochastic effects of radiation. The effective dose again has units of sievert, Sv.

$$E = \sum w_T \cdot H_T \qquad \textbf{(33)}$$

Radiation weighting factors for particles not specified in ECSS-E-ST-10-12C Table 11-1 are determined by evaluation of the $Q(L)$ from the ICRU sphere at 10mm, *e.g.*:

$$\frac{H^*(10)}{dose} \qquad \textbf{(34)}$$

where H*(10) is the *ambient dose equivalent* at 10 mm (defined in Clause 10.2.3) and is evaluated using the $Q(L)$ function for the deposited dose (see ECSS-E-ST-10-12C clause 11.2.3.2), e.g. you get $\overline{Q}$ (see paragraph A14 of [RDH.3]):

$$\overline{Q} = \frac{\int_0^\infty Q(L) D_L(L) dL}{D} \tag{35}$$

where $D_L(L)$ is the absorbed dose at 10 mm due to radiation with LET L, and $Q(L)$ is the associated quality factor at 10 mm (see ECSS-E-ST-10-12C clause 11.2.3.2).

Tissue equivalent doses are not measurable in general and neither are effective doses. For their determination a calculation of the dose distribution in an anthropoid phantom (an artificial object representing the anthropoid) is performed. There are several ways published in the literature to calculate E from physical quantities characterizing the external fields. An appropriate set of conversion factors can be found in chapter 4.1 of 'ICRP-26' [RDH.2]. With a few exceptions these operational quantities meet their objective. For some irradiation geometries the discrepancies are significant, this is the case for electrons and photons of low energy, intermediate neutrons and high-energy neutrons. ICRP-26 concluded that the high-energy radiations, such as found in high-flying aircraft, need separate study. This is of course valid also for space missions.

The quality factor or weighting factor is defined for stochastic effects only. In 1990 the ICRP made a first attempt to address the fact that an adequate approach for deterministic effects is missing by specifying RBE values for deterministic effects from exposures to densely ionising α-particles from incorporated radionuclides in case of accidental, i.e. high-dose exposures [RDH.10]. In space it is unavoidable that a finite probability that high-dose exposures occurs in SPEs so that deterministic effects can also ensue. The US National Council on Radiation Protection and Measurements, NCRP, in drawing on the ICRP recommendations [RDH.10] has suggested such weighting factors for space radiation applications in its recent report on that topic [RDH.9]. However, a satisfactory solution appears not to have been achieved yet as in its most recent report the ICRP once more states [RDH.22]:

> *"In special circumstances where one deals with higher doses that can cause deterministic effects, the relevant RBE values are applied to obtain a weighted dose. The question of RBE values for deterministic effects and how they should be used is also treated in the report, but it is an issue that will demand further investigations."*

Therefore, the assessment of the risk for early deterministic effects from SPE exposure suffers from the added uncertainty that the proper values for the RBE pertaining to a given effect can be only poorly known.

10.2.3. Operational quantities

Operational quantities are defined by the International Commission on Radiation Units and Measurements (ICRU) and have been defined with the aim of never underestimating the relevant protection quantities, in particular the effective dose, E, under exposure conditions in conventional terrestrial radiation fields.

For area monitoring the appropriate operational quantity is the *ambient dose equivalent* $H^*(d)$ of strongly penetrating radiation and the *directional dose equivalent* $H'(d,\Omega)$ for weakly penetrating radiation.

The ***ambient dose equivalent***, $H^*(d)$, at a point is the dose equivalent that is produced by the corresponding expanded and aligned radiation field in the ICRU sphere[4] at a depth, d, in millimetres on the radius opposing the direction of the aligned field. For measurement of strongly penetrating radiations the reference depth used is 10 mm and the quantity denoted $H^*(10)$.

The ***directional dose equivalent***, $H'(d,\Omega)$, at a point is the dose equivalent that is produced by the corresponding expanded field in the ICRU sphere at a depth, d mm, on a radius in a specified direction, Ω. For measurement of weakly penetrating radiations the reference depth is 0.07 mm and the quantity denoted $H'(0.07,\Omega)$.

The operational quantity for individual monitoring is the ***personal dose equivalent***, $H_P(d)$. For strongly penetrating radiation H_P is defined as the dose equivalent in ICRU soft tissue at a depth of 10 mm in the body and for weakly penetrating radiation at a depth of 0.07 mm in the body. H_P can vary both between individuals and location. Calibration of H_P can therefore be performed on phantoms (slab, pillar and rod) only.

Even though the ICRP-60 recommendation means that the protection quantities are now calculated using the radiation weighting factor, it still recommends that the operational quantities are calculated using the Q-L relationship given in ECSS-E-ST-10-12C clause 11.2.3.2.

Typically and in contrast to ICRU stipulations, the ambient radiation fields surrounding astronauts are omnidirectional or even isotropic so that it can become important to verify that in a given field the premise still does hold that the operational quantities overestimate the effective dose.

The relationships between these various parameters are shown in Figure 25 (adapted from Annals of the ICRP Vol. 26 [RDH.2]). For the calibration of instruments, standards and reference fields are available in national and international standards laboratories.

[4] The ICRU sphere is a sphere of 30 cm diameter made of tissue equivalent material with a density of 1 g/cm^3 and a mass composition of 76.2 % oxygen, 11.1 % carbon, 10.1 % hydrogen and 2.6 % nitrogen.

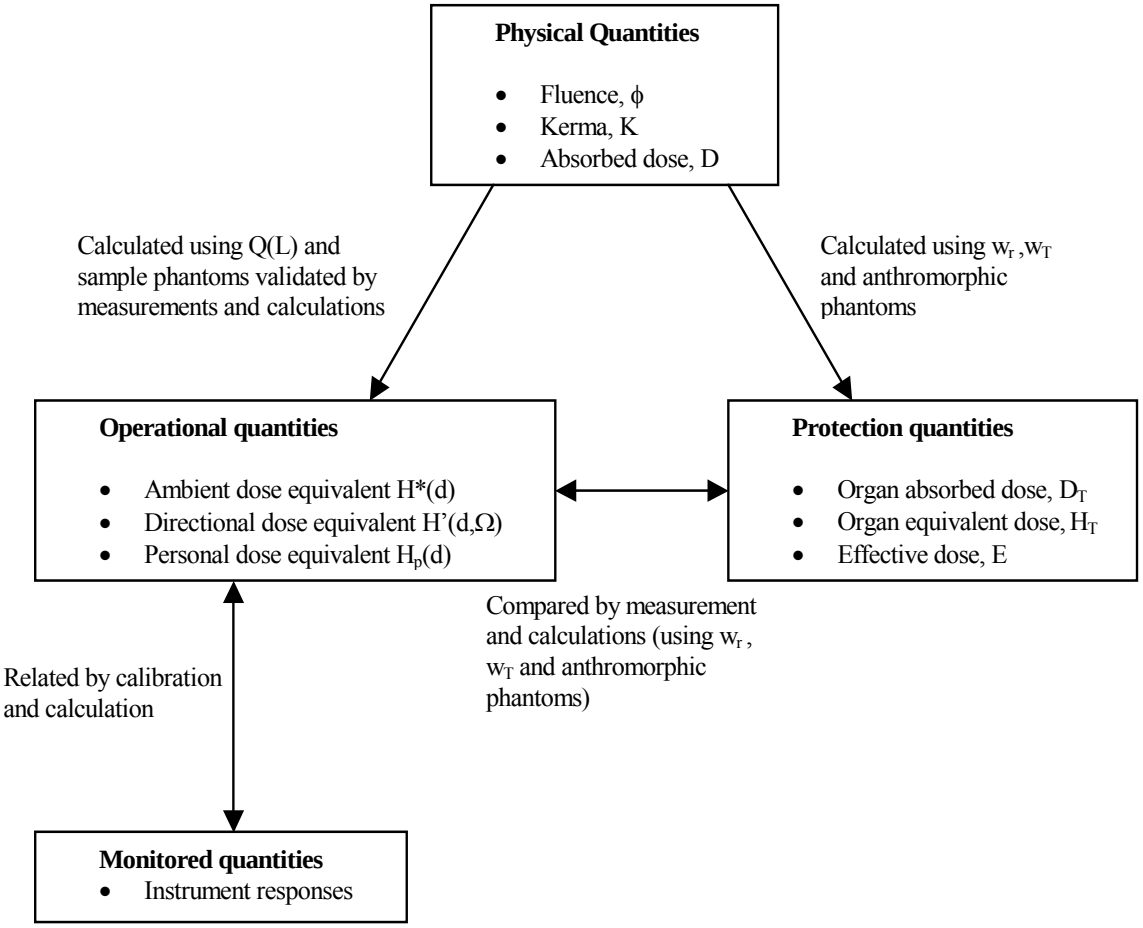

Figure 25: Relationship of quantities for radiological protection.

10.3. Radiation effects in biological systems

10.3.1. Overview

Irreversible molecular changes, produced by radiation, can alter the function of cellular pathways and can lead to a situation in which cells can permanently lose the ability to perform one or more functions. This damage can be expressed in the cell after several cell cycles, or the immediate death of the damaged cell as a part of an organ can lead to changed or altered functions of the organ. The time scale for the events on the physical, chemical, macromolecular and cellular or organ level ranges from 10^{-16} s to years, even decades. The subcellular and cellular radiation effects can finally give rise to deterioration of tissue or organ functions with the expression of clinically observable symptoms.

Radiation effects in man have been – somewhat artificially – divided into stochastic and deterministic radiation effects. For deterministic radiation effects the magnitude or severity of the effect depends on dose, with a possible lower threshold dose below which no response at all is produced. For stochastic radiation effects, no threshold dose is postulated to exist and here the probability for the manifestation of a radiation effect, rather than its magnitude, becomes a function of dose.

10.3.2. Source of data

The primary human database consists, in the overwhelming majority of cases, of exposures to photons and electrons under terrestrial exposure conditions only. These data are supported by general relations observed in cellular and especially animal systems between dose-modifying factors, such as radiation quality or dose-rate, and cell killing or transformation. Such findings can tentatively be drawn upon to supply the information lacking for human response data which are available only for radiation qualities and exposure conditions vastly different from those prevailing in the space radiation field.

These general principles, which can be derived from the vast amount of data covered by the general literature on radiobiological effects, are indispensable as guidance for the interpretation of the database concerning the specific human response to ionising radiation. The most important source of human exposures for the dose-effect relations for stochastic radiation effects, *i.e.* radiation induced cancer, is the Japanese population of atomic bomb survivors. But even this source suffers from severe restrictions concerning the dosimetry, the medical or epidemiological methodology, or both.

For early radiation effects part of the same database as used for stochastic effects and, in addition, findings from therapeutic exposure in cancer therapy and from accident victims in the nuclear industry constitute the respective database.

The primary and secondary sources of human exposures are constantly reviewed and updated by national and international committees as well as ad hoc study groups constantly. The UNSCEAR reports are most widely recognised as the most thorough and balanced summaries of the field [RDH.1].

10.3.3. Early effects

Symptoms becoming manifest from within minutes to 30 to 60 days subsequent to exposure are classified as early effects. For early effects the biologically plausible hypothesis can be advanced that the severity of tissue response depends on the fraction of constituent cells having been killed in relation to the tissue's intrinsic capacity to regenerate this fractional cell loss.

Manifestations of early effects in man usually appear to be threshold phenomena, *i.e.* stochastic phenomena, and occur only after acute exposures to comparatively high doses, which under terrestrial standards are ruled out as impermissible under regular circumstances. However, in space-flight activities such high acute doses are considered, due to very large solar particle events or for missions that encounter high intensities of trapped radiation. Apart from early mortality that is rarely to be expected at instantaneous exposures below 2 Sv, early forms of radiation sickness, which occur already at lower doses and can impair the functional performance of space personnel, are considered as relevant effects. The threshold, below which no symptoms of the prodromal syndrome - the most sensitive symptom complex - such as anorexia, nausea, fatigue, vomiting and diarrhoea should occur is about 200 mSv if the model of the NUREG report [RDH.6] is taken with parameter values for instantaneous exposure. The risk drops below 5 % around that dose value. Another report, the PSR report [RDH.7], uses a higher threshold of 500 mSv (free-in-air!) below which no early radiation related symptoms should be observable, which can affect performance.

10.3.4. Late effects

10.3.4.1. Overview

Radiation effects not occurring within this period generally do not become manifest for many months or even years of a latent period and these effects are then classified as late or delayed effects. Among late effects those that don't become manifest in the irradiated individual but in its progeny, are classified as genetic or more properly as hereditary effects. Hereditary late effects from exposure to ionising radiation have never been observed in human populations and therefore are not treated as a health risk.

For late effects, the transformation (mutation) of a single cell rather than cell killing is probably the primary relevant cellular "initiation" event, especially for carcinogenesis, although additional interfering and contributing biological "promotion"-mechanisms assume greater importance for the final outcome. Very recently evidence has increased that cell killing per se in cells surrounding the initiated (transformed) cells is also an important factor in the promotion (towards the full malignant status of a tissue) of the initiated progenitor cells [RDH.23].

10.3.4.2. Stochastic late effects

Life shortening, the primary reference risk, is considered to be mainly due to either the induction or the acceleration of appearance of neoplastic diseases (*i.e.* tumour development). Hence the dose-response relationship for carcinogenesis is the basic empirical datum from which exposure limits are to be derived. The human database again consists mainly of observations on the atomic bomb victims. Less specific data on general life shortening exist for the shortened life expectancy of American radiologists prior to 1950, while data on the induction of leukaemia can be supplemented by observations on patients irradiated for ankylosing spondylitis.

Detailed information on the estimates of probability for fatal cancers and expected years of life lost from fatal cancer is described in [RDH.3]. The fatality probability coefficients for different organs per Sv are given in Table 12 taken from this report.

Genetic manifestations never place a limit on radiation exposure as far as population dose is concerned, due to the vanishing contribution of the space crew population to the gene pool of the general population. However, on an individual basis it is important to consider the gonads as an additional critical organ.

Table 12: Lifetime mortality in a population of all ages from specific cancer after exposure to low doses.

Organ	Fatality Probability coefficient (10^{-4} Sv^{-1})
Bladder	30
Bone marrow	50
Bone surface	5
Breast	20
Colon	85
Liver	15
Lung	85
Oesophagus	30
Ovary	10
Skin	2
Stomach	110
Thyroid	8
Remainder	50
Total	500

10.3.4.3. Deterministic late effects

Secondary or ancillary reference risks relating to distinct organs are "late" cateractogenesis in the ocular lens and permanent or late skin effects.

The thresholds for deterministic effects in humans are given in Table 13. Temporary sterility appears to be around 0.15 Sv of low-LET radiation and about 0.4 Sv if exposure is fractionated. In the case of highly fractionated exposures cataract formation is the

most important deterministic effect. The latent period varies from about 0.5 to 35 years with an average of about 2 to 3 years.

Dose response relationships for late skin effects, other than cancer, such as late loss of reproductive capacity of fibroblasts are not available.

Table 13: Estimates of the thresholds for deterministic effects in the adult human testes, ovaries, lens and bone marrow.

Tissues	Effects	Threshold	
		Total dose equivalent received in a single brief exposure (Sv)	Annual dose equivalent (Sv/y) ‡
Testes	Temporary sterility	0.15	0.4
	Permanent sterility	3.5 – 6	2.0
Ovaries	Sterility	2.5 – 6	> 0.2
Lens	Detectable opacities	0.5 – 2.0	> 0.1
	Visual impairment (cataract)	5.0	> 0.15
Bone Marrow	Depression of haematopoiesis	0.5	> 0.4

10.4. Radiation protection limits in space

10.4.1. Overview

The International Space Station (ISS) Multilateral Radiation Health Working Group (MRHWG) acts as the primary working level body for coordinating Partner input on radiation protection into ISS Multilateral Medical Operations Panel (MMOP) for ISS medical operations. The authority of MRHWG is from ISS MMOP, which is empowered by the Article 11.4 of the Memoranda of Understanding between the Partners and ISS Program (ISSP). Empowerment within the ISSP is authorized through SSP 50200-01, Station Program Implementation Plan, Volume 1, Station Program Management Plan.

The MRHWG is the primary working level body for development of common exposure limits for radiation from space environment and man made radiation sources, radiation protection requirements and strategies, crew member radiation training content, operational countermeasures, radiation hardware responsibilities, radiation monitoring requirements, radiation health risk assessment procedures, and operational procedures.

Radiation protection activities relevant to ISS operations under the auspices of this group include, but are not limited to:

- establishment of operational principles to ensure proper protection of crew members from radiation exposure for ISS missions;
- procedures for crew training on the use of radiation monitors;
- coordination of radiation dosimetry between Partners;
- radiation monitoring and countermeasures definition and implementation;
- development and implementation for in-flight radiation events, *e.g.*, SPE, procedures;
- development of requirements for radiation protection support;
- radiation health risk assessment.

The charter of the MRHWG pertains to all ISS radiation protection for medical operations activities and is applicable to all Partner medical organizations and crewmembers, including the Canadian Space Agency (CSA), European Space Agency (ESA), National Aeronautics and Space Administration (NASA), Japan Aerospace Exploration Agency (JAXA), and the Russian Space Agency (RSA).

Based on the inputs of the agencies of the ISS partners the MRWHG needs to elaborate an operational scenario that is agreed by all partners.

10.4.2. International agreements

Until now an agreement on international exposure limits for low Earth orbit activities can only be achieved for one organ specific equivalent dose limit, namely that of the BFO (blood forming organ). The limit was set to 0.25 Sv for 30 days exposure interval and to 0.50 Sv for an annual exposure

The crew exposures are always managed according to the ALARA principle, which formulates that doses are maintained ***as low as reasonably achievable***. The ALARA principle is not a methodology for quantifying radiation exposure or protection, but is more a widely accepted objective of radiation protection.

The current career limits for each agency are shown in Clause 10.4.4.

For the calculation of effective doses for astronauts, the MRHWG has recommended to use the $Q(L)$-L relationship instead of w_R. There is no agreement on the human shielding model to calculate organ doses, NASA uses the CAM/CAF model [RDH.8] for organ dose evaluation. A comparison of the effective doses predicted by various models in a given field should prepare decisions to adopt the most appropriate one as a common standard.

10.4.3. Other considerations in calculating crew exposure

The exposure of an astronaut (or part of an astronaut), and the consequential increased risk to the crew, cannot be appropriately calculated without information on the primary radiation environment (see ECSS-E-ST-10-04 [RDB.1]) and the effects of shielding in changing the nature of the radiation field both outside the human, and inside (*i.e.* self-shielding).

The types of calculation which can be performed to quantify shielding are discussed in Clause 5.6. The variation of the type of radiation *i.e.* its quality as a function of shielding material (and not just areal mass of shield in g/cm^3) is very important. As mentioned in 5, lower-Z (particularly hydrogenous) materials can slow energetic protons and heavier nuclei with minimal production of nuclear fragments and secondary neutrons compared with high-Z shields. The latter also produce greater fluxes of bremsstrahlung for electron sources. However, engineering requirements force a compromise on the composition of materials used. Depending upon the radiation source, simple sector shielding calculations can be insufficient, thus implying the use of more detailed calculations that treat the production and transport of secondary radiations.

Furthermore, for manned-spaceflight it is particularly important that shielding issues be considered hand-in-hand with mission planning of crew activities within spacecraft habitats, lunar or planetary habitats, or extra-vehicular activities. It is also important to consider this as a function of the radiation environment for nominal and exceptional circumstances, and during the mission, this is obviously linked with local environment and space weather monitoring to recognise the need to perform operational changes. For instance, almost all parts of the habitable spacecraft structure can be designed to meet the ALARA requirement for normal space weather conditions, whilst if there is a risk of enhanced exposure during a solar particle event, activities are restricted to better shielded parts of the vehicle/habitat for the duration. EVAs can likewise be restricted depending upon spatial (orbital) variations as well as temporal variations of the radiation field. Whilst the trade-off between the ALARA requirement, mission requirements (which also drive spacecraft design and crew activities), radiation

protection (including shielding), environment monitoring/forecasting, and overall mission risk is important, such discussions are beyond the scope of this document and is treated in [RDH.9].

10.4.4. Radiation limits used by the space agencies of the partners of the International Space Station (ISS)

10.4.4.1. Proposed CSA Limits

- Short-term limits

  The US short-term exposure limits apply to CSA crewmembers (see Clause 10.4.4.3).

- Career limits

  The following career limits for CSA crewmembers are shown in Table 14.

Table 14: CSA career ionising radiation exposure limits.

Exposure interval	Organ-specific exposure limits (Sv)		
	BFO (5.0 cm)	Eye (0.3 cm)	Skin (0.01 cm)
Career	1.0	4.0	6.0

10.4.4.2. Proposed ESA Limits

The European limits, shown in Table 15, are based on thresholds of radiation effects in organs as represented by ICRP-60 [RDH.3].

Table 15: ESA ionising radiation exposure limits.

Exposure interval	Organ-specific equivalent dose limits (Sv)		
	BFO	Eye	Skin
30 days	0.25	0.5	1.5
Annual	0.50	1	3

Exposures are managed as follows:

- Crew exposures are managed in adherence to the ALARA principle, which directs that exposures always be maintained As Low As Reasonably Achievable.
- The administrative career exposure limit is 1 Sv independent on gender and age.

10.4.4.3. Proposed NASA limits

The US limits are based on the recommendations of NCRP, which released in December 2000 its second report on radiation protection guidance [RDH.9]. The limits provided in Table 17, Table 18, and Table 19 are mainly for late deterministic effects and cancer risks. Since report No. 132 only covers manned activities in low earth orbit, early deterministic effects are not of major concern. This is generally true even during a major SPE. Only EVA exposures can be of concern, but those can be properly controlled by operational measures. To limit late deterministic effects, such as cataracts, damage to the bone marrow and skin, is a requirement. NCRP considers that the Sv is not the adequate unit to derive limits for short term exposures. Instead of applying Q and w_R, NCRP have recommended for the calculation of the organ doses appropriate RBE's and adapted the RBE values of ICRP Publication 58 as given in Table 16.

Table 16: NCRP-132 recommended RBEs.

Radiation Type	Recommended RBE	Range of RBE
1-5 MeV neutrons	6.0	(4 – 8)
5-50 MeV neutrons	3.5	(2 – 5)
Heavy ions (helium, carbon, neon, argon)	2.5	(1 – 4)
Proton > 2 MeV	1.5	-

The new recommended career dose limits for different ages and gender are based on a 3 % probability of lifetime excess cancer mortality risk derived from the risks of Pierce *et al* 1996 [RDH.11]. NASA ensures that these limits are not exceeded at a 95 % confidence level based on a statistical assessment of the uncertainties that entered in the NCRP 132 cancer risk projection model. Short-term limits are designed to prevent deterministic effects resulting from acute exposure. This risk is comparable to the risk for a workers occupational exposure of 20 mSv/y using current nominal risk coefficients for an adult population of 4×10^{-2} Sv^{-1}. Compared to other lifetime risks the choice of this risk seems to be reasonable and justified.

Table 17: NCRP-132 Deterministic dose limits for all ages and genders (Gy-Eq.).

Exposure interval	Bone marrow	Eye	Skin
30 days	0.25	1.0	1.5
Annual	0.5	2.0	3

Table 18: NCRP-132 career ionising radiation exposure limits.

Exposure interval	Over all Organs (Sv)	Eye (Gy-eq.)	Skin (Gy-eq.)
Career	0.40 to 3.0 (see Table 19 below)	4.0	6.0

Table 19: NCRP-132 career effective dose limits for age and gender specific ionising radiation exposure for 10-year careers.

Age at exposure	Effective dose (Sv)	
	Female	Male
25	0.4	0.7
35	0.6	1.0
45	0.9	1.5
55	1.7	3.0

10.4.4.4. Proposed JAXA Limits

The Japanese limits, shown in Table 20 to Table 22, are set so that the attributable lifetime cancer mortality equals nearly 3 % assuming the most probable pattern of stay but never exceeding 5 % even if the cosmonauts stay in space every year within the dose limit.

All values given are pending final approval.

Table 20: JAXA short-term ionising exposure limits

Exposure interval	Testes	Bone marrow	Lens of eye	Skin
Single/brief	-	-	0.50	2.0
Annual	1.0	0.5	2.0	7.0

Table 21: JAXA career ionising radiation exposure limits (Sv).

Exposure interval	Effective dose Over all Organs	Dose Eqv. Eye	Dose Eqv. Skin
Career	See following table (Table 22)	5.0	20.0

Table 22: JAXA current career exposure limits by age and gender

Age at exposure	Effective dose equivalent (Sv)	
	Female	Male
27-29	0.6	0.6
30-35	0.8	0.9
36-39	0.9	1.0
>40	1.1	1.2

10.4.4.5. Proposed RSA Limits

The general principle underlying the Russian protection concept are: manned spaceflight belongs to a high risk category of human activity, such spaceflights are carried out under conditions of potentially harmful exposure to a variety of factors, including radiation; a successful flight program depends on adequate crew performance; the objectives of the space radiation safety system is to preserve health of flight participants as well as restrict the risk of injuries late effects; considering the relative low number of people to be expected to participate in space flights in the immediate future, genetic radiation effects are assumed to be practically absent [RDH.12].

The acute BFO limit was proposed as an upper limit of a single acute exposure, which can occur during a SPE. This exposure limits the working capacity decrease to about 1 to 2 %.

The choice of an age independent career limit of 1 Sv is due to the fact that Russian studies show with increasing age an increase of non-cancer risks due to radiation, which compensates the cancer risk decrease with age. It is stated that this limit equals to a total fatal risk of 10 % for cancer and non-cancer risks.

It is assumed that the corresponding eye and skin limits are defined by the scaling factors adopted for the short-term limits.

Table 23: RSA short-term ionising exposure limits.

Exposure interval	Organ specific exposure limits (Sv)		
	BFO	Eye(0.3 cm)	Skin (0.01 cm)
Acute (from 1 day)	0.15	-	
30 days	0.25	0.5	1.5
Annual	0.50	1.0	3.0

The career limits for Russian crewmembers are shown in Table 24.

Table 24: Russian career ionising radiation exposure limits

Exposure interval	Organ Specific Exposure Limits (Sv)		
	BFO (5.0 cm)	Eye(0.3 cm)	Skin (0.01 cm)
Career	1.0	2.0	6.0

10.5. Uncertainties

10.5.1. Overview

There are a lot of uncertainties involved in the estimate of radiation risk due to the exposure to the space radiation field. An optimal radiation protection programme cannot be carried out if more information in the areas covered in Clauses 10.5.2 to 10.5.8 is not available.

10.5.2. Spacecraft shielding interactions

As mentioned in 5, the range of particle species and energies leads to a wide range of interaction processes and hence a very complex radiation field. Of particular importance is the consideration of potential adverse effects of shielding against energetic protons and heavier nuclei (galactic cosmic ray, solar particles or trapped protons). The high energies increase the probability of nuclear interactions, and multiplicities of secondary and often more intensely ionising particles.

Since the radiation incident on the human body is scattered, fragmented and degraded in energy as it penetrates to the deeper organs, the effective LET, as well as dose and dose rate, all change with depth; all three are factors that influence RBE, but not necessarily in the same direction. Fragmentation can lead to an enhancement (build up) of high LET components at the expense of low LET components. Of particular importance for dose modifications towards higher quality factors is the increase of the number of nuclear disintegration “stars” with higher multiplicities near the bone marrow in osseous structures.

10.5.3. The unique effects of heavy ions

The findings to be discussed are:

- the effects of accelerated heavy ions on cells and tissues;
- the observation of microlesions engendered in various tissues by irradiation with a single heavy ion;

- the non-additive effect on tissue cultures of sequential irradiation with heavy ions and sparsely ionising radiation;
- the different kinetics of expression of late effects in mammals;
- the reversed dose rate effect observed in the life shortening of mice and the induction of neoplastic transformations in tissue cultures by high LET radiation in the context of other endpoints and systems.

Immediately evident in the simplified version for the calculation of the dose equivalent as a function of the quality factor alone, is the huge range of LET values occurring in the terrestrial space radiation field. Application of the "adopted" dependence of Q as a function of LET rests on the assumption that the underlying terrestrial experience, gained from completely different sources of ionising radiation, can be applied to the space radiation and is the same for the relevant effects in critical organs. This approach loses its conceptual basis, especially for the extremely densely ionising radiation of HZE (high mass energy) particles and nuclear disintegration stars, since the definition of absorbed dose as a measure of radiation exposure, and hence that of RBE and Q, break down [RDH.13][RDH.14].

10.5.4. Extrapolation from high-dose effects to low-dose effects

One of the most important questions under permanent discussion is the estimation of radiation risk gathered at high dose irradiations compared to that at very low doses. In radiation protection the linear, no threshold (LNT) hypothesis fits a straight line through the origin. Numerous radiobiological investigations indicate that mammalian cells have the potential to respond adaptively to the stress imposed by ionising radiation. Even “beneficial” effects of low doses were observed in such investigations, and increased resistance to higher levels of radiation exposure can be induced by low doses. The LNT hypothesis is therefore highly questionable. However, once total exposures surpass say 500 mSv, the importance of its validity starts to become minor.

10.5.5. Variability in composition, space and time

With respect to time-dependent factors it is evident that the radiobiological conditions in space differ quite substantially from those which usually apply for "reference" experiments on Earth. Compared to typical dose rates in terrestrial experiments with photon sources and particle accelerators, the fluxes in space are lower by orders of magnitude. Thus all the spread of dose rate effects observed with low and high LET radiation impacts the calculation of dose equivalents under spaceflight conditions.

10.5.6. Effects of depth-dose distribution

Radiation exposures in space do not result in uniform whole-body dose distribution. The dose distribution is non-uniform both with respect to depth and with respect to area or region of the body involved. Rapidly decreasing absorbed dose with depth in tissue is a result from the spectral characteristics of the significant space radiations. As an example, the integral-energy spectrum (and consequently the absorbed-dose deposition) of primary solar-flare protons is a continuum with negative slope that varies from flare to flare, with time during the course of a flare, and with shielding. Qualitatively, it is generally accepted, that partial or non-uniform exposure in man entails less damage than uniform total-body exposure, although the existence of abscopal – usually deterministic – radiation effects hints at the possibility that this assumption can imply further scrutiny.

10.5.7. Influence of spaceflight environment

During spaceflight man is exposed to several stressors:

- flight dynamic factors, such as, above all microgravity, acceleration and vibration and noise;
- work environment factors, such as hypoxia (lack of oxygen in body tissue), hyperoxia (excess of oxygen in body tissue), hypo- and hyperthermia (abnormally low and abnormally high body temperature respectively) and noise;
- internal body factors, such as exercises, trauma, infection, altered biorhythms and psychological factors;
- energetic particle radiation.

The interrelationship between the pathologies of radiation syndromes and the influence of external and internal factors, so far, is merely understood at the level of two factor combinations – if at all. Up to now, only a few data on the interaction of the first three factors with radiation for humans are available. Most of the investigations are done using cellular systems, plant seeds and animal systems, such as insect eggs, larvae pupae and adults, as well as rats, mice and dogs. Irradiation was performed with gamma sources before or after spaceflight or with an onboard source. The combination of microgravity and radiation yields mostly an additive interaction when using pre- or postflight irradiation, whereas in experiments with onboard irradiation, synergistic effects (greater than the sum of the effects of each factor) dominate. A compilation of the experiments is given in Horneck (1988) [RDH.15].

Regarding the important question of a modification of the radiation response to heavy ions by microgravity, one important result has been obtained by the use of the Biostack[5] concept in combination with the 1-g centrifuge of BIORACK. For the investigation, eggs of the stick insect *Carausius morosus* were exposed in the Spacelab D1 mission and allowed to continue their development during spaceflight. After retrieval, hatching rates, growth kinetics and anomaly frequency were determined. A synergistic action of heavy ions and microgravity was established in the unexpectedly high frequency of anomalous larvae. Neither cosmic radiation nor microgravity alone produced an effect of similar extent, nor was this extremely high anomaly rate reached by adding up the effects of the two parameters [RDH.16]. Although suggestive, this result cannot be applied without further elaboration and additional experiments before answers can be given with some confidence.

The combined influence of different spaceflight factors is one of the key problems in space medicine; it is of particular interest to understand the mechanisms underlying the interaction of radiation and microgravity. Along the radiobiological chain of events every step can be affected by internal and external modifiers, thereby influencing the final radiation response. Concerning the observed synergistic effects of microgravity and radiation, microgravity can exert its influence:

- at the molecular level, *e.g.* by changing diffusion controlled processes;
- at the cellular level, *e.g.* by modifying repair processes or by changing the metabolic/physiological state;
- at the tissue and organ level, *e.g.* by modifying self-assembly intercellular communication, cell migration, pattern formation, or differentiation.
- at the level of the whole organism where microgravity induced systemic changes of, e.g., fluid distributions lead to an altered humoral status of the endocrine system and in particular of the immune system.

It is unlikely that microgravity interferes with the number of primary molecular radiation lesions. Cellular enzymatic processes, such as DNA repair, are more likely to

[5] The Biostack experiment was designed to study the effect of single heavy nuclei of the cosmic radiation environment upon individual biological systems during actual spaceflight.

be gravity-dependent. This hypothesis was tested during the IML1 mission with X-ray pre-irradiated yeast cells. The results suggest that DNA double strand repair is inhibited or at least delayed under microgravity. A replication of this experiment on the SMM-03 mission can not confirm the previous result. Again no effect of microgravity can be observed in a third yeast experiment using an on board radiation source [RDH.17]. The effectiveness and kinetics of DNA repair in pre-irradiated bacteria (*E. coli, B. subtilis* and *D. radiodurans*) and human fibroblasts remains unchanged under microgravity [RDH.18]. On the opposite, the systemic scale, the increasing evidence that expression of late radiogenic cancer is to a significant fraction controlled by immune surveillance raises the possibility that the manifest reductions of immune competence which accompany prolonged exposure to microgravity render the assessment of space radiation risk by terrestrial risk coefficients tenuous.

10.5.8. Uncertainties summary

Table 15 and Table 16 give the major uncertainties from the atomic bomb data and from the space radiation field. The uncertainties in risk estimates have been evaluated in detail in 'NCRP 1997' [RDH.19]. The risk estimates are presented in a distribution that ranges from 1.15 to 8.1 x 10^{-2} Sv^{-1} for the 90 % confidence interval for the nominal value of 4 % per Sv for an adult US population.

The uncertainties due to spaceflight environment, *e.g.* microgravity, are not assessed at all due to non-availability of appropriate data.

10.6. References

[RDH.1] ICRU, International Commission on Radiation Units and Measurements, "The quality Factor in Radiation Protection," ICRU Report **40**, 1986.

[RDH.2] ICRP International Commission on radiation Protection, "Recommendations of the ICRP," ICRP Publication 26, Annals of the ICRP **1** (3), Pergamon Press, 1977.

[RDH.3] ICRP "1990 Recommendations of the International Commission on Radiobiological Protection," ICRP Publication 60, Annals of the ICRP **21** (1-3), Pergamon Press Oxford, 1991.

[RDH.4] NCRP, National Council on Radiation Protection and Measurements, "Limitation of Exposure to Ionizing Radiation," NCRP Report 116, Bethesda, Maryland, 1993.

[RDH.5] UNSCEAR, United Nations Scientific Committee on the Effects of Atomic Radiation Sources, "Effects and Risks of Ionizing Radiation," UNSCEAR reports 1993-2001 to the UN General assembly, with Annexes, United Nations, New York.

[RDH.6] J S Evans, D W Moeller, and D W Cooper, (Eds), "Health effect model for nuclear power plant accident consequence analysis," NUREG/CR-4214, SAND85-7185, Sandia Nat. Laboratory for the Department of Energy, Washington, DC, 1985.

[RDH.7] G H Anno, D B Wilson, and S J Baum, "Severity levels and symptoms for acute radiation sickness," Pacific-Sierra, Research Corporation for the Defense Nuclear Agency, Rep. DNA-TR-86-94, Washington, DC, 1985.

[RDH.8] M P Billings and W R Yucker, "The Computerized Anatomical Man (CAM) Model," NASA CR-134043, September 1973.

[RDH.9] NCRP, National Council on Radiation Protection and Measurements, "Radiation Protection Guidance for Activities in Low-earth Orbit," NCRP Report No.132, Bethesda, Maryland, 2000.

[RDH.10] ICRP, International Commission on radiation Protection, "RBE for deterministic effects," Annals of the ICRP 20 (4), Pergamon Press, 1989.

[RDH.11] D A Pierce, Y Shimizu, D L Preston, M Vaeth, K Mabuchi, "Studies of the mortality of atomic bomb survivors", Report 12 Part 1, Cancer, pp 1950-1990, *Rad Res*, **146**, pp1-27, 1996.

[RDH.12] E E Kovalev, "Radiation Protection during Spaceflight," *Aviat Space Environ Med*, Dec 1983.

[RDH.13] R Facius, M Schäfer, and H Bücker, "Unique radiobiological aspects of high-LET radiation," *Adv Space Res,* **4**, No 10, pp175-185, 1984.

[RDH.14] G Reitz *et al*, "Results of space experiments," *Radiat Environ Biophys*, **34**, pp139-144, 1995.

[RDH.15] G Horneck, "Impact of spaceflight environment on radiationresponse," Terrestrial Space Radiation and its Biological Effects, P C McCormack, C E Swenberg, H Bücker, (Eds.), Plenum Press, New York, Series A: Life Sciences, Vol. **154**, pp707 -714, 1988.

[RDH.16] H Bücker, R Facius, G Horneck, G Reitz, E H Graul, H Berger, H Höffken, W Rüther, W Heinrich, R Beaujean, W Enge, "Embryogenesis and Organogenesis of Carausius Morosus under Spaceflight conditions," *Adv Space Res*, **6**, No 12, pp115, 1986.

[RDH.17] H D Pross, J Kiefer, "Repair of cellular Radiation Damage in Space under Microgravity Conditions," *Radiat Environ Biophys*, **38**, pp133-138, 1999.

[RDH.18] G Horneck, "Impact of Microgravity on radiobiological processes and efficiency of DANN Repair," *Mutation Research*, **430**, No 2, pp221-228, 1999.

[RDH.19] NCRP, National Council on Radiation Protection and Measurements, "Uncertainties in Fatal Cancer risk estimated Used in Radiation Protection," NCRP Report **126**, Bethesda, Maryland, 1997.

[RDH.20] W K Sinclair, "Science, Radiation Protection and the NCRP," Lauriston Taylor Lecture, Proceedings of the 29th Annual Meeting, April 7-8, 1993, NCRP, Proceedings No 15, pp209-239, 1994.

[RDH.21] T C Yang, L M Craise, "Biological Response to heavy ion exposures," Shielding Strategies for Human Space Exploration, J W Wilson, J Miller, A Konradi, F A Cucinotto, (Eds.), pp91-107, NASA CP3360, National Aeronautics and Space Administration, Washington, DC, 1997.

[RDH.22] International Commission on Radiological Protection, "Relative Biological Effectiveness (RBE), Quality Factor (Q), and Radiation Weighting Factor (WR)," ICRP Publication 92, Elsevier, 2004.

[RDH.23] Committee to Assess Health Risks from Exposure to Low Levels of Ionizing Radiation, National Research Council. Health Risks from Exposure to Low Levels of Ionizing Radiation: BEIR VII - Phase 2. National Academy of Sciences Press, Washington D. C., p425, 2005.